2014

Synthesis, Characterization, and Investigation of the Catalytic Activity of NiO, CuO, and NiO-CuO Nanoparticles on Silica as Surrogates of Combustion-Generated Nanoparticles

Nuwan Nilanka Balapitiya Liyanage
Louisiana State University and Agricultural and Mechanical College

www.manaraa.com

SYNTHESIS, CHARACTERIZATION, AND INVESTIGATION OF THE CATALYTIC ACTIVITY OF NiO, CuO, AND NiO-CuO NANOPARTICLES ON SILICA AS SURROGATES OF COMBUSTION-GENERATED NANOPARTICLES

A Dissertation

Submitted to the Graduate Faculty of the
Louisiana State University and
Agricultural and Mechanical College
in partial fulfillment of the
requirements for the degree of
Doctor of Philosophy

in

The Department of Chemistry

by
Nuwan Nilanka Balapitiya Liyanage
B.S., University of Colombo, 2007
December 2014

This dissertation is dedicated to

My parents (Premarathna and Chandra),

My cousin Chirath,

and

My loving wife Elizabeth

ACKNOWLEDGEMENTS

I would like to thank my parents (Mr. Balapitiya L. Premarathna and Mrs. Chandra Sellahewa) and my brother (Balapitiya L. Buddima) for encouraging me to achieve my goals. I am also grateful to my dearest cousin Chirath Amadoru for believing in me and supporting me in every possible way to complete this journey. I would also like thank my host family (Prof. John Whittaker and Ms. Judy Kahn) for taking care of me and making my stay in the US an enjoyable one. Finally, I would like to thank my loving wife Elizabeth Balapitiya and my in-laws (Mr. Tim Conner and Mrs. Mary Conner) for their support and encouragement in every step of the way.

TABLE OF CONTENTS

LIST OF TABLES

LIST OF FIGURES

x

LIST OF SCHEMES

ABSTRACT

Transition metal oxide nanoparticles contained in fly ash are known to catalyze the formation of polychlorinated dibenzo-*p*-dioxins and polychlorinated dibenzofurans (PCDD/Fs) during the waste incineration process. The potential catalytic activity of silica-supported NiO, CuO, and NiO-CuO nanoparticles for the formation of PCDD/Fs will be discussed in this dissertation. The successful synthesis of silica-supported NiO, CuO, and NiO-CuO nanoparticles as surrogates of combustion-generated nanoparticles was important to this study. The synthesis was followed by the characterization of the nanoparticle surrogates by X-ray photoelectron spectroscopy (XPS), X-ray absorption spectroscopy (XAS), transmission electron microscopy (TEM), and energy-dispersive X-ray spectroscopy (EDS). Finally, the catalytic activity of these nanoparticle surrogates for the formation of PCDD/Fs was investigated.

Silica-supported metal oxide nanoparticles were prepared by wetness impregnation of metal ion−dendrimer complexes (WI-D) and wetness impregnation of metal ion solutions (WI-M), both followed by oxidative thermal treatment (calcination). NiO nanoparticles with low size dispersity (14%) and an average diameter of 3.6 ± 0.5 nm were formed by the WI-D method followed by calcination at 500 °C for 5 h. NiO nanoparticles prepared by the WI-M method showed of low size dispersity (14%) and an average diameter 2.9 ± 0.4 nm followed by calcination at 500 °C for 5 h. For the first time, mixed NiO-CuO nanoparticles were synthesized with the ability to control their Ni:Cu (1:1, 1:3, 1:10, 10:1, and 3:1) molar composition by altering the amounts of metal ions in the starting solutions.

Catalytic activity of NiO, CuO, and NiO-CuO nanoparticles was investigated by reacting 2-monochlorophenol (2-MCP)−a known PCDD/Fs precursor−on their surface at cool-zone temperatures of waste incinerators (300–500 °C with 50 °C intervals). Results indicated nearly

85% of the 2-MCP was reacted at 300 °C, while close to 100% conversion was achieved for 2-MCP at temperatures above 450 °C. It is proposed that the reactions associated with PCDD/Fs formation were initiated by binding of 2-MCP to the metal-oxide sites on the silica support, followed by formation of surface-bound chlorinated phenol molecule. PCDD/Fs yields as a function of reaction temperature and the nature of the catalyst (NiO, CuO and NiO-CuO) will be discussed.

CHAPTER 1: INTRODUCTION

1.1   Research Goal and Aims

The overall goal of the research described here is delineation of the potential catalytic activity of silica-supported NiO, CuO, and NiO-CuO nanoparticles for the formation of polychlorinated dibenzo-*p*-dioxins (PCDDs) and polychlorinated dibenzofurans (PCDFs), which are collectively known as dioxins or PCDD/Fs, under simulated reaction conditions of a municipal solid waste (MSW) incinerator. Fly ash is a product of waste incineration, which consists of a silica/alumina substrate, transition metals/metal oxides (CuO, NiO, and Fe_2O_3), and different aromatic compounds (chlorobenzenes and chlorophenols).[1-3] PCDD/Fs have been isolated from fly ash obtained from municipal waste incinerators,[2, 4-5] which supports the hypothesis of chlorobenzenes and chlorophenols acting as precursors and transition metal oxides acting as the catalyst in aiding the formation of PCDD/Fs.[6-8]

Laboratory studies of the catalytic activity of combustion-generated, transition metal-oxide nanoparticles requires a surrogate fly ash system that is comparable to real fly ash but with less complexity. Amorphous silica was selected as the substrate for surrogate fly ash instead of the complex silica/alumina mixtures that are present in real fly ash. One transition metal oxide (NiO or CuO) or known combinations of metal oxides (NiO-CuO) with total 5% weight coverage on silica were included in the surrogate fly ash, as opposed to a large number of unknown metal/metal-oxide combinations in real fly ash. However, organic precursors were not introduced to the surrogate fly ash until the beginning of the catalytic experiment. Surrogate fly ash was tested for its catalytic activity under the cool-zone temperatures (< 600 °C) similar to that in MSW incinerator.

1

Observation of real fly ash via transmission electron microscopy (TEM) has demonstrated the presence of transition metal-oxide nanoparticles on the fly ash surface.[1, 9] Nanoparticles are generally known to have greater reactivity compared to micron-sized or larger particles of the same composition, due to an increased surface-to-volume ratio.[10-13] Therefore, it was important to produce the surrogate fly ash containing metal-oxide nanoparticles for a comparable investigation. Here, generation-3 poly(propylene imine) dendrimer was used as a chelating ligand to avoid metal ion agglomeration on silica surfaces and to aid in the formation of NiO, CuO, and NiO-CuO nanoparticles.[14] TEM images confirmed the formation of nanoparticles on the silica support. X-ray photoelectron spectroscopy (XPS) and X-ray absorption spectroscopy (XAS) were used to determine the oxidation states of the metal ions and interaction of metal-oxides with the silica surface in surrogate fly ash. Mixed NiO-CuO nanoparticle surrogate fly ashes were investigated using single-particle energy-dispersive X-ray spectroscopy (EDS) to determine the composition of Ni and Cu in individual nanoparticles.

Hydroxyl groups on silica surfaces (Si−OH) are known to act as cation exchangers as a result of their coordination to transition metal ions (M) to form Si−O−M complexes on the surface.[15-17] Anchoring of transition metal ions on the silica surface is presumed to limit their mobility, thus avoiding agglomeration of the nanoparticles even without a chelating agent. To test this hypothesis, surrogate fly ash samples were also prepared without dendrimer or any other chelating agent. Their particle size, composition, and catalytic activity were compared with the surrogate fly ash prepared using generation-3 poly(propylene imine) dendrimer.

The catalytic experiments were carried out using the system for thermal diagnostic studies (STDS) in the Dellinger research group at LSU (details in Chapter 2). The surrogate fly ash was exposed to 2-monochlorophenol (2-MCP) precursor molecules for 1 h (reaction time) at

temperatures 300 to 550 °C with 50 °C intervals. Products were collected at −60 °C and then analyzed by gas chromatography–mass spectrometry (GC–MS). Products were quantified using calibration standards.

1.2   Municipal solid waste (MSW) incineration and its products

Municipal solid waste (MSW) incineration is the most efficient way to reduce the volume of solid waste to approximately 80% and thereby save landfill space.[18-21] However, particulate matter (PM), fly ash, and other hazardous materials released during the MSW incineration create complications to both the environment and the human health.[9, 19-23] Once inhaled, PM with average diameter of < 2.5 μm ($PM_{2.5}$) is taken up by bronchial epithelial cells via endocytosis, which induce the cells to respond by producing reactive oxygen species (ROS), ultimately leading to cardiopulmonary disease and cancer.[24-29] However, this study is focused on possible reactions inside MSW incinerators during their operation and the resulting products, such as PCDD/Fs.

MSW incineration is a complex process wherein the solid waste is volatilized and combusted at high temperatures.[19] MSW incinerator kilns operate at 1200 °C during the combustion process.[18, 30] However, the decline in temperature away from the combustion site in the kiln prompts condensation of fly ash inside the walls and filters of the incinerator.[22] In the same way, cooling down the kiln after a combustion operation creates low temperature zones inside the incinerator, that lead to various reactions in these temperature zones as depicted in Scheme 1.1.[25] Zone 1: the pre-flame zone operates at temperatures higher than 1200 °C where all the waste materials are promoted into the gas phase and exist in their atomic or molecular form. Zone 2: the flame zone operates at ~1200 °C and the gas-phase atoms or molecules convert to their thermodynamically most stable form, namely, carbon dioxide (CO_2), water (H_2O),

3

hydrochloric acid (HCl), and nitric oxide (NO$_X$).[25] Zone 2 also generates large quantities of

vaporized metals and chlorinated organic compounds that are crucial in the next zone.[31] Zone 3:

post-flame zone is at 1200 °C–600 °C and contains both oxygen-rich and oxygen-depleted

pockets where several radical/molecular reactions occur in the gas-phase. Vaporized metals are

oxidized and deposited onto silica surfaces thereby forming PM and fly ash in the oxygen-rich

pockets; whereas PAHs, chlorinated hydrocarbons (Cl-HCs), and brominated hydrocarbons (Br-

HCs) are formed within the oxygen-depleted pockets.[25, 31-32] The major product of the Zone 3 is

collectively known as "Soot".
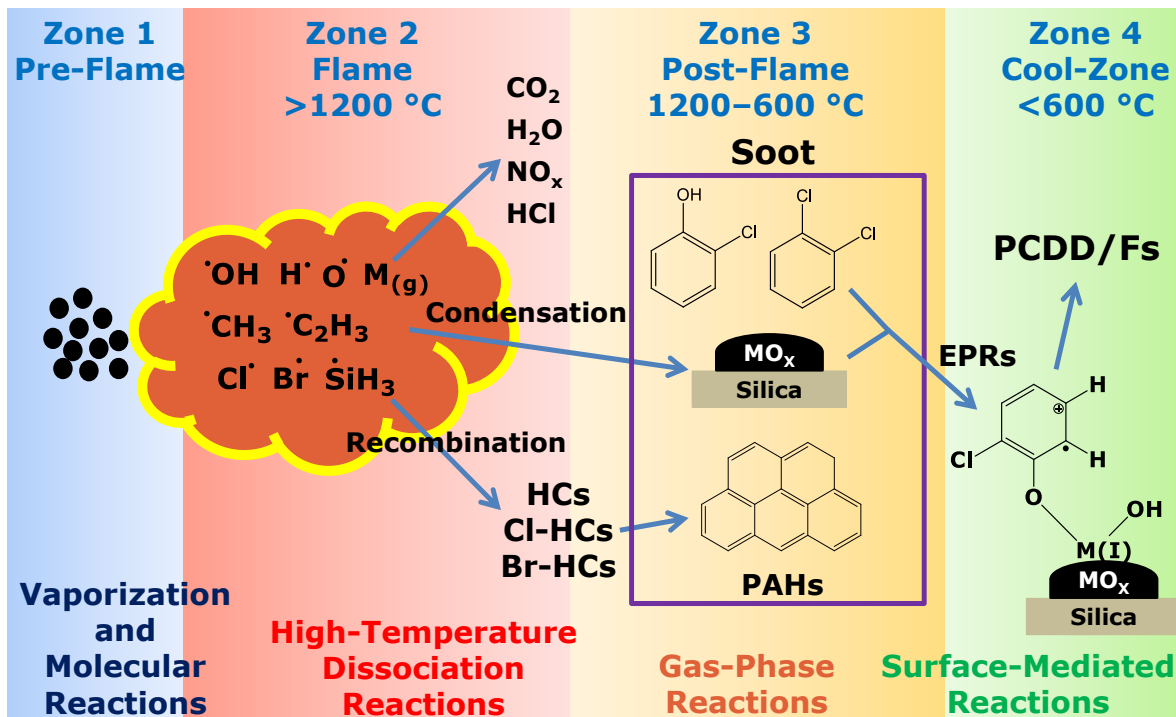
Scheme 1.1 Depiction of different temperature zones and the associated reactions inside a municipal solid waste incinerator. Adapted from Cormier et al.,[25] and modified.

Zone 4: cool zone has temperatures < 600 °C and is a mostly oxygen-depleted zone due

to oxidation reactions in the upstream zones. Surface-mediated reactions occur in this region

between 200 °C and 600 °C under pyrolytic conditions.[33-38] Transition metal oxides, formed on

الملارة للاستشارات

www.manaraa.com

silica surfaces in Zone 3, catalyze reactions in the cool zone that result in products like PCDD/Fs, which are released to the environment because the temperature in this zone is not enough to degrade them in the gas-phase.[25, 35-36] This dissertation focuses on the surface-mediated reactions occurring in the cool-zone (Zone 4) and the resulting pollutants.

1.2.1 Composition of the fly ash

Fly ash is a complex mixture consisting of a silica/alumina substrate, transition metals/metal oxides (Fe, Cu, V, Pb, and Ni), and organic compounds, such as chlorophenols, chlorobenzenes, and PCDD/Fs.[2, 6-7] The chlorobenzenes and chlorophenols are recognized as precursors for formation of PCDD/Fs, while transition metal oxides catalyze the reaction to form PCDD/Fs.[8-9, 22-23, 39-40] The silica/alumina and metal composition of the fly ash varies depending on the nature of the starting material (ex: solid waste, residual oil, etc.).

Silica/alumina in fly ash has provided the surface for metal-oxides and organic compounds to thrive. Fly ash has previously been analyzed using SEM, TEM, and EDS, and some of those images are displayed in Figure 1.1. The size of a fly ash particle can vary from 200 nm to 200 μm depending on its source.[13, 21, 41] In Figure 1.1A are shown fly ash particles from an incinerator in China where fly ash particles were observed as agglomerated spheres.[21] Fly ash particles about 60 μm was reported by a study in France where the deposited metals were observed as needles on the surface of the fly ash particle (Figure 1.1B).[42] Fly ash particles containing both Si and Al were observed in another study where the diameter was around 200 nm (Figure 1.1C and 1.1D).[13]

5
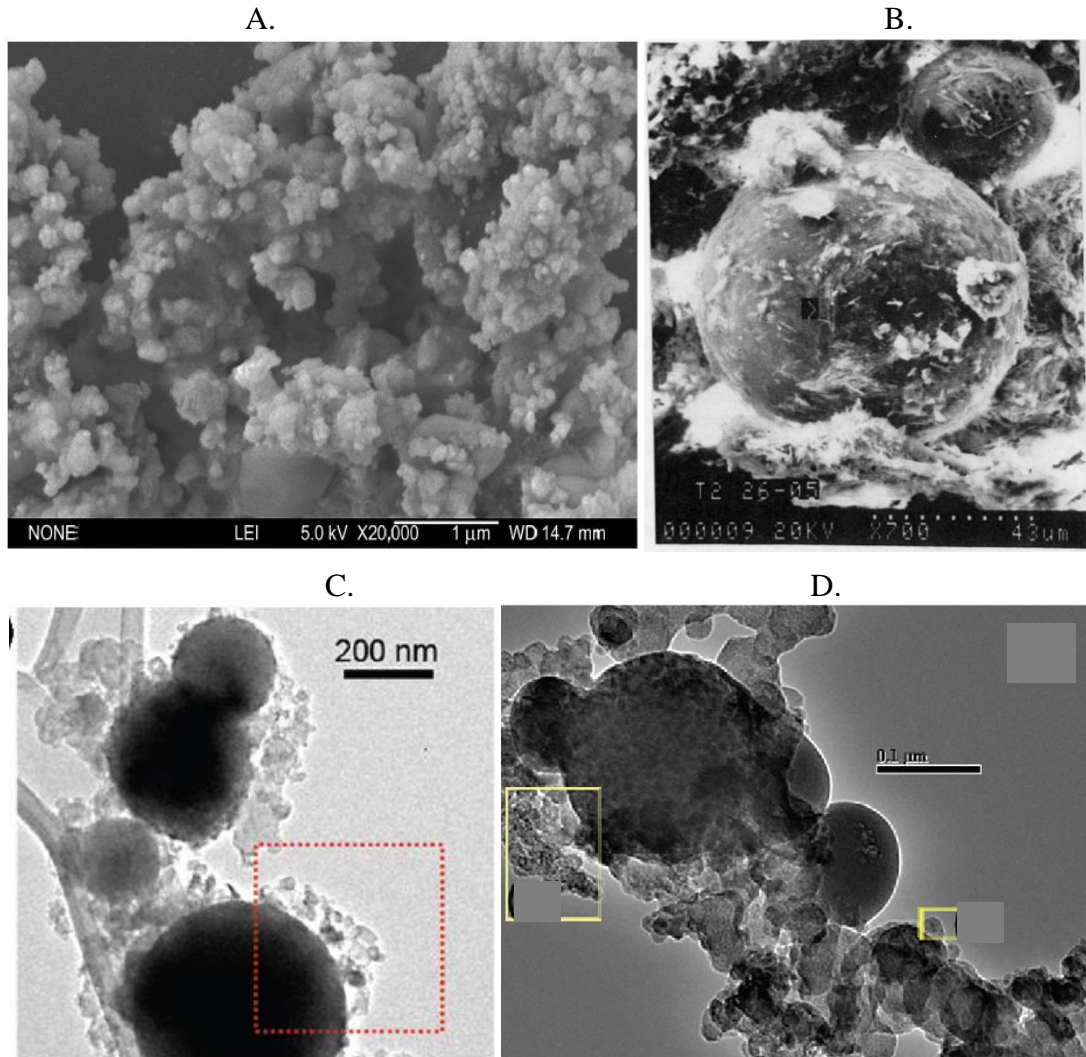
Figure 1.1 A. SEM of fly ash from MSW incinerator in China,[21] B. SEM of Fly ash extracted from MSW incinerator in France,[42] C. and D. TEM of Si-Al fly ash particles from a coal plant in Kentucky.[13]

Transition metals, such as Fe, Cu, V, Pb, and Ni were identified with various fly ash particles.[1-2, 13, 43] In Figure 1.2 are shown various transition metal-oxide nanoparticles found on the surfaces of fly ash. Fe nanoparticles immersed on Al-Si fly ash spheres were identified using electron energy loss spectroscopy (EELS), as displayed in Figure 1.2A and 1.2B.[13] Vanadium oxide (Figure 1.2C) and nickel oxide (Figure 1.2D) nanoparticles have been discovered on the surface of residual oil fly ash by TEM and selected-area electron diffraction (SAED).[1]
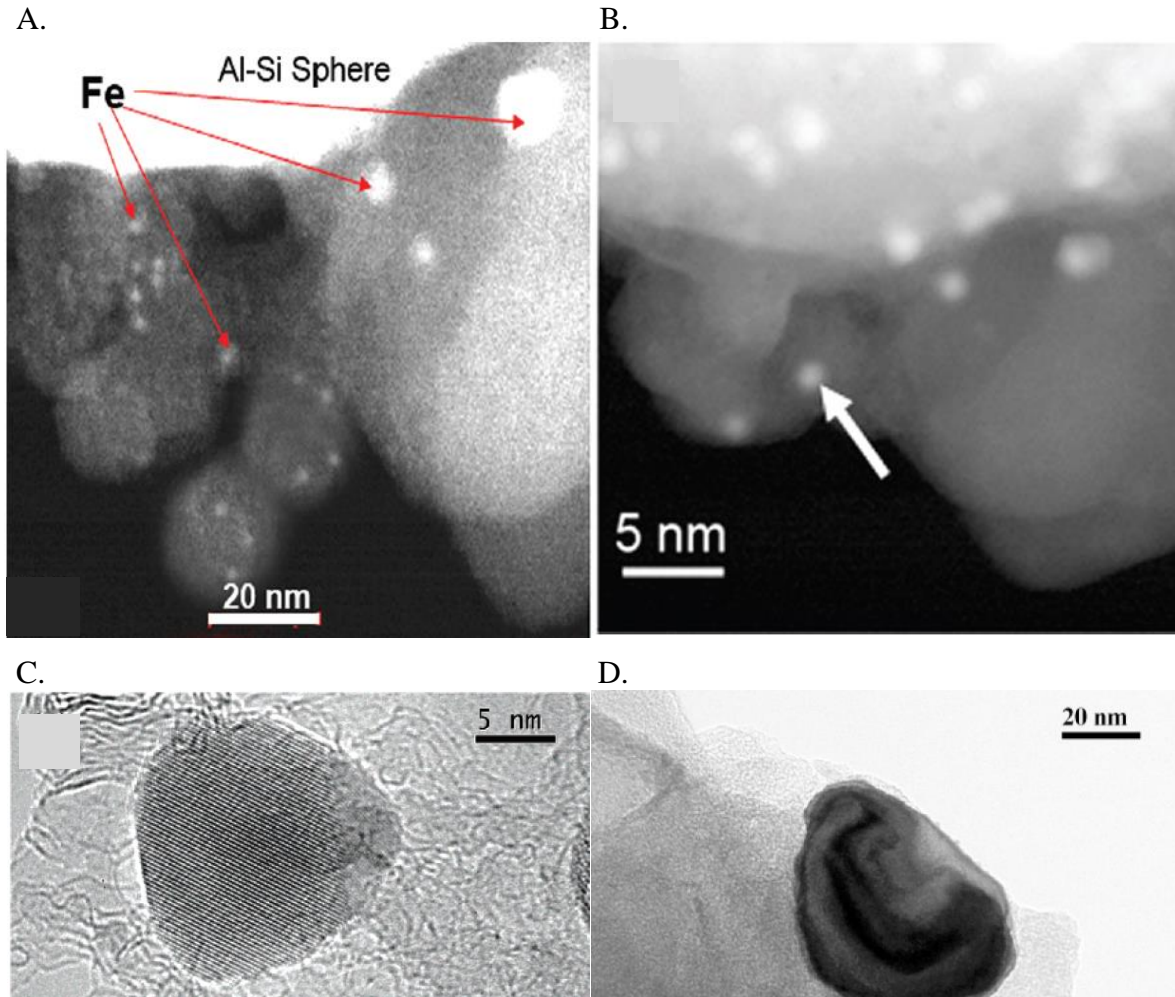
Figure 1.2 TEM images of various nanometer-sized metal/metal oxides on fly ash particles A. and B. iron nanoparticles on Si-Al fly ash spheres,[13] C. vanadium oxide nanoparticle,[1] and D. Nickel oxide nanoparticle.[1]

The metal composition of the fly ash is a function of the starting materials in the incineration process (waste, residual oil, etc.). Some of the metals found in the fly ash from MSW incinerators are given in Tables 1.1 and 1.2. Zn was the metal found in the highest amount for this sample, along with Pb in second place.[2] In addition, toxic heavy metals, such as Hg and Cd, were also found. In contrast, residual oil fly ash contains only Ni, Fe, and V as the transition metals, thus indicating the importance of the starting materials on the composition of the fly ash.[1]

7

Table 1.1 Amounts of metals found in fly ash of a MSW incinerator.[2]

Metal	Min (μg/g)	Max (μg/g)
Cu	220	1800
Ni	36	110
Zn	4900	44000
V	24	113
Cr	200	1600
Pb	730	36000
Co	2	120
Hg	1	22
Cd	4	310
W	12	50

Table 1.2 % Metal found in residual oil incinerator fly ash.[3]

Metal	Weight%
Ni	12.8
Fe	34.0
V	17.6
Na	1.7
Mg	6.2
Ca	14.8

Transition metal oxides such as Fe_2O_3 and CuO have been studied extensively for their ability to catalyze the formation of PCDD/Fs under MSW incinerator cool-zone conditions.[36, 44-47] Additionally, it has been found that $PbCl_2$ catalyzes the formation of chlorinated aromatic compounds, which are known precursors of PCDD/Fs.[43] ZnO and NiO are well known for their ability to form environmentally-persistent radical species after those being exposed to chlorobenzenes and chlorophenols: this is the first step in the proposed mechanism of PCDD/Fs formation.[48-49] Ni is a common metal in incinerator fly ash (Table 1.1 and 1.2), and the catalytic activity of NiO for the formation of PCDD/Fs under MSW incinerator conditions had not been

studied prior to the work here. This dissertation aims to fill this knowledge gap by exploring the catalytic ability of NiO and simple combinations of NiO/CuO for the formation of PCDD/Fs.

1.2.2 Significance of polychlorinated dibenzo-*p*-dioxins and polychlorinated dibenzofurans (PCDD/Fs)

PCDD/Fs are environmental pollutants originating from waste incineration, pesticide synthesis, paper manufacturing, and activity of the textile industry.[25, 50-54] Even though PCDD/Fs are emitted from natural processes, like forest fires and volcanic eruptions, the amounts that originate from anthropogenic sources exceeds that of natural processes, with waste incineration alone contributing 45% of the total emissions.[53, 55] PCDD/Fs belong to the family of persistent organic pollutants (POPs), which polychlorinated biphenyls (PCBs), polycyclic aromatic hydrocarbons (PAHs), and organochlorine pesticides (e.g. DDT) are also included.[40, 56] Once released, POPs last a long time in the environment and have the ability to spread long distances from their source, until they encounter cold temperatures or rain that cause them to precipitate, thereby contaminating the water and soil (Scheme 1.2).[53]

Due to their hydrophobic and lipophilic (soluble in lipids) properties, PCDD/Fs associate with materials with high organic content, such as microscopic plants and animals in water and soil.[53] When those microorganisms are consumed by macro organisms, the PCDD/Fs make their way to the next level of the food chain. Likewise, PCDD/Fs make their way up in the food chain while accumulating at each level due to their solubility in body fat (lipophilic), thus increasing in concentration at each level; this is a phenomenon referred to as biomagnification.[53] Being at the top of the food chain, humans are exposed to the highest levels of PCDD/Fs through the consumption of contaminated animal products (meat, fish, milk, and eggs).[51, 57-58]

9

POPs (persistent organic pollutants)

1. In warm temperatures POPs evaporate
2. POPs move in air by winds to colder places such as the North
3. In cold temperatures POPs condense and fall to earth
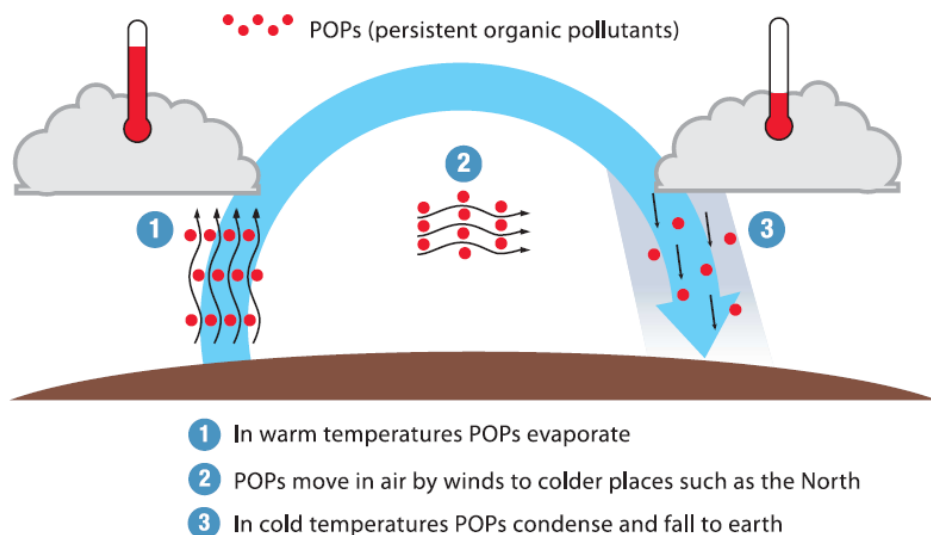
Scheme 1.2 Fate of persistent organic pollutants (POPs), including PCDD/Fs in the environment.[59]

PCDD/Fs belong to a group of compounds that consists of 210 different congeners (75 PCDDs and 135 PCDFs) distinguished by the number and position of Cl atoms attached to aromatic rings (Figure 1.3).[53] Only 17 of these congeners (7 PCDDs and 10 PCDFs) are known to be toxic.[53, 60] 2,3,7,8-tetrachlorodibenzo-*p*-dioxin (2,3,7,8-TCDD) is the most toxic congener known (Figure 1.4), and the toxicity of the other congeners is reported with respect to that of 2,3,7,8-TCDD using International Toxic Equivalents I-TEQ (Table 1.3).[53, 60-61] Based on animal toxicity and human epidemiology data, 2,3,7,8-TCDD is now considered a human carcinogen by the World Health Organization (WHO) and the US National Toxicology Program.[62]
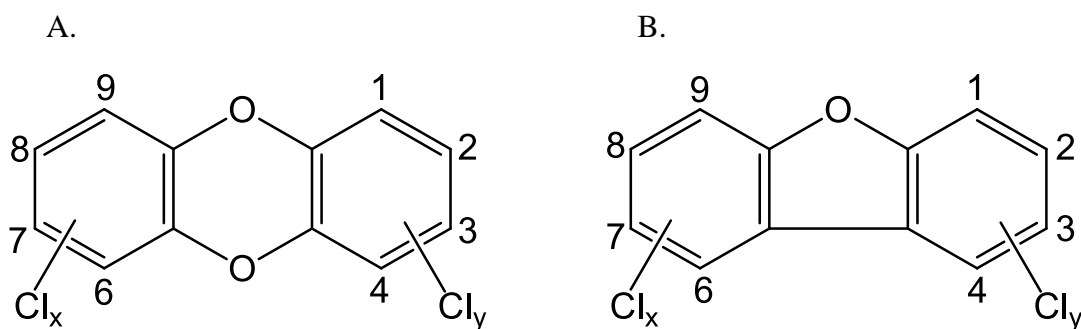
Figure 1.3 Structures of A. polychlorinated dibenzo-*p*-dioxins and B. polychlorinated dibenzofurans.

10
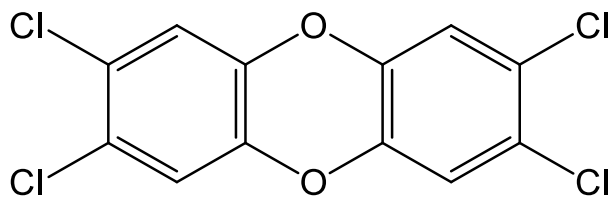
Figure 1.4 The most toxic congener in the PCDD/Fs family; 2,3,7,8-tetrachlorodibenzo-*p*-dioxin (2,3,7,8-TCDD).

Table 1.3 International Toxicity Equivalence Factors (I-TEFs) for the 17 known toxic PCDD/F congeners.[60]

PCDD/Fs Congeners	I-TEF
2,3,7,8-tetrachlorodibenzo-*p*-dioxin	1
2,3,7,8-tetrachlorodibenzofuran	0.1
1,2,3,7,8-pentachlorodibenzofuran	0.05
2,3,4,7,8-pentachlorodibenzofuran	0.5
1,2,3,7,8-pentachlorodibenzo-*p*-dioxin	0.5
1,2,3,4,7,8-hexachlorodibenzofuran	0.1
1,2,3,6,7,8-hexachlorodibenzofuran	0.1
2,3,4,6,7,8-hexachlorodibenzofuran	0.1
1,2,3,7,8,9-hexachlorodibenzofuran	0.1
1,2,3,4,7,8-hexachlorodibenzo-*p*-dioxin	0.1
1,2,3,6,7,8-hexachlorodibenzo-*p*-dioxin	0.1
1,2,3,7,8,9-hexachlorodibenzo-*p*-dioxin	0.1
1,2,3,4,6,7,8-heptachlorodibenzofuran	0.01
1,2,3,4,7,8,9-heptachlorodibenzofuran	0.01
1,2,3,4,6,7,8-heptachlorodibenzo-*p*-dioxins	0.01
octachlorodibenzofuran	0.001
octachlorodibenzo-*p*-dioxin	0.001

The lipophilic nature of 2,3,7,8-TCDD allows its purge through the cell membrane into the cytosol. Once in the cytosol, TCDD binds with the aryl hydrocarbon receptor (AhR), a protein that is designed to recognize lipophilic compounds entering the cell.[62-64] Then the AhR-TCDD complex migrates to the nucleus with the help of AhR nuclear translocator protein (Arnt).

11

The AhR-TCDD-Arnt complex binds with a specific DNA sequence called the xenobiotic-response element (XRE) inside the nucleus (Scheme 1.3) followed by the expression of several genes, generating response proteins and enzymes associated with PCDD/F poisoning.[62]
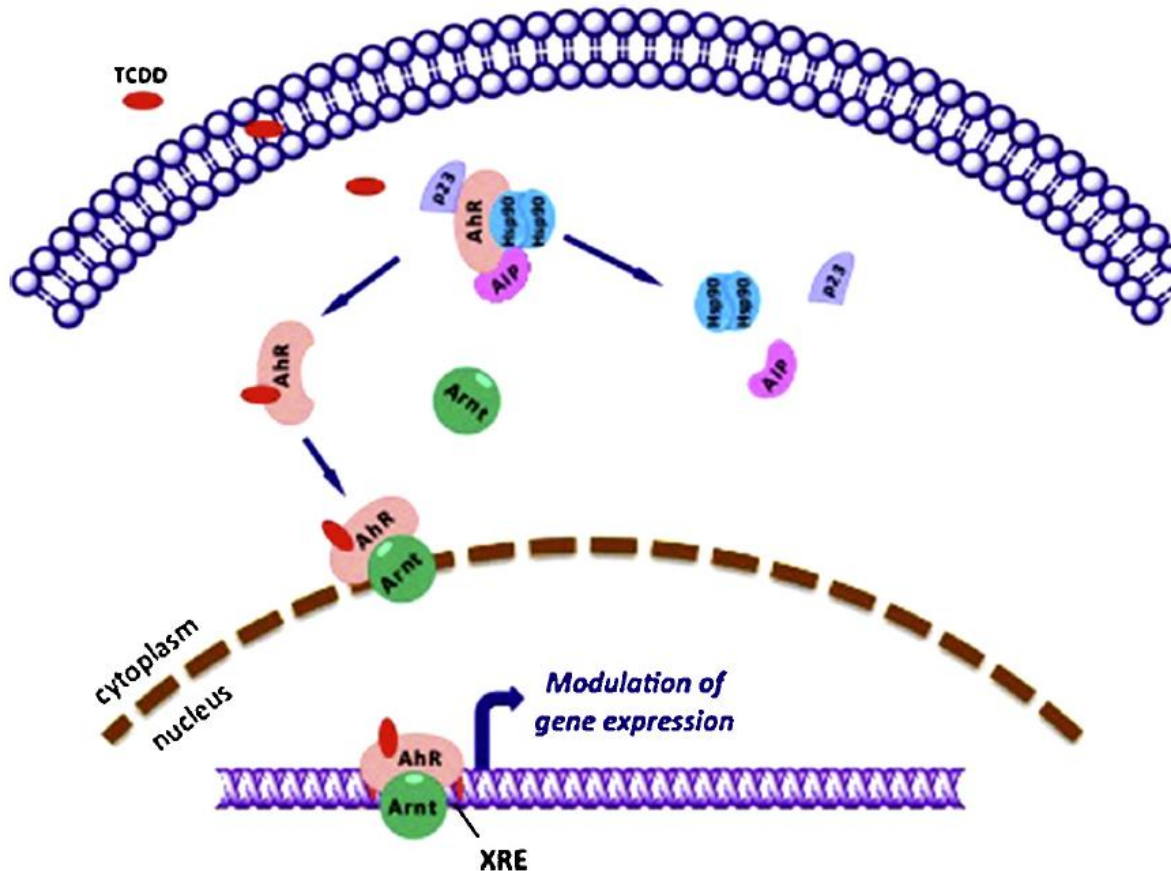
Scheme 1.3 Fate of 2,3,7,8-TCDD inside the cell after binding to aryl hydrocarbon receptor (AhR).[62]

Many human tissues−including those of the lung, liver, kidney, skin, spleen, and placenta−contain AhR; thus acute exposure to PCDD/Fs can result in failure of one or more of the above organisms, leading to death.[62] Chloracne is the main physiological symptom of dioxin poisoning, where the sebaceous gland on the skin is depleted creating skin discoloration and cysts.[53, 62-63] Liver and kidney damage, gastrointestinal pain, and appetite loss are some of the other symptoms.[50] Due to the long biological half-lives of PCDD/Fs (7−10 years), these symptoms may last for a long time; however, the outcomes may vary based on the amount of

toxin ingested and the genetic variations of individuals.[65] Adverse effects on reproductive systems (birth defects and miscarriage) and disruption in the endocrine system have been reported as long-term abnormalities.[56, 66]

The general population usually carries minor levels of PCDD/Fs in body fat due to environmental exposure (2 pg g^{-1} body fat),[67] but accidental and occupational exposure to large quantities of PCDD/Fs elevates the levels in body fat thereby creating health complications. Several incidents of accidental and occupational exposure have been reported throughout the 20th century and early 21st century.[53] Monsanto Chemical Company in the USA (1930s) was a large producer of PCBs, pesticides, and herbicides that contained high levels of PCDD/Fs as byproducts.[53] Several Monsanto workers developed chloracne due to occupational exposure.

During the Vietnam War from 1961 to 1971, the US military used a plant defoliant called "Agent Orange" to destroy the forest cover and vegetation so that enemy combatants lost both defenses and food supplies.[53, 66] Agent Orange was manufactured by US chemical companies, including Monsanto, and was later found to be contaminated with the most toxic dioxin congener 2,3,7,8-TCDD.[53] This discovery led to the termination of Agent Orange operations within Vietnam in 1971 (four years prior to the end of the Vietnam War in 1975), but an estimated 72 million liters of Agent Orange had already been sprayed over Vietnam by that time.[53, 66] The exact number of deaths caused by Agent Orange is not known, even though reports of long-term health defects, like miscarriages and congenital birth defects, have been reported in affected areas even as late as 2000, a quarter of a century after the Vietnam War.[66] Exposure to high levels of Agent Orange caused health problems among US war veterans who were actively involved in the operation, and to date, several lawsuits have been filed against chemical companies, claiming over $180 million in compensation.[53]

13

The explosion of a 2,4,5-trichlorophenol reactor on ICMESA chemical plant in Seveso (25 Km/13 miles north of Milan), Italy in 1976, released a cloud of dioxins over the city of Seveso.[50, 53, 68] The seemingly harmless mist began to precipitate on streets, buildings, and gardens and as a result, entire town was contaminated. The effects were not visible until several days later when children began to develop chloracne.[69] Italian officials later confirmed the presence of dioxins in the area and ordered an evacuation.[68]

Several cases of occupational exposure have been reported throughout the 21st century, and one such case explains the symptoms of two office workers at a textile research institute in Vienna, Austria.[50] Patient 1, a 30-year old woman in 1997, had developed severe chloracne over her entire body within days after moving into new office space. Scientists at the Department of Dermatology of the University of Vienna Medical School have identified 2,3,7,8-TCDD as the cause for her chloracne, and TCDD was detected at 144,000 pg g^{-1} body fat (25 μg Kg^{-1} body weight), the highest recorded in a human at the time.[50] Besides the skin condition, which lasted for several years, during the initial stage the patient had also experienced gastrointestinal symptoms including nausea, vomiting, and loss of appetite. Follow up with Patient 1 after seven years from the first symptoms, led to a report of significant improvement in the inflammatory conditions and cysts, even though today she still suffers from skin disfigurations, scars, and occasional abscesses.[65] Patient 2, a 27-year old woman who worked in the same room with Patient 1, had exhibited similar symptoms in 1997 and had 2,3,7,8-TCDD amounts of 26,000 pg g^{-1} body fat (6 μg Kg^{-1} body weight).[50] Due to comparatively lower concentrations of 2,3,7,8-TCDD, Patient 2 suffered only from mild chloracne, which resolves after 1 year from the first symptoms.[65] Neither of the patients were directly associated with laboratory work, and due to the high concentrations the in the body, oral ingestion was suggested as the possible route of

14

exposure.[65] Examination of 30 other coworkers reported only three people (2 men and 1 woman) with slightly elevated levels of 2,3,7,8-TCDD (856, 149, and 93 pg g^{-1} body lipids) with none of them showing symptoms.[50]

The poisoning of Ukrainian President Viktor Yushchenko in 2004 was the most notorious dioxin poisoning case of the 21st century, which baffled the medical and political communities, and attracted worldwide media attention.[53, 67] The news was escalated after the release of President Yushchenko's photos before and after the poisoning (Figure 1.5).[67] The transformation from a handsome gentleman to the disfigured apparent older fellow within a matter of weeks continues to stun the world. After dinner with the security services of Ukraine in September 2004, just prior to the Presidential elections, Viktor Yushchenko (the opposition leader at the time) fell seriously ill with nausea, severe headache, and abdominal pain followed by severe back pain and chloracne within the next couple of weeks.[67] Two months later, British toxicologists suggested a dioxin poisoning but the diagnosis was not completed until a month later (three months after the first symptoms) by a gas chromatography-mass spectrometry (GC-MS) group at the Geneva University Hospital in Switzerland.[53, 67] Tests confirmed the presence of 2,3,7,8-TCDD in his blood serum with 108,000 pg g^{-1} body lipids; this value is 50,000 times higher than the background level (2 pg g^{-1} body lipids) in the general population.[53] The presence of high concentrations of one congener 2,3,7,8-TCDD raised the suspicion of an assassination attempt, but not enough evidence was found to prove such claims.

With many incidents of occupational and accidental exposure, and having been used in chemical warfare and political assassination attempts, PCDD/Fs are a group of compounds that shaped human history, and their presence will continue to haunt our present and impact our future. Therefore, it is important to explore routes of their formation and ways to eliminate such

15

processes. MSW incineration is one of the major routes of PCDD/Fs formation, contributing to 45% of the total emissions; thus mechanisms involved in that process will be discussed in the Section 1.3.

Before   After

Figure 1.5 Ukrainian President Viktor Yushchenko (September 2004) before and after exposure to 2,3,7,8-TCDD.[67, 70]

1.3   Pathways of PCDD/Fs formation during MSW incineration

Two pathways have been identified as contributing to the formation of PCDD/Fs, namely, gas-phase reactions and surface-mediated reactions.[22, 36] Gas-phase reactions predominantly form PCDD/Fs at temperatures higher than 600 °C, and they are responsible for 30% of the total PCDD/F emissions.[35] However, PCDD/Fs were reported to be unstable at temperatures above 900 °C, making gas-phase reactions insignificant at flame zone temperatures.[22, 35]

Surface-mediated processes are predominant under cool-zone temperatures (< 600 °C), and they account for 70% of the total PCDD/Fs emissions.[35] Surface-mediated reactions are further divided into *de novo* pathway and precursor pathway.[35-36] Regardless of the difference in

16

the mechanism of these pathways, both require transition metal oxides contained in fly ash as the catalysts.[22, 71] In *de novo* pathway, carbonaceous deposits and soot converts to PCDD/Fs under the cool-zone temperature mostly in the presence of oxygen, moisture, and chlorine sources (inorganic chlorides or Cl_2/HCl in the flue gas).[22, 39, 71] Studies of fly ash models doped with ^{13}C-labeled carbon resulted in the formation of ^{13}C-PCDD/Fs, ^{12}C-PCDD/Fs and [13]C-^{12}C-PCDD/Fs,[72-74] confirming the formation of PCDD/Fs from the unreacted carbon on the matrix via *de novo* pathway.

The precursor pathway is the most predominant surface-mediated process inside MSW incinerators, which is responsible for PCDD/Fs formation 10^5 times higher than that of the *de novo* pathway.[71] In the precursor pathway, chlorophenols and chlorobenzenes are converted to PCDD/Fs in the cool-zone temperatures under oxygen-depleted conditions.[35] The surface-mediated precursor pathway has been extensively studied using surrogate fly ash containing different transition metals. Exposure of surrogate fly ash, containing Fe, Cu, Ni, and Zn, to precursor molecules (chlorophenols and chlorobenzenes) resulted in the formation of chlorophenoxyl radicals as previously observed by electron paramagnetic resonance (EPR).[35, 48-49, 75] These radicals are stable under ambient conditions for several days, but they will quickly react with other compounds under the conditions inside a MSW incinerator.[48-49, 75] The chlorophenoxyl radical is the first step in PCDD/Fs formation via precursor pathway.[35] Nganai *et al.* studied reactions of 2-chlorophenol on Fe_2O_3 surrogate fly ash and reactions of 1,2-dichlorobenzene on CuO surrogate fly ash under pyrolysis (helium carrier gas) to determine yields and mechanisms of PCDD/Fs formation under cool-zone temperatures (200 °C–550 °C).[44-45] The pyrolysis of 2-chlorophenol on Fe_2O_3 surrogate fly ash resulted in dibenzo-*p*-dioxin (DD), 1-chloro-dibenzo-*p*-dioxin (1-MCDD), dibenzofuran (DF), and 4,6-dichloro-dibenzofuran

17

(4,6-DCDF), as displayed in Figure 1.6A. The product % yield varied with the reaction temperature. Similar products were observed when 2-chlorophenol and 1,2-dichlorophenol was reacted on CuO surrogate fly ash (Figure 1.6B).[45] These studies indicate that the transition metal oxides, such as Fe_2O_3 and CuO, catalyze the pyrolytic conversion of chlorophenols and chlorobenzenes to PCDD/Fs at cool-zone temperatures. Chapter 4 in this study focuses on the reactions of 2-chlorophenol on NiO surrogate fly ash. Also, for the first time, reactions of chlorophenols on mixed metal-oxide (NiO-CuO) fly ash surrogates are studied so as to examine the effect of two transition metals on the % yields of PCDD/Fs.
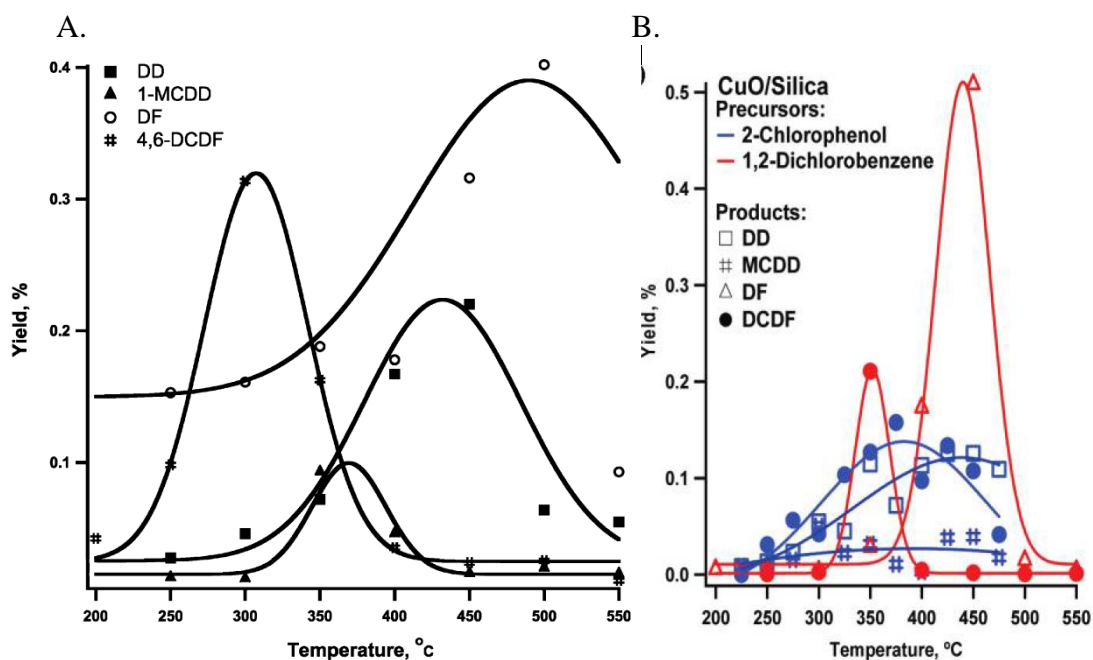
Figure 1.6 PCDD/F % yields from the pyrolysis of A. 2-chlorophenol over Fe_2O_3 surrogate fly ash[44] and B. 2-chlorophenol and 1,2-dichlorobenzene over CuO surrogate fly ash.[45]

1.4 Preparation of silica-based surrogate fly ash

Incipient wetness impregnation (IWI), followed by calcination, was the most common method used in previous studies to prepare surrogate fly ash.[44-45, 48-49, 75-76] In IWI, aqueous solution of metal nitrates, such as Fe(III) nitrate, Cu(II) nitrate, etc., were mixed with silica gel powder and allowed to equilibrate for 24 h at room temperature, followed by drying at 120 °C

18

for 12 h. Subsequent calcination at 450 °C for 5 h resulted in metal oxide particles on silica. Then the sample was ground using a mortar and pestle to obtain a fine powder similar to real fly ash.

Surrogate fly ash was also prepared by wetness impregnation of metal-dendrimer complexes on silica surfaces followed by calcination.[77-78] Solutions were prepared in methanol because the dendrimer is insoluble in water. Metal nitrate solutions were mixed with a solution of poly(propylene imine) dendrimer to form the metal-dendrimer complex. Then the solution of the metal-dendrimer complex was mixed with silica and allowed to reach equilibrium at room temperature for 1 h. Subsequent calcination at 450 °C for 5 h resulted in the surrogate fly ash. TEM studies revealed the presence of CuO nanoparticles < 5 nm in diameter on silica when generation-4 poly(propylene imine) dendrimer (DAB-Am$_{32}$) was used in the preparation (Figure 1.7).[79]

The sol-gel method followed by calcination has been utilized to prepare metal-oxide nanoparticles coated with silica. In one study, NiO nanoparticles coated with silica were prepared by starting with nickel nitrate, tetraethoxysilane (TEOS), a water-ethanol mixture, and citric acid.[80-81] All the above materials were stirred in a round-bottom flask for 1 h, and the pH of the solution was adjusted to 2.5 using aqueous ammonia. The resulting slurry was dried at 50 °C in air for 20 h followed by calcination at 500 °C for 2 h in air. Silica-coated NiO nanoparticles of 2–8 nm (average ~5 nm) in diameter were observed by TEM, as displayed in Figure 1.8.

1.5   Impact of studying silica-based NiO and NiO-CuO surrogate fly ash

Ni and Cu are commonly found transition metals in MSW incinerator fly ash.[1-3] Also, CuO is a well-known catalyst in both *de novo* and precursor pathways of PCDD/F formation inside MSW incinerators.[22, 71] EPR spectroscopy studies on both CuO and NiO surrogate fly ash

19

demonstrated a reduction of the metal center followed by formation of a chlorophenoxyl radical upon exposure to precursor molecules (chlorobenzenes and chlorophenols).[49, 82] The formation of chlorophenoxyl radical on CuO and NiO surrogate fly ash is the first step of PCDD/F formation in the precursor pathway.[35-36] Previously, CuO surrogate fly ash was studied for its catalytic activity for the formation of PCDD/Fs (Figure 1.6B).[45] However, such a study has not been done for NiO until now. The ability of NiO to form chlorophenoxyl radicals upon exposure to precursor molecules is a good indication that NiO has the ability to catalyze the formation PCDD/Fs, which provides incentive for this study of NiO surrogate, fly ash-catalyzed reactions of chlorophenol.
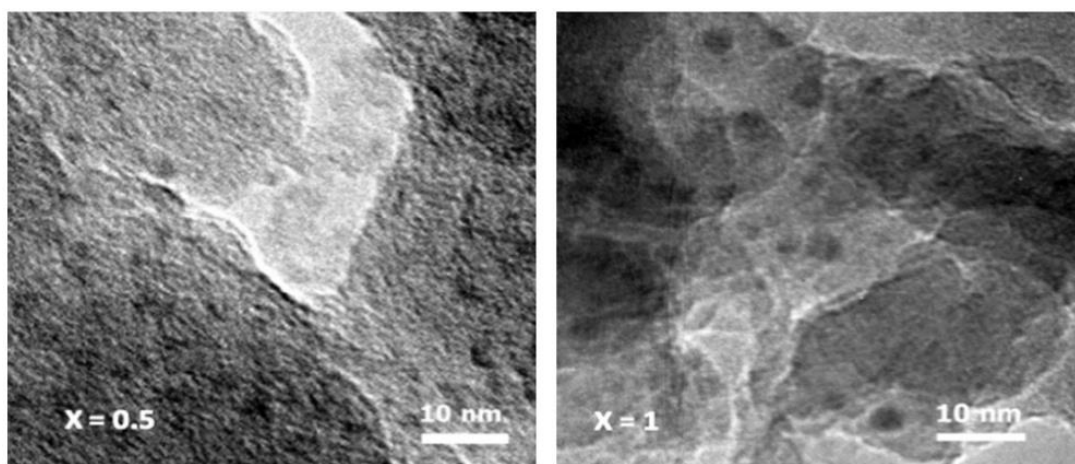
Figure 1.7 TEM of CuO surrogate fly ash prepared by wetness impregnation of DAB-Am$_{32}$-Cu(II)$_{16}$ on silica.[79]
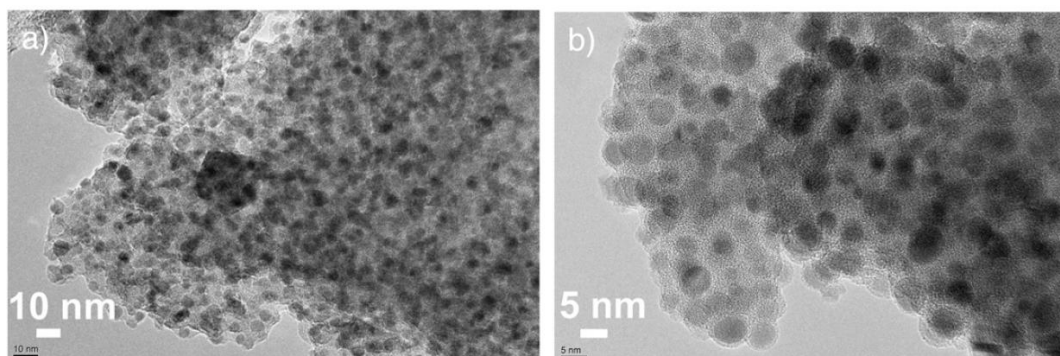
Figure 1.8 TEM of silica-coated NiO nanoparticles prepared by the sol-gel method.[80]

www.manaraa.com

Ni and Cu are consecutive *d*-block transition metals in the periodic table. Both Ni and Cu inhabit a face-centered cubic lattice (fcc) structure with similar lattice parameters (a_{Ni}=0.352 nm and a_{Cu}=0.362 nm); hence, their alloys have been studied in the past.[83-84] The formation of NiO-CuO mixed oxides in the presence of oxygen has also been observed.[85-86] TEM studies on MSW incinerator fly ash revealed the presence of metal-oxide particles (micrometer and nanometer sized) containing more than one transition metal including Ni and Cu.[1] Therefore, it is highly likely for Ni and Cu to form a mixed metal-oxide under the conditions inside MSW incinerator. However, such a mixed metal-oxide surrogate fly ash system has never been investigated as potential catalysts for PCDD/Fs formation prior to this study.

Equation 1.1 $$Ni^{2+} + 2e^- \rightarrow Ni \qquad E^\circ = -0.25V$$

Equation 1.2 $$Cu^{2+} + 2e^- \rightarrow Cu \qquad E^\circ = +0.34V$$
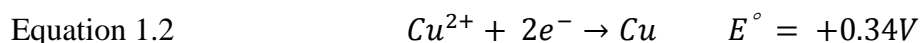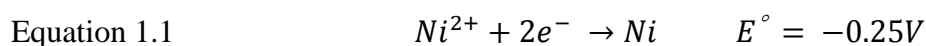
According to Equations 1.1 and 1.2, Cu(II) has the ability to reduce itself readily than Ni(II). The reduction of the metal center is important in the first step of PCDD/Fs formation reaction.[35-36] Also, incorporation of Cu metals into a Ni system brings an extra electron to the NiO-CuO lattice.[87] Consequently, an enhancement in catalytic activity can be expected when Cu is incorporated with Ni due the changes in the lattice.[84, 87] Therefore, it is important to study NiO-CuO surrogate fly ash systems for their catalytic activity in forming PCDD/Fs so as to gain some understanding of how the presence of multiple metal-oxides in MSW incinerator fly ash affects pollutant formation.

1.6   References

1.   Chen, Y.; Shah, N.; Huggins, F. E.; Huffman, G. P., Investigation of the Microcharacteristics of PM$_{2.5}$ in Residual Oil Fly Ash by Analytical Transmission Electron Microscopy. *Environmental Science & Technology* **2004,** *38* (24), 6553-6560.

21

2. Öberg, T.; Öhrström, T.; Bergström, J., Metal catalyzed formation of chlorinated aromatic compounds: A study of the correlation pattern in incinerator fly ash. *Chemosphere* **2007,** *67* (9), S185-S190.

3. Allouis, C.; Beretta, F.; D'Alessio, A., Structure of inorganic and carbonaceous particles emitted from heavy oil combustion. *Chemosphere* **2003,** *51* (10), 1091-1096.

4. Addink, R., Bakker, WCM, Olie, K, Influence of H_2O and HCl on the formation of polychlorinated dibenzo-*p*-dioxins/dibenzofurans in a carbon/fly ash mixture. *Organohalogen Compounds* **1992,** *8*, 205 - 208.

5. Addink, R.; Drijver, D. J.; Olie, K., Formation of polychlorinated dibenzo-*p*-dioxins/dibenzofurans in the carbon/fly ash system. *Chemosphere* **1991,** *23* (8–10), 1205-1211.

6. Öberg, T.; Bergbäck, B.; Öberg, E., Different Catalytic Effects by Copper and Chromium on the Formation and Degradation of Chlorinated Aromatic Compounds in Fly Ash. *Environmental Science & Technology* **2007,** *41* (10), 3741-3746.

7. Öberg, T.; Bergbäck, B.; Filipsson, M., Catalytic effects by metal oxides on the formation and degradation of chlorinated aromatic compounds in fly ash. *Chemosphere* **2008,** *71* (6), 1135-1143.

8. Shaub, W. M.; Tsang, W., Dioxin formation in incinerators. *Environmental Science & Technology* **1983,** *17* (12), 721-730.

9. Vejerano, E. P.; Leon, E. C.; Holder, A. L.; Marr, L. C., Characterization of particle emissions and fate of nanomaterials during incineration. *Environmental Science: Nano* **2014,** *1* (2), 133-143.

10. Martinello, K.; Oliveira, M. L. S.; Molossi, F. A.; Ramos, C. G.; Teixeira, E. C.; Kautzmann, R. M.; Silva, L. F. O., Direct identification of hazardous elements in ultra-fine and nanominerals from coal fly ash produced during diesel co-firing. *Science of The Total Environment* **2014,** *470–471* (0), 444-452.

11. Navrotsky, A., Thermochemistry of Nanomaterials. *Reviews in Mineralogy and Geochemistry* **2001,** *44* (1), 73.

12. Banfield, J. F.; Zhang, H., Nanoparticles in the Environment. *Reviews in Mineralogy and Geochemistry* **2001,** *44* (1), 1.

13. Hower, J. C.; Graham, U. M.; Dozier, A.; Tseng, M. T.; Khatri, R. A., Association of the Sites of Heavy Metals with Nanoscale Carbon in a Kentucky Electrostatic Precipitator Fly Ash. *Environmental Science & Technology* **2008,** *42* (22), 8471-8477.

14. Mitran, E.; Dellinger, B.; McCarley, R. L., Highly Size-Controlled, Low-Size-Dispersity Nickel Nanoparticles from Poly(propylene imine) Dendrimer−Ni(II) Complexes. *Chemistry of Materials* **2010,** *22* (24), 6555-6563.

15. Hathaway, B. J.; Lewis, C. E., Electronic properties of transition-metal complex ions adsorbed on silica gel. Part I. Nickel(II) complexes. *Journal of the Chemical Society A: Inorganic, Physical, Theoretical* **1969**, 1176-1182.

16. Hathaway, B. J.; Lewis, C. E., The electronic properties of transition-metal complex ions adsorbed on silica gel. Part III. Copper(II). *Journal of the Chemical Society A: Inorganic, Physical, Theoretical* **1969**, 2295-2299.

17. Hathaway, B. J.; Lewis, C. E., Electronic properties of transition-metal complex ions adsorbed on silica gel. Part II. Cobalt(II) and cobalt(III). *Journal of the Chemical Society A: Inorganic, Physical, Theoretical* **1969**, 1183-1188.

18. Decision Makers' Guide to Municipal Solid Waste Incineration. The International Bank for Reconstruction and Development, THE WORLD BANK, 1818 H Street, N.W. Washington, D.C. 20433, U.S.A.: 1999; pp 1-20.

19. Chagger, H. K.; Jones, J. M.; Pourkashanian, M.; Williams, A., The Formation of VOC, PAH and Dioxins During Incineration. *Process Safety and Environmental Protection* **2000,** *78* (1), 53-59.

20. Bie, R.; Li, S.; Wang, H., Characterization of PCDD/Fs and heavy metals from MSW incineration plant in Harbin. *Waste Management* **2007,** *27* (12), 1860-1869.

21. Chen, M.; Meng, Y.; Shi, J.; Ni, G.; Jiang, Y.; Yu, X.; Zhao, P., Effect of feed forms on the results of melting of fly ash by a DC plasma arc furnace. *Plasma Science & Technology (Bristol, U. K.)* **2009,** *11* (5), 592-597.

22. Addink, R.; Olie, K., Mechanisms of Formation and Destruction of Polychlorinated Dibenzo-*p*-dioxins and Dibenzofurans in Heterogeneous Systems. *Environmental Science & Technology* **1995,** *29* (6), 1425-1435.

23. Vejerano, E. P.; Holder, A. L.; Marr, L. C., Emissions of Polycyclic Aromatic Hydrocarbons, Polychlorinated Dibenzo-*p*-Dioxins, and Dibenzofurans from Incineration of Nanomaterials. *Environmental Science & Technology* **2013,** *47* (9), 4866-4874.

24. Truong, H.; Lomnicki, S.; Dellinger, B., Potential for Misidentification of Environmentally Persistent Free Radicals as Molecular Pollutants in Particulate Matter. *Environmental Science & Technology* **2010,** *44* (6), 1933-1939.

25. Cormier, S. A.; Lomnicki, S.; Backes, W.; Dellinger, B., Origin and health impacts of emissions of toxic by-products and fine particles from combustion and thermal treatment of hazardous wastes and materials. *Environmental Health Perspectives* **2006,** *114* (6), 810-817.

26. Díaz-Robles, L. A.; Fu, J. S.; Vergara-Fernández, A.; Etcharren, P.; Schiappacasse, L. N.; Reed, G. D.; Silva, M. P., Health risks caused by short term exposure to ultrafine particles generated by residential wood combustion: A case study of Temuco, Chile. *Environment International* **2014,** *66* (0), 174-181.

23

27. Fahmy, B.; Ding, L.; You, D.; Lomnicki, S.; Dellinger, B.; Cormier, S. A., In vitro and in vivo assessment of pulmonary risk associated with exposure to combustion generated fine particles. *Environmental Toxicology and Pharmacology* **2010,** *29* (2), 173-182.

28. Gehling, W.; Khachatryan, L.; Dellinger, B., Hydroxyl Radical Generation from Environmentally Persistent Free Radicals (EPFRs) in $PM_{2.5}$. *Environmental Science & Technology* **2013,** *48* (8), 4266-4272.

29. Silva, L. F. O.; da Boit, K. M., Nanominerals and nanoparticles in feed coal and bottom ash: implications for human health effects. *Environmental Monitoring and Assessment* **2011,** *174* (1-4), 187-197.

30. Municipal Solid Waste Incineration (World Bank Technical Guidance Report). The International Bank for Reconstruction and Development / THE WORLD BANK, 1818 H Street, N.W.. Washington, D.C. 20433, U.S.A.: 1999; pp 1 - 111.

31. Cundy VA, L. T., Sterling AM, Montestruc AN, Morse JS, Leger CB, et al., Rotary kiln incineration. 3. An in-depth study: kiln exit afterburner stack train and kiln exit pattern factor measurements during liquid CCI_4 processing. *Journal of Air and Waste Management Association* **1989,** *39*, 944-952.

32. Russell, J. J.; Seetula, J. A.; Gutman, D.; Senkan, S. M., Kinetics of reactions of chlorinated vinyl radicals (CH_2CCl and C_2Cl_3) with molecular oxygen. *Journal of Physical Chemistry* **1989,** *93* (5), 1934-8.

33. Huang, H.; Buekens, A., On the mechanisms of dioxin formation in combustion processes. *Chemosphere* **1995,** *31* (9), 4099-4117.

34. Ryu, J.-Y.; Mulholland, J. A.; Kim, D. H.; Takeuchi, M., Homologue and Isomer Patterns of Polychlorinated Dibenzo-*p*-dioxins and Dibenzofurans from Phenol Precursors: Comparison with Municipal Waste Incinerator Data. *Environmental Science & Technology* **2005,** *39* (12), 4398-4406.

35. Lomnicki, S.; Dellinger, B., A Detailed Mechanism of the Surface-Mediated Formation of PCDD/F from the Oxidation of 2-Chlorophenol on a CuO/Silica Surface. *The Journal of Physical Chemistry A* **2003,** *107* (22), 4387-4395.

36. Lomnicki, S.; Dellinger, B., Formation of PCDD/F from the pyrolysis of 2-chlorophenol on the surface of dispersed copper oxide particles. *Proceedings of the Combustion Institute* **2002,** *29* (2), 2463-2468.

37. Altwicker, E. R.; Konduri, R. K. N. V.; Lin, C.; Milligan, M. S., Rapid formation of polychlorinated dioxins/furans in the post combustion region during heterogeneous combustion. *Chemosphere* **1992,** *25* (12), 1935-1944.

38. Gullett, B. K.; Lemieux, P. M.; Dunn, J. E., Role of combustion and sorbent parameters in prevention of polychlorinated dibenzo-*p*-dioxin and polychlorinated dibenzofuran

24

formation during waste combustion. *Environmental Science & Technology* **1994,** *28* (1), 107-18.

39. Milligan, M. S.; Altwicker, E., The relationship between *de novo* synthesis of polychlorinated dibenzo-*p*-dioxins and dibenzofurans and low-temperature carbon gasification in fly ash. *Environmental Science & Technology* **1993,** *27* (8), 1595-1601.

40. Procaccini, C.; Bozzelli, J. W.; Longwell, J. P.; Sarofim, A. F.; Smith, K. A., Formation of Chlorinated Aromatics by Reactions of Cl•, Cl_2, and HCl with Benzene in the Cool-Down Zone of a Combustor. *Environmental Science & Technology* **2003,** *37* (8), 1684-1689.

41. Silva, L. F. O.; Oliveira, M. L. S.; Sampaio, C. H.; de Brum, I. A. S.; Hower, J. C., Vanadium and Nickel Speciation in Pulverized Coal and Petroleum Coke Co-combustion. *Energy & Fuels* **2013,** *27* (3), 1194-1203.

42. Carignan, J.; Libourel, G.; Cloquet, C.; Le Forestier, L., Lead Isotopic Composition of Fly Ash and Flue Gas Residues from Municipal Solid Waste Combustors in France: Implications for Atmospheric Lead Source Tracing. *Environmental Science & Technology* **2005,** *39* (7), 2018-2024.

43. Fujimori, T.; Tanino, Y.; Takaoka, M., Thermochemical Behavior of Lead Adjusting Formation of Chlorinated Aromatics in MSW Fly Ash. *Environmental Science & Technology* **2013,** *47* (5), 2169-2176.

44. Nganai, S.; Lomnicki, S.; Dellinger, B., Ferric Oxide Mediated Formation of PCDD/Fs from 2-Monochlorophenol. *Environmental Science & Technology* **2008,** *43* (2), 368-373.

45. Nganai, S.; Lomnicki, S. M.; Dellinger, B., Formation of PCDD/Fs from the Copper Oxide-Mediated Pyrolysis and Oxidation of 1,2-Dichlorobenzene. *Environmental Science & Technology* **2010,** *45* (3), 1034-1040.

46. Alderman, S. L.; Farquar, G. R.; Poliakoff, E. D.; Dellinger, B., Reaction of 2-chlorophenol with CuO: XANES and SEM analysis. *Proceedings of the Combustion Institute* **2005,** *30* (1), 1255-1261.

47. Takaoka, M.; Fujimori, T.; Shiono, A.; Yamamoto, T.; Takeda, N.; Oshita, K.; Uruga, T.; Sun, Y.; Tanaka, T., Formation of chlorinated aromatics in model fly ashes using various copper compounds. *Chemosphere* **2010,** *80* (2), 144-149.

48. Vejerano, E.; Lomnicki, S.; Dellinger, B., Lifetime of combustion-generated environmentally persistent free radicals on Zn(ii)O and other transition metal oxides. *Journal of Environmental Monitoring* **2012,** *14* (10), 2803-2806.

49. Vejerano, E.; Lomnicki, S. M.; Dellinger, B., Formation and Stabilization of Combustion-Generated, Environmentally Persistent Radicals on Ni(II)O Supported on a Silica Surface. *Environmental Science & Technology* **2012,** *46* (17), 9406-9411.

50. Geusau, A.; Abraham, K.; Geissler, K.; Sator, M. O.; Stingl, G.; Tschachler, E., Severe 2,3,7,8-tetrachlorodibenzo-*p*-dioxin (TCDD) intoxication: Clinical and laboratory effects. *Environmental Health Perspectives* **2001,** *109* (8), 865-869.

51. Kaiser, J., Toxicology: Just how bad is dioxin? *Science (Washington, D. C.)* **2000,** *288* (5473), 1941, 1943-1944.

52. Jorling, T., No Longer a Source of Dioxin. *Science* **2000,** *290* (5493), 934-935.

53. Marinkovic, N.; Pasalic, D.; Ferencak, G.; Grskovic, B.; Stavljenic Rukavina, A., Dioxins and human toxicity. *Archives of Industrial Hygiene and Toxicology* **2010,** *61* (4), 445-453.

54. Facts on health and the environment. Scientic facts on Dioxins 2004 *GreenFacts* [Online], 2010. http://www.greenfacts.org/en/dioxins/dioxins-greenfacts-level2.pdf.

55. Ren, Z.; Zheng, M., Impacts of human activities on dioxins emissions at national scale. *Chemosphere* **2009,** *76* (6), 853-859.

56. Nakamoto, M.; Arisawa, K.; Uemura, H.; Katsuura, S.; Takami, H.; Sawachika, F.; Yamaguchi, M.; Juta, T.; Sakai, T.; Toda, E.; Mori, K.; Hasegawa, M.; Tanto, M.; Shima, M.; Sumiyoshi, Y.; Morinaga, K.; Kodama, K.; Suzuki, T.; Nagai, M.; Satoh, H., Association between blood levels of PCDDs/PCDFs/dioxin-like PCBs and history of allergic and other diseases in the Japanese population. *International Archives of Occupational and Environmental Health* **2013,** *86* (8), 849-859.

57. Beck, H.; Eckart, K.; Mathar, W.; Wittkowski, R., PCDD and PCDF body burden from food intake in the Federal Republic of Germany. *Chemosphere* **1989,** *18* (1-6), 417-24.

58. Berg, M. V. d.; De Jongh, J.; Poiger, H.; Olson, J.; Van den Berg, M.; De Jongh, J.; Poiger, H.; Olson, J. R., The Toxicokinetics and Metabolism of Polychlorinated Dibenzo-*p*-Dioxins (PCDDs) and Dibenzofurans (PCDFs) and Their Relevance for Toxicity. *Critical Reviews in Toxicology* **1994,** *24* (1), 1-74.

59. Dioxins and Furans *Northwest Territories contaminants fact sheets, Contaminants and Remediation Directorate, Aboriginal Affairs and Northern Development Canada* [Online], March 2004 http://www.aadnc-aandc.gc.ca/eng/1100100023383/1100100023391.

60. Stanmore, B. R., The formation of dioxins in combustion systems. *Combustion and Flame* **2004,** *136* (3), 398-427.

61. Steenland, K.; Bertazzi, P.; Baccarelli, A.; Kogevinas, M., Dioxin revisited: developments since the 1997 IARC classification of dioxin as a human carcinogen. *Environmental Health Perspectives* **2004,** *112* (13), 1265-1268.

62. Sorg, O., AhR signalling and dioxin toxicity. *Toxicology Letters* **2013**.

26

63. Bock, K. W., The human Ah receptor: hints from dioxin toxicities to deregulated target genes and physiological functions. *The Journal of Biological Chemistry* **2013,** *394* (6), 729-739.

64. Abel, J.; Haarmann-Stemmann, T., An introduction to the molecular basics of aryl hydrocarbon receptor biology. *The Journal of Biological Chemistry* **2010,** *391* (11), 1235-1248.

65. Geusau, A.; Abraham, K., Severe 2,3,7,8-Tetrachlorodibenzo-*p*-dioxin intoxication: A follow-up of the patients from Vienna. *Organohalogen Compounds* **2005,** *67*, 1702 - 1704.

66. Nham Tuyet, L. T.; Johansson, A., Impact of chemical warfare with agent orange on women's reproductive lives in Vietnam: A pilot study. *Reproductive Health Matters* **2001,** *9* (18), 156-164.

67. Ryan, J. J., The Yushchenko dioxin poisoning: chronology and pharmacokinetics. *Dioxins and Health (3rd Edition)* **2012**, 567.

68. Stone, R., New Seveso findings point to cancer. *Science* **1993,** *261* (5127), 1383.

69. Assennato, G.; Cervino, D.; Emmett, E. A.; Longo, G.; Merlo, F., Follow-up of subjects who developed chloracne following TCDD exposure at Seveso. *American journal of industrial medicine* **1989,** *16* (2), 119-125.

70. Herbschleb, C. T. ReactorSTM : imaging catalysts under realistic conditions. Faculty of Science, Leiden University, http://hdl.handle.net/1887/17620, 2011.

71. Dickson, L. C.; Lenoir, D.; Hutzinger, O., Quantitative comparison of *de novo* and precursor formation of polychlorinated dibenzo-*p*-dioxins under simulated municipal solid waste incinerator postcombustion conditions. *Environmental Science & Technology* **1992,** *26* (9), 1822-8.

72. Stieglitz, L.; Bautz, H.; Roth, W.; Zwick, G., Investigation of precursor reactions in the *de novo* synthesis of PCDD/PCDF on fly ash. *Chemosphere* **1997,** *34* (5–7), 1083-1090.

73. Milligan, M. S.; Altwicker, E. R., Mechanistic Aspects of the *de novo* Synthesis of Polychlorinated Dibenzo-*p*-dioxins and Furans in Fly Ash from Experiments Using Isotopically Labeled Reagents. *Environmental Science & Technology* **1995,** *29* (5), 1353-8.

74. Hell, K.; Stieglitz, L.; Dinjus, E., Mechanistic Aspects of the *de novo* Synthesis of PCDD/PCDF on Model Mixtures and MSWI Fly Ashes Using Amorphous ^{12}C- and ^{13}C-Labeled Carbon. *Environmental Science & Technology* **2001,** *35* (19), 3892-3898.

75. Vejerano, E.; Lomnicki, S.; Dellinger, B., Formation and Stabilization of Combustion-Generated Environmentally Persistent Free Radicals on an Fe(III)$_2$O$_3$/Silica Surface. *Environmental Science & Technology* **2010,** *45* (2), 589-594.

27

76. Ungureanu, A.; Dragoi, B.; Chirieac, A.; Ciotonea, C.; Royer, S.; Duprez, D.; Mamede, A. S.; Dumitriu, E., Composition-Dependent Morphostructural Properties of Ni–Cu Oxide Nanoparticles Confined within the Channels of Ordered Mesoporous SBA-15 Silica. *ACS Applied Materials & Interfaces* **2013,** *5* (8), 3010-3025.

77. Mitran, E. Synthesis and characterization of transition metal and metal oxide nanoparticles using dendritic complexes. Louisiana State University, Electronic Thesis and Dissertation Library, Graduate School, 2010.

78. Rodrigo, U. I. Geometrical and electronic structure of metal oxide nanoparticles on silica and alumina. Louisiana State University, Electronic Thesis and Dissertation Library, Graduate School, 2012.

79. Lomnicki, S. M.; Wu, H.; Osborne, S. N.; Pruett, J. M.; McCarley, R. L.; Poliakoff, E.; Dellinger, B., Size-selective synthesis of immobilized copper oxide nanoclusters on silica. *Materials Science and Engineering: B* **2010,** *175* (2), 136-142.

80. Tadić, M.; Panjan, M.; Marković, D., NiO/SiO$_2$ nanostructure and the magnetic moment of NiO nanoparticles. *Materials Letters* **2010,** *64* (19), 2129-2131.

81. Tadić, M.; Panjan, M.; Marković, D.; Milošević, I.; Spasojević, V., Unusual magnetic properties of NiO nanoparticles embedded in a silica matrix. *Journal of Alloys and Compounds* **2011,** *509* (25), 7134-7138.

82. Lomnicki, S.; Truong, H.; Vejerano, E.; Dellinger, B., Copper Oxide-Based Model of Persistent Free Radical Formation on Combustion-Derived Particulate Matter. *Environmental Science & Technology* **2008,** *42* (13), 4982-4988.

83. Pabi, S. K.; Joardar, J.; Manna, I.; Murty, B. S., Nanocrystalline phases in Cu-Ni, Cu-Zn and Ni-Al systems by mechanical alloying. *Nanostructured Materials* **1997,** *9* (1–8), 149-152.

84. Mainardi, D. S.; Balbuena, P. B., Monte Carlo Simulation of Cu−Ni Nanoclusters: Surface Segregation Studies. *Langmuir* **2001,** *17* (6), 2047-2050.

85. Eric, H.; Timuçin, M., Equilibrium relations in the system nickel oxide-copper oxide. *MTB* **1979,** *10* (4), 561-563.

86. Kellogg, H. H., Thermodynamic properties of the oxide of copper and nickel. *Journal of chemical and Engineering Data* **1969,** *14* (1), 41-4.

87. Hristova, E.; Dong, Y.; Grigoryan, V. G.; Springborg, M., Structural and Energetic Properties of Ni−Cu Bimetallic Clusters. *The Journal of Physical Chemistry A* **2008,** *112* (34), 7905-7915.

CHAPTER 2: INSTRUMENTATION AND METHODS

2.1   X-ray photoelectron spectroscopy (XPS)

Surface elemental analyses of the NiO, CuO, and NiO-CuO nanoparticles were performed using a custom-designed Kratos Axis Ultra X-ray photoelectron spectroscopy system.[1] The surface analysis chamber was equipped with aluminum Kα X-ray gun and a 500 mm Rowland circle silicon single-crystal monochromator. The X-ray gun was operated using a 15 mA emission current at an accelerating voltage of 15 kV. Low-energy electrons were used for sample charge compensation. High-resolution spectra were acquired in the region of interest using the following experimental parameters: 20–40 eV energy window, pass energy of 20 eV, step size of 0.1 eV, and dwell time of 1000 ms. One sweep was used to acquire a survey spectrum of all binding regions (1200–0 eV) at a pass energy 160 eV, step size of 1 eV, and a dwell time of 100 ms. The absolute energy scale was calibrated to the Cu $2p_{3/2}$ peak binding energy of 932.6 eV using an etched copper plate. Samples were mounted by pressing them to indium foil for analysis. All spectra were calibrated using the adventitious C1s peak at 285.0 eV. A Shirley-type background was subtracted from each spectrum to account for inelastically scattered electrons contributing to the broad background. CasaXPS software[2] and Origin software version 6.1 were used for XPS data processing. Transmission-corrected relative sensitivity factor (RSF) values from the Kratos library were used for elemental quantification. An error of ±0.2 eV is reported for all peak binding energies. Uncertainties in atomic concentrations were calculated using CasaXPS Monte Carlo simulations.

2.2   Transmission electron microscopy (TEM)

TEM was performed with a JEOL JEM-2010 high-resolution transmission-electron microscope operating at 200 kV accelerating voltage. Metal-oxide/silica samples were suspended

29

in methanol, and 10 μL of the solutions were deposited onto Formvar holey carbon-coated gold grids and then allowed to dry in air. Average particle diameter was determined using ImageJ software version 1.45s, and the size distribution histograms were constructed using Origin software version 6.1.

2.3   Energy-dispersive X-ray spectroscopy (EDS)

The composition of the mixed NiO-CuO nanoparticles was determined using a JEOL 2100F field-emission, transmission-electron microscope equipped with Thermo Noran Nanotrace 40 mm^2 Si(Li) X-ray detector and a Schottky emitter operating in scanning transmission (STEM) mode. The accelerating voltage was 200 kV, and the diameter of the electron beam was 0.7 nm. Samples were suspended in methanol, and 10 μL of the suspensions were deposited onto Formvar holey carbon-coated gold grids and then allowed to dry in air. The electron beam was focused on single metal-oxide nanoparticles, and energy-dispersive X-ray spectra were obtained. Integrated characteristic X-ray intensities of Kα lines of both Ni and Cu were used for the quantification using the Cliff-Lorimer method.[3]

2.4   X-ray absorption spectroscopy (XAS)

Ni and Cu K-edge X-ray absorption spectroscopic measurements were conducted at the electron storage ring of the Center for Advanced Microstructures and Devices (CAMD), Louisiana State University, Baton Rouge, LA. The ring was operated at 1.3 GeV. The experiments were performed at the wiggler double-crystal monochromator (WDCM) beam line located on a seven Tesla wavelength shifter. Germanium (220) crystals were used in the WDCM, which is a Lemonnier-type monochromator,[4] with design modifications made at the University of Bonn, Germany. Ni and Cu foil were used for monochromator calibration. The measurements in fluorescence mode were obtained with a 13-element germanium solid-state detector (Canberra

30

Industries, Meridian, CT, USA). The powder samples were thinly spread between two pieces of Kapton tape, and this assembly was placed in the path of the X-ray beam. No degradation of the samples was observed over time or due to exposure to radiation. At least two scans were performed for each sample. Ni samples were scanned from 8233 to 9333 eV, and Cu samples were scanned from 8879 to 9979 eV in both fluorescence and transmission mode at room temperature. The two scans were averaged using Athena in Demeter software (Ravel and Newville, 2005), and the experimental data were fitted with Artemis in Demeter.

2.5   System for thermal diagnostic studies (STDS)

Surface-mediated precursor reactions on surrogate fly ash were carried out using a system for thermal diagnostic studies (STDS).[5] It consists of four components: (1) controller, (2) thermal reactor housed within a Varian CP-3800 gas chromatographic oven, (3) Varian CP-3800 gas chromatographic (GC) system, and (4) Varian Saturn 2000 ion-trap mass spectrometer.[6] The main components of the STDS are displayed in Figure 2.1A. The controller helps to maintain a constant temperature inside the thermal reactor and the transfer line. Different types of gases are used as the carrier gas depending on the type of experiment (Figure 2.1B). In this study, both breathing air (20% O_2 + 80% N_2) and ultra-high pure (Alpha gas) helium were used as carrier gases. The thermal reactor was placed inside a GC oven (Varian CP-3800) as displayed in Figure 2.2B. The temperature inside the oven was maintained at 200 °C to avoid condensation of precursor compounds (chlorophenols) in the lines. The quartz reactor containing the catalyst was placed inside the thermal reactor (Figure 2.2C). The temperature of the thermal reactor was controlled by the controller (Figure 2.1A), and it was varied from 300 °C to 550 °C with 50 °C intervals for each experiment to simulate the temperature inside a municipal solid waste incinerator in the cooling-down mode.

31

A.

B.

Figure 2.1 System for thermal diagnostic studies (STDS) A. Front and B. Back.

Precursor compounds were injected using a GC syringe attached to an injector pump (Figure 2.2A), which allows control of the flow rate at 0.21 μL h^{-1} to maintain a constant gas phase precursor concentration of 50 ppm. Carrier gas (helium) flow rate (15 mL min^{-1}) was controlled by the electronic flow controller in the GC oven and was always verified using a flow meter (Figure 2.3A). Chlorophenol precursor passed over the quartz reactor and interacted with the contained catalyst. Products from the reaction were transported to the front end of the GC column in the Varian CP-3800 gas chromatographic system by the transfer line maintained at 200 °C (Figure 2.3A). The temperature inside the GC oven was maintained at −60 °C during the catalytic reaction (for 1 h) to cryogenically-trap the products at the front end of the GC column

(Agilent HP-5ms, length 30 m, inner diameter 0.25 mm, dimethylpolysiloxane stationary phase thickness 0.25 μm wrapped around a 7 inch diameter cage; Figure 2.3C). Once a catalytic reaction was complete (after 1 h), the GC/MS was initiated to separate and identify products (temperature program: -60 °C to 300 °C at 10 °C min^{-1}). Products were quantified using calibration standards.
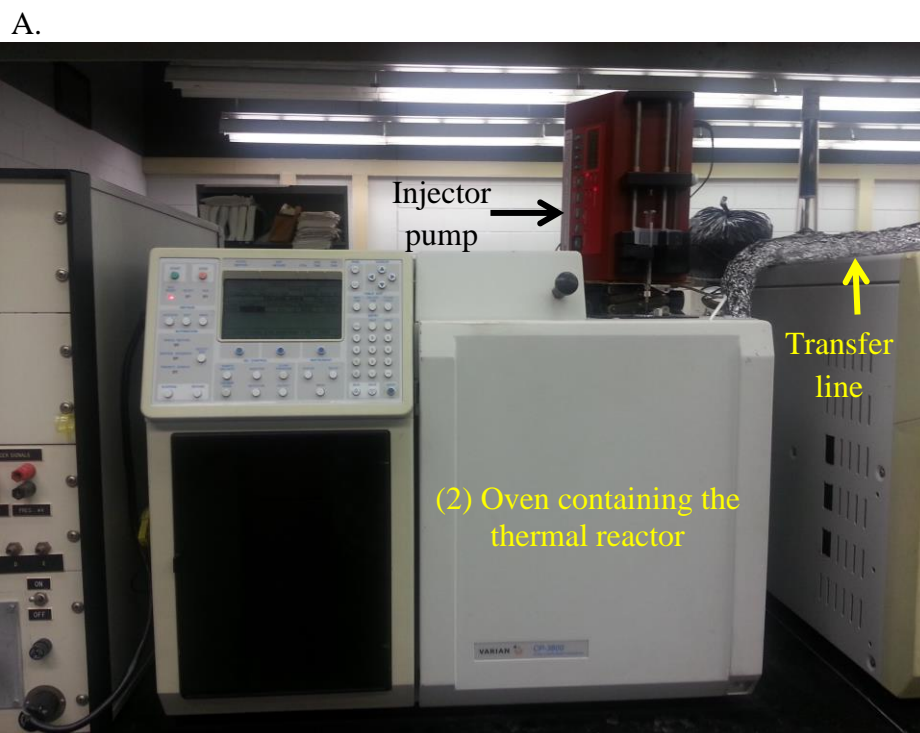
Figure 2.2 A. Varian CP-3800 gas chromatographic oven, B. thermal reactor inside the oven, and C. quartz reactor containing the catalyst.

A.

Transfer line

Flow meter

GC

MS

B.

C.
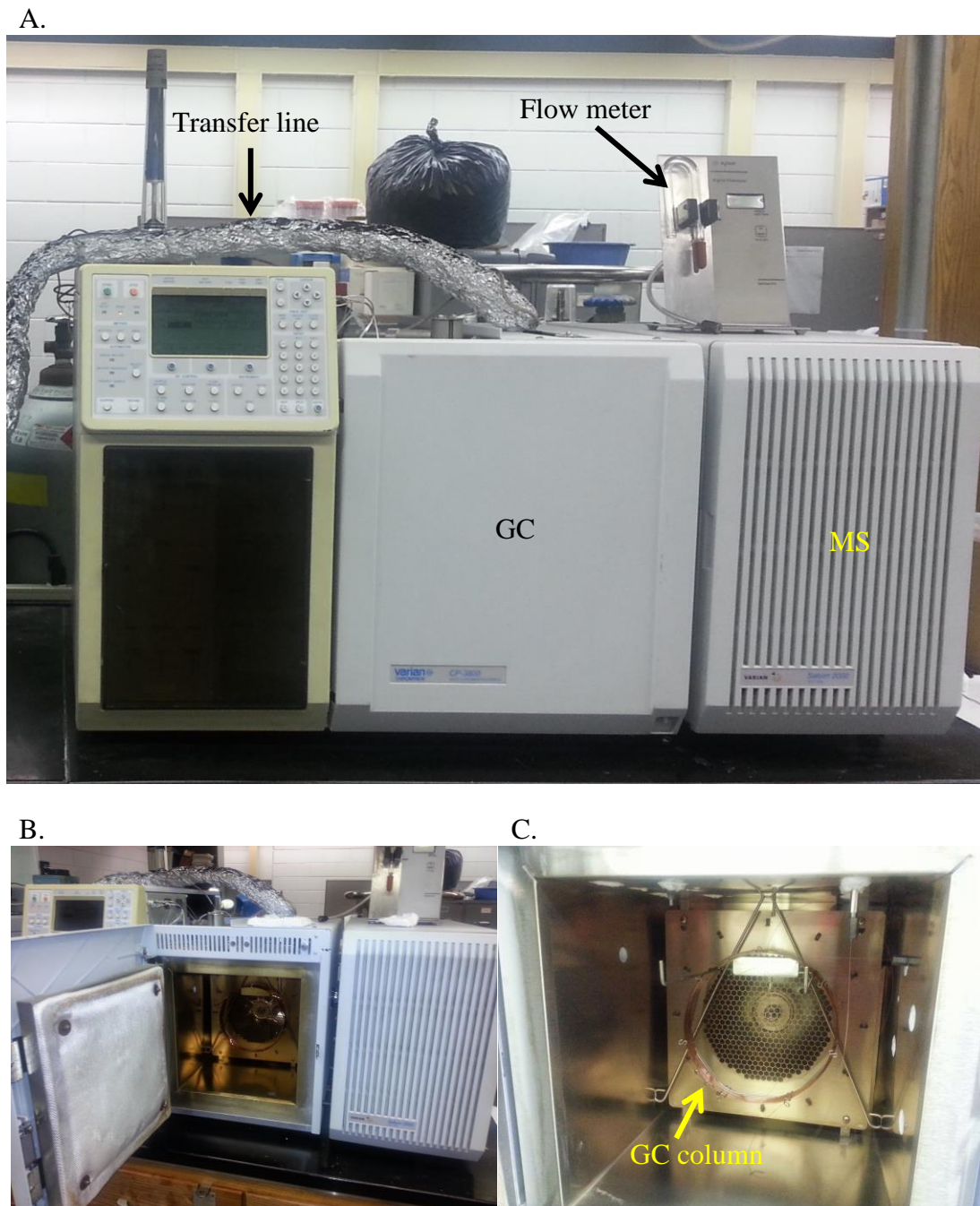
GC column

Figure 2.3 A. Varian CP-3800 gas chromatographic (GC) system in line with Varian Saturn 2000 ion trap mass spectrometer, B. Inside the GC oven, and C. GC column.

2.6 References

1. Baltrusaitis, J.; Usher, C. R.; Grassian, V. H., Reactions of sulfur dioxide on calcium carbonate single crystal and particle surfaces at the adsorbed water carbonate interface. *Physical Chemistry Chemical Physics* **2007,** *9* (23), 3011-3024.

2.   Fairley, N. C., CasaXPS 2.3.17. www.casaxps.com. **1999-2012**.

3.   Nacucchi, M.; Alvisi, M.; Altamura, D.; Pfister, V.; Re, M.; Signore, M. A.; Antisari, M. V., Quantitative EDS analysis in transmission electron microscopy using unconventional reference materials. *IOP Conference Series: Materials Science and Engineering* **2010,** *7* (1), 012020.

4.   Lemonnier, M.; Collet, O.; Depautex, C.; Esteva, J.-M.; Raoux, D., High vacuum two crystal soft X-ray monochromator. *Nuclear Instruments and Methods* **1978,** *152* (1), 109-111.

5.   Rubey, W. A.; Grant, R. A., Design aspects of a modular instrumentation system for thermal diagnostic studies. *Review of Scientific Instruments* **1988,** *59* (2), 265-269.

6.   Wehrmeier, A.; Lenoir, D.; Sidhu, S. S.; Taylor, P. H.; Rubey, W. A.; Kettrup, A.; Dellinger, B., Role of Copper Species in Chlorination and Condensation Reactions of Acetylene. *Environmental Science & Technology* **1998,** *32* (18), 2741-2748.

CHAPTER 3: SYNTHESIS OF NiO, CuO, AND NiO-CuO NANOPARTICLES SUPPORTED ON SILICA

Metal-oxide nanoparticles were prepared in methanol, using three different methods, namely, wetness impregnation of metal-dendrimer complexes (WI-D), wetness impregnation of metal ion solutions (WI-M), and incipient wetness impregnation (IWI). NiO, CuO, and NiO-CuO nanoparticles were prepared by both WI-D[1] and WI-M methods in methanol so as to yield mixed NiO-CuO nanoparticles of varying Ni:Cu molar ratios (1:1, 1:3, 1:10, 10:1, and 3:1). Nanoparticle size and size dispersity were obtained by obtaining TEM images of each sample produced using the given experimental conditions. IWI is a well-documented method for preparing metal-based catalysts on substrates in aqueous media.[2-4] Nanoparticles such as, Fe_2O_3,[5-6] CuO,[7-8] and NiO[9] were previously prepared on silica by this method. However, these reports lack TEM data to support the formation of nanoparticles on silica when starting with aqueous metal-nitrate solutions, an issue which has motivated this study to prepare NiO/silica nanoparticles in aqueous media in addition to the ones prepared in methanol.

3.1 Materials

Generation-3 Poly(propyleneimine) dendrimer , $Ni(NO_3)_2 \cdot 6H_2O$ (99.999%) and $Cu(NO_3)_2 \cdot XH_2O$ (99.999%) were purchased from Sigma-Aldrich Co. LLC, St. Louis, MO. Pesticide-grade methanol was purchased from MACRON Chemicals, Phillipsburg, NJ. Silica (SiO_2, Cab-O-Sil, particle size < 1 μm, surface area = 380 m^2g^{-1}) was donated by Cabot Corporation, Boston, MA. Indium foil (99.99% pure, 0.5mm thickness) was purchased from Refining Systems Inc., Las Vegas, NV. Formvar holey carbon-coated gold TEM grids (400 mesh) were purchased from Structure Probe Inc., West Chester, PA. Ultra-thin Formvar holey carbon-coated gold TEM grids (300 mesh) were purchased from Ted Pella Inc., Redding, CA. All chemicals and materials were used as received without further purification.

3.2 Wetness impregnation of metal-dendrimer complexes (WI-D)

3.2.1 Preparation of solutions

Solutions of Ni(II) and Cu(II) for the WI-D method were prepared by dissolving Ni(NO$_3$)$_2 \cdot 6$H$_2$O and Cu(NO$_3$)$_2 \cdot X$H$_2$O in methanol. The concentrations of Ni(II) and Cu(II) stock solutions were determined using atomic absorption spectroscopy (see appendix), and they were found to be 1.09×10^{-2} ($\pm 0.01 \times 10^{-2}$) M and 1.02×10^{-2} ($\pm 0.03 \times 10^{-2}$) M, respectively. Poly(propylene imine) dendrimer (Generation-3) solutions were prepared in methanol (2.00×10^{-2} M with respect to terminal amino groups). The stoichiometric amount of metal species was added to silica for each time to achieve 5% weight coverage of metal oxide on silica surfaces after calcination.

3.2.2 Preparation method

Generation-3 poly(propylene imine) dendrimer, DAB-Am$_{16}$, consists of a 1,4-diaminobutane (DAB) core with extending propylene imine units.[1, 10-11] Coordination of Cu(II) and Ni(II) ions to DAB-Am$_{16}$ occurs via two terminal amino groups and one tertiary amino group of the dipropylenetriamine (dpt) subunits of the dendrimer periphery as depicted in Scheme 3.1.[12-14] With DAB-Am$_{16}$ containing 16 terminal amino groups (Am), the maximum number of metal ions binding to DAB-Am$_{16}$ is 8, and this metal ion-dendrimer complex is denoted as DAB-Am$_{16}$–M(II)$_8$, where M = Ni or Cu.

The DAB-Am$_{16}$–Ni(II)$_8$ complex was prepared by adding equal volumes of Ni(NO$_3$)$_2$ and DAB-Am$_{16}$. The DAB-Am$_{16}$–Ni(II)$_8$ aliquot was transferred to a round-bottom flask containing silica and stirred every 10 min for 1 h. The solvent was removed by rotary evaporation, which leads the DAB-Am$_{16}$–Ni(II)$_8$ complexes to impregnate on silica. Subsequent calcination at 500 °C for 5 h in breathing air (20% O$_2$ + 80% N$_2$) degraded the DAB-Am$_{16}$ dendrimer to CO, CO$_2$,

37

and NO_x, while the resulting NiO nanoparticles remained on silica.[1] CuO nanoparticles were prepared from $Cu(NO_3)_2$ using a similar procedure. Mixed NiO-CuO nanoparticles having different Ni:Cu molar ratios (1:1, 1:3, 1:10, 10:1, and 3:1) were synthesized by altering the amounts of $Ni(NO_3)_2$ and $Cu(NO_3)_2$ in solution. A procedure similar to the preparation of NiO nanoparticles was followed to prepare mixed NiO-CuO nanoparticles on silica.
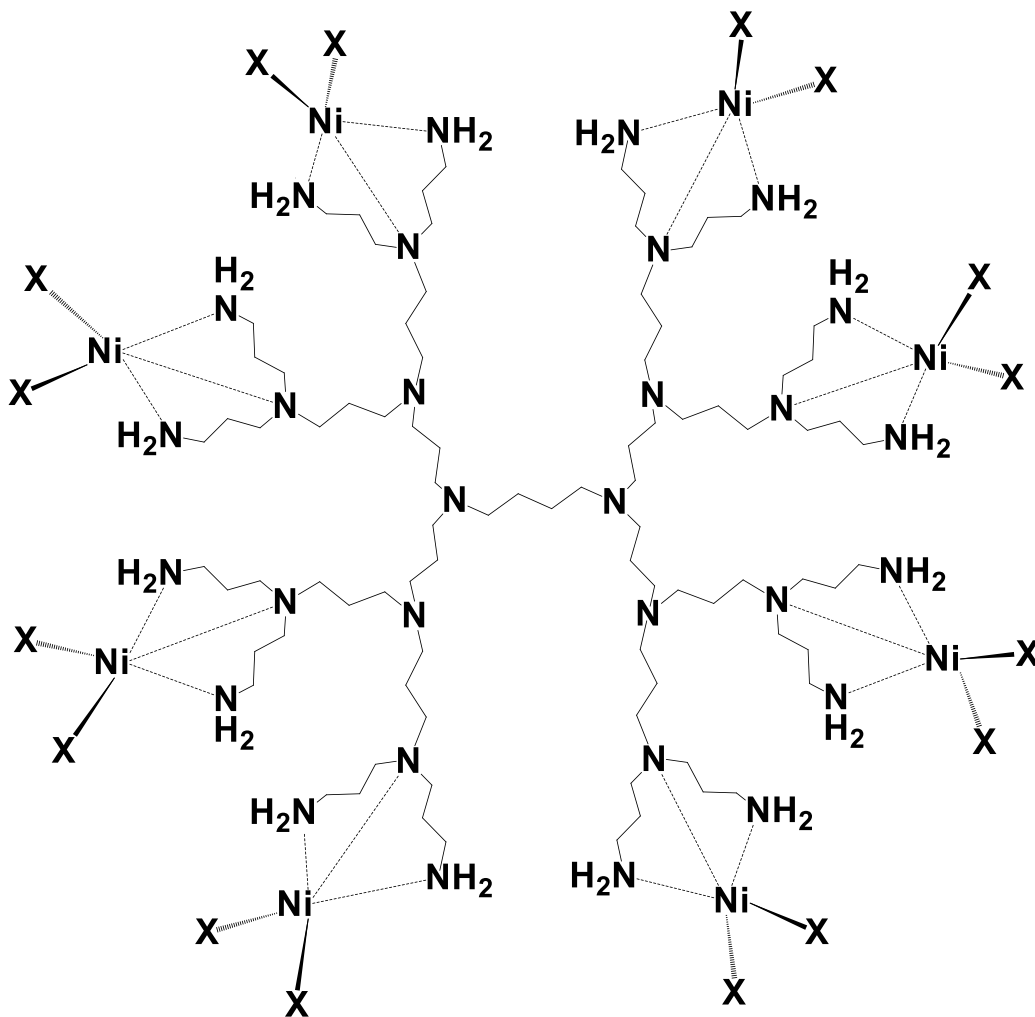
Scheme 3.1 Schematic depiction of DAB-Am$_{16}$-Ni(II)$_8$ complex with an oxygen-containing ligand (X).

3.2.3 Thermogravimetric analysis (TGA) of metal-dendrimer complexes

Metal-dendrimer complexes were analyzed by TGA (2950 TGA, TA Instruments New Castle, DE) to determine the best calcination temperature to remove the dendrimer from the

38

silica surface. Poly(propylene imine) dendrimers are known for their high thermal stability; for example, generation-4 poly(propylene imine) dendrimer, DAB-Am$_{32}$, was reported to be stable to as high as 470 ℃.[15] The TGA curve for silica displayed the loss of surface-bound water above 200 ℃ (Figure 3.1). However, DAB-Am$_{16}$–Ni(II)$_8$/silica, DAB-Am$_{16}$–Cu(II)$_8$/silica, and DAB-Am$_{16}$–Ni(II)$_4$–Cu(II)$_4$/silica complexes displayed identical TGA curves with larger weight loss. The weight loss observed between 200 ℃ and 400 ℃ was the loss of surface-bound water followed by the degradation of the dendrimer. Therefore, a temperature higher than 400 ℃ was required for the removal of generation-3 poly(propylene imine) dendrimer, DAB-Am$_{16}$. Hence, calcination was carried out at 500 ℃ for all the samples prepared during this study.
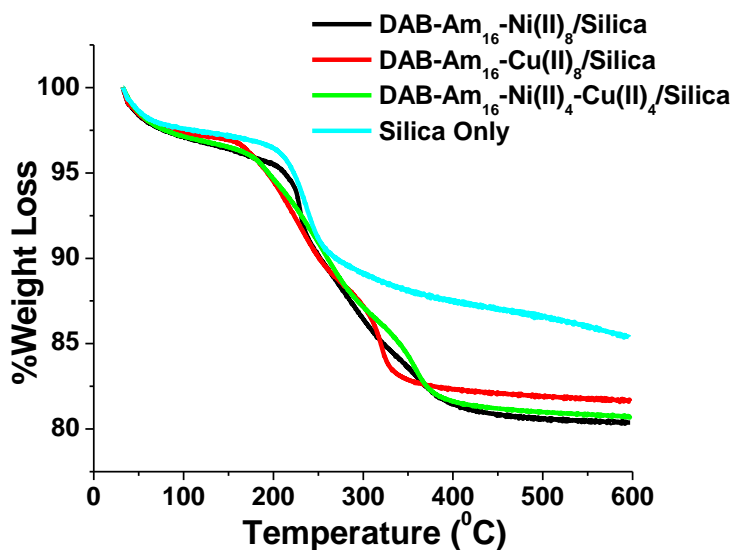
Figure 3.1 TGA curves for DAB-Am$_{16}$–Ni(II)$_8$/silica, DAB-Am$_{16}$–Cu(II)$_8$/silica, DAB-Am$_{16}$–Ni(II)$_4$–Cu(II)$_4$/silica, and silica from 25 °C to 600 °C in breathing air (20%.O$_2$ + 80% N$_2$).

3.2.4 X-ray photoelectron spectroscopy (XPS) studies

NiO/silica nanoparticles prepared by the WI-D method were examined by XPS to determine the changes occurring throughout calcination (500 ℃ for 5 h). High-resolution X-ray photoelectron spectra in the N 1s region were obtained before and after calcination of the

39

nanoparticles to probe for the presence of DAB-Am$_{16}$ on the silica surface. The N 1s peak was observed at 399.3 eV before sample calcination, indicating the presence of DAB-Am$_{16}$ on the silica surface (Figure 3.2A). However, the N 1s was virtually undetectable after calcination of the samples, indicating the removal of DAB-Am$_{16}$ at 500 ºC for 5 h.

NiO is a charge-transfer oxide possessing a mixture of three ground state configurations known as 3d^8, 3d^{9}L, and 3d^{10}L^2 (L denotes a hole in the ligand band).[16-18] Hence, high-resolution X-ray photoelectron spectra of the Ni 2p region possess three peaks: the Ni 2p$_{3/2}$ main line (c3d^{9}L); the Ni 2p$_{3/2}$ charge-transfer satellite (c3d^{10}L^2) (c stands for hole in the Ni 2p core level); and a Ni 2p$_{1/2}$ peak. Thus, high-resolution X-ray photoelectron spectra in the Ni 2p region of the NiO/silica nanoparticles prepared by the WI-D method exhibited three peaks before and after the calcination (Figure 3.2B), corresponding to the main 2p$_{3/2}$ and its satellite, and the 2p$_{1/2}$, in agreement with a material having Ni-O bonds.[16-20] The Ni 2p$_{3/2}$ main peak at 854.7 eV and the Ni 2p$_{1/2}$ peak at 872.4 eV were observed in samples prior to calcination; the 2p$_{3/2}$ and the 2p$_{1/2}$ peaks are at higher values of 855.3 eV and 873.2 eV, respectively, after calcination. The shifts of the main Ni 2p$_{3/2}$ and the Ni 2p$_{1/2}$ transitions to higher binding energies upon sample calcination (Figure 3.2B) indicate possible changes in the ligands associated with Ni(II) on the silica surface.[19-21]

The hydroxylated silica surface was previously demonstrated to act as a cation exchanger, where protons are substituted by metal ions.[22-23] Thus, transition metal ions, such as Ni(II) and Cu(II), can readily bind to the silica surface by coordination with surface silanol (Si–OH) groups forming Si–OH–M(II).[22, 24-25] Previous research in our group has suggested that the DAB–Am$_{16}$–M(II)$_8$ in methanol has the M(II) bound to two terminal amino groups, one tertiary amino group, and two oxygen-containing ligands as demonstrated for Ni(II) and Cu(II)

dendrimer complexes in methanol.[12-13] Therefore, I hypothesized the DAB–Am$_{16}$–Ni(II)$_8$ complex is chemisorbed to the silica surface via –OH groups through coordination of Ni(II) as a result of replacing two oxygen containing ligands (X) as displayed in Scheme 3.2. High-resolution X-ray photoelectron spectra of the Ni 2p region of the NiO/silica nanoparticles prepared by the WI-D method before calcination suggested the presence of Ni-O species on the silica surface (Figure 3.2B).[20] This suggests the binding of DAB–Am$_{16}$–Ni(II)$_8$ complex to the silica surface via surface –OH groups as depicted in Scheme 3.2A.
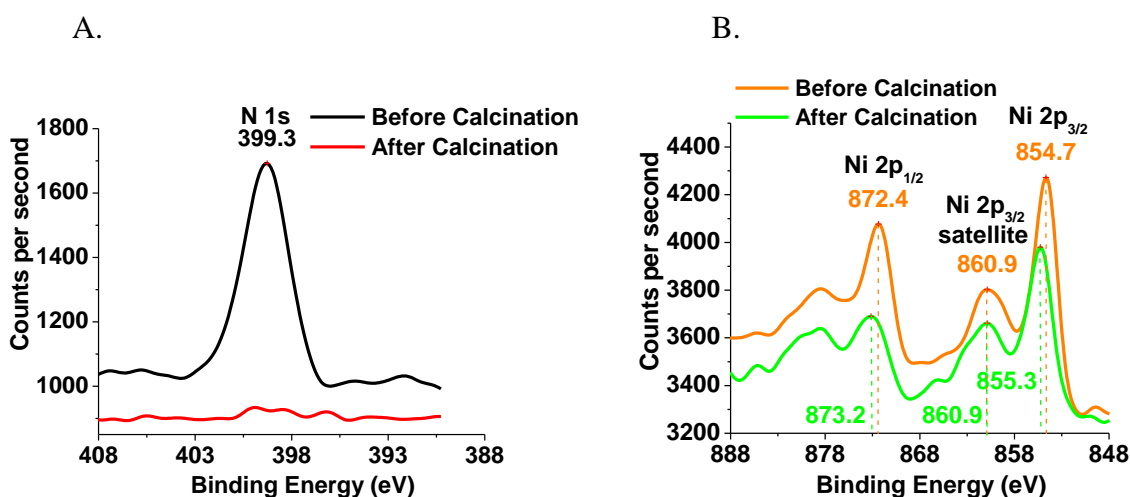
Figure 3.2 Representative high-resolution X-ray photoelectron spectra for NiO/silica (prepared by the WI-D method) before and after calcination at 500 ºC for 5 h; A. N 1s and B. Ni 2p regions.

Results similar to NiO/silica were observed after calcination for CuO/silica. The N 1s peak was observed at 399.2 eV before sample calcination, indicating the presence of DAB-Am$_{16}$ on the silica surface (Figure 3.3A). However, the N 1s was virtually undetectable after calcination of the samples, indicating the removal of DAB-Am$_{16}$ at 500 ºC, which was previously proved for DAB-Am$_{16}$–Cu(II)$_8$.[1] Cu 2p$_{3/2}$ and Cu 2p$_{1/2}$ peaks shifted to higher binding energy, similar to that of Ni, indicating changes on the surface (Figure 3.3B). Both Ni and Cu

41

were observed on the surface of NiO-CuO(1:1)/silica samples, following a similar trend to NiO/silica and CuO/silica before and after calcination (Figure 3.4). Thus, NiO, CuO, and NiO-CuO particles are proven to form by calcination of DAB-Am$_{16}$–M(II)$_8$ on silica surface.

A.   B.
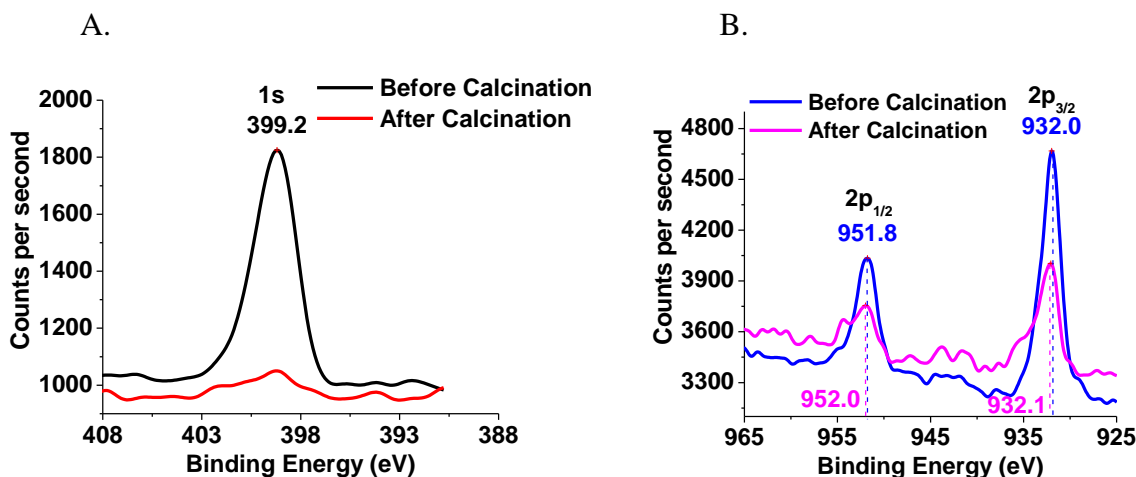
Figure 3.3 Representative high-resolution X-ray photoelectron spectra for CuO supported on silica (prepared by the WI-D method) before and after calcination at 500 °C for 5 h; A. N 1s and B. Cu 2p regions.

A.   B.
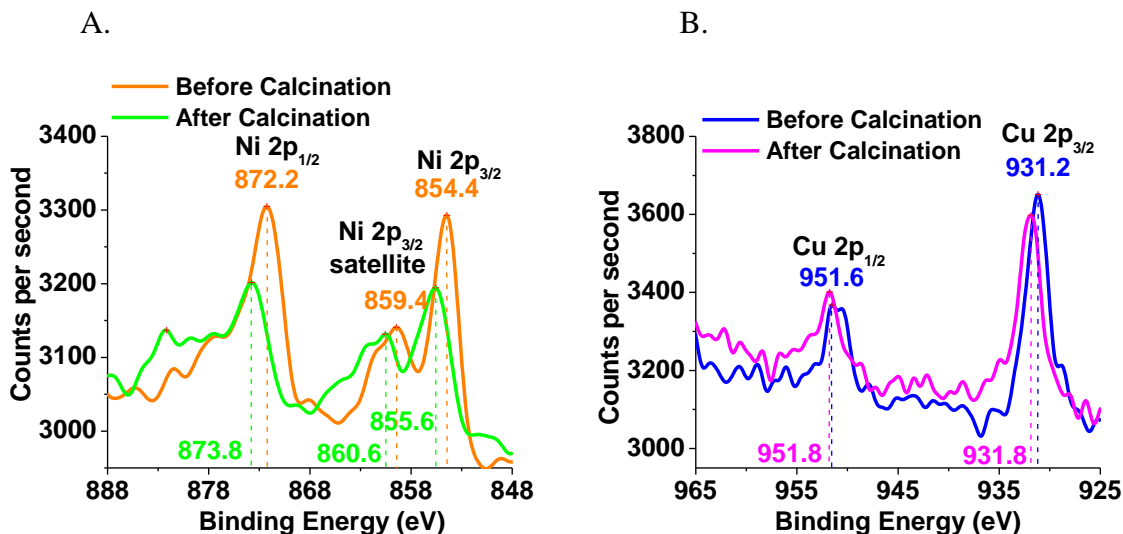
Figure 3.4 Representative high-resolution X-ray photoelectron spectra for NiO-CuO (1:1) supported on silica (prepared by the WI-D method) before and after calcination at 500 °C for 5 h; A. Ni 2p and B. Cu 2p regions.

42
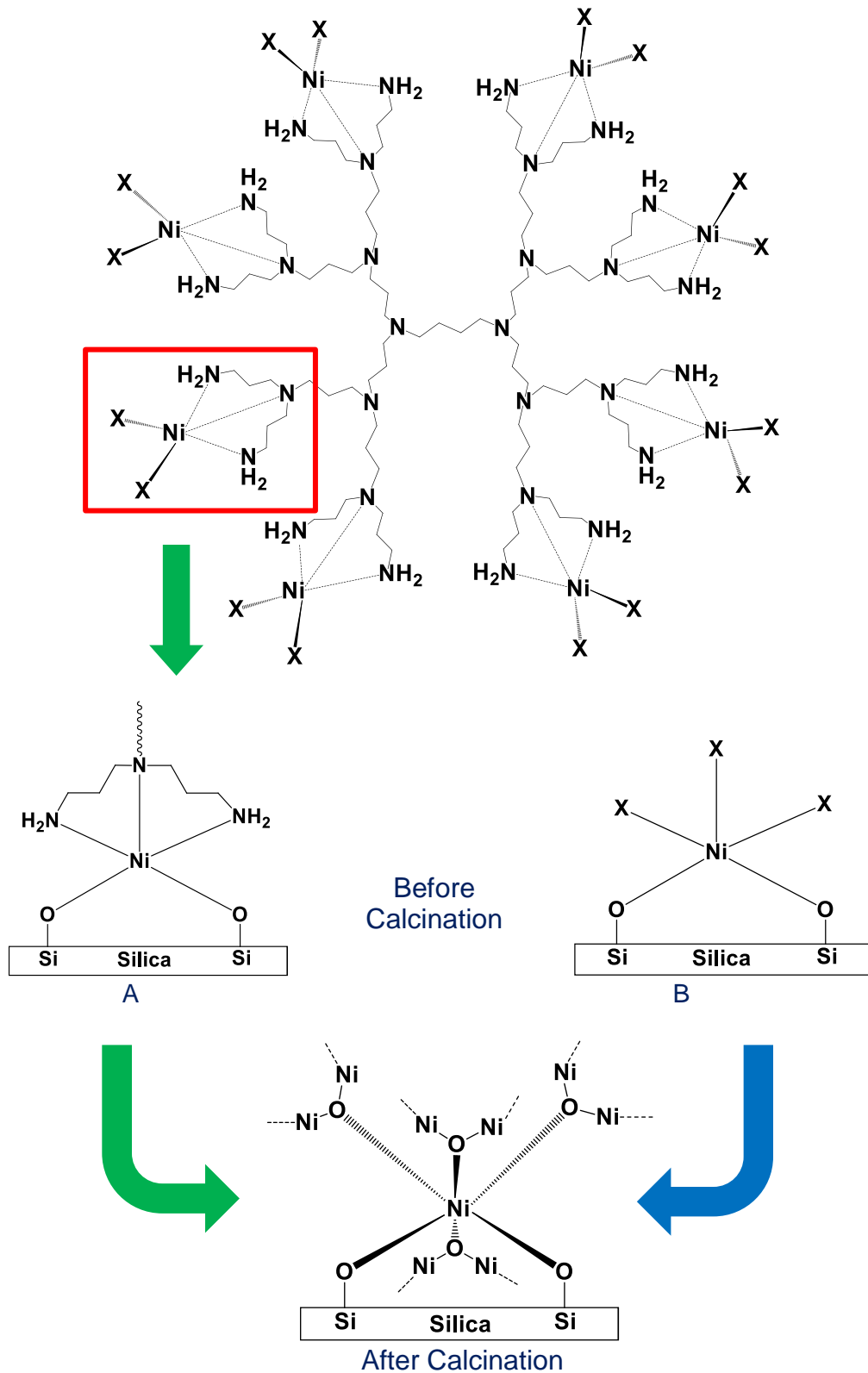
Scheme 3.2 The chemisorption of A. DAB–Am$_{16}$–Ni(II)$_8$ complex on silica and B. Ni(X)$_3$ complex, with subsequent NiO/silica structure after calcination. X = oxygen-containing ligand (nitrate ions or methanol).

43

3.2.5 X-ray absorption spectroscopy (XAS) studies (XANES and EXAFS)

The effect of calcination on DAB–Am$_{16}$–Ni(II)$_8$ and DAB–Am$_{16}$–Cu(II)$_8$ complexes on silica was further studied by XANES and EXAFS. Analysis of XANES at the Ni and Cu K absorption edges (Figure 3.5) yielded values very close to those of reagent grade (RG) NiO and CuO. Thus, all the silica-supported metal-dendrimer complexes, before and after calcination, were comprised of Ni and Cu with +2 oxidation state.
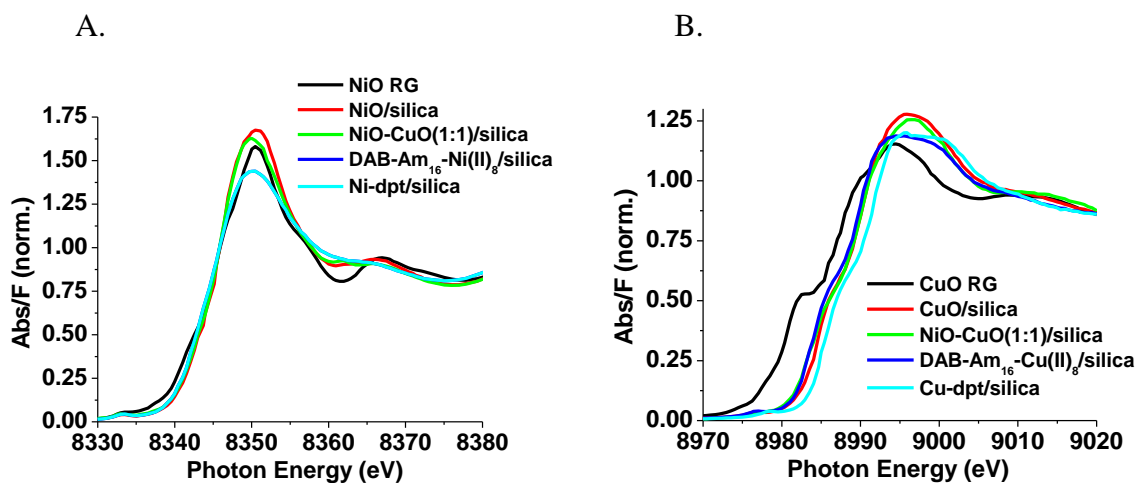
Figure 3.5 A. Normalized spectra at: A. Ni K edge for NiO RG (reagent grade), NiO/silica, NiO-CuO(1:1)/silica, DAB−Am$_{16}$–Ni(II)$_8$/silica, and Ni-dpt/silica; and B. Cu K edge for CuO RG, CuO/silica, NiO-CuO(1:1)/silica, DAB−Am$_{16}$–Cu(II)$_8$/silica, and Cu-dpt/silica.

EXAFS fittings were conducted to determine the coordination number and bond distances of DAB–Am$_{16}$–Ni(II)$_8$ and DAB–Am$_{16}$–Cu(II)$_8$ complexes on silica. EXAFS fitting parameters for Ni are listed in Table 3.1, and those for Cu are listed in Table 3.2. The amplitude reduction factor, (S_0^2) for Ni compounds was obtained from the fitting of RG NiO ($S_0^2 = 0.94$), and used for all subsequent fits. The same edge shift (E_0) was used for all the paths (both first shell and the second shell) in NiO/silica, NiO-CuO(1:1)/silica, and Ni-dpt/silica. But using different E_0 for different paths in DAB-Am$_{16}$-Ni(II)$_8$/silica improved the fitting. The total number of O and N atoms in the first shell was set to five (three N atoms and two O atoms) for

44

the fit of the DAB-Am$_{16}$-Ni(II)$_8$/silica data, based on modeling assumptions (Scheme 3.2A). Varying the number of O and N atoms in the first shell, while keeping the total number of atoms fixed at five, lead to an even slightly lower bond distance (R) and improves the fitting drastically. The correlation of < 90% was achieved with the number of N atoms fixed at three and number of O atoms fixed at 2. Keeping a fixed number of Si and Ni atoms in the subsequent shells improved the fit quality significantly. RG CuO was used for the fittings of Cu compounds.

Fourier transforms of the EXAFS spectra for Ni species are displayed in Figure 3.6A, and their fitting parameters are listed in Table 3.1. The data for the RG NiO led to a Ni-O bond distance of 2.07 ± 0.01 Å with six O atoms in the first coordination shell; the Ni-Ni bond distance was determined to be 2.94 ± 0.01 Å, with twelve Ni atoms in the second coordination shell.[16, 26] Assessment of the data of NiO/silica (after calcination) indicated similarities in bond distances to that of RG NiO, with a Ni-O bond distance of 2.01 ± 0.01 Å (4.22 ± 0.59 number of O atoms in the first coordination shell) and Ni-Ni bond distance of 3.05 ± 0.01 Å (8.06 ± 2.70 number of Ni atoms in the second coordination shell). The determination of the Ni-Ni bond distance in the second coordination shell indicates long range order in NiO particles formed on the silica surface. These results also support the high-resolution X-ray photoelectron spectroscopy data (Figure 3.2) and confirm the removal of dendrimer, as well as the conversion of DAB-Am$_{16}$-Ni(II)$_8$/silica to NiO/silica upon calcination.

Analysis of EXAFS data for silica-supported mixed metal oxides of NiO-CuO in a 1:1 Ni:Cu ratio yielded a Ni-O/Cu-O bond distance of 2.05 ± 0.01 Å for an environment of six O atoms in the first coordination shell. The second coordination shell consisted of 4.48 ± 0.49 Ni/Cu atoms with a bond distance of 2.98 ± 0.01 Å indicating long range ordered structure

45

within particles. Due to their proximity in the periodic table, differentiating between Ni and Cu is difficult in EXAFS.

A.

B.
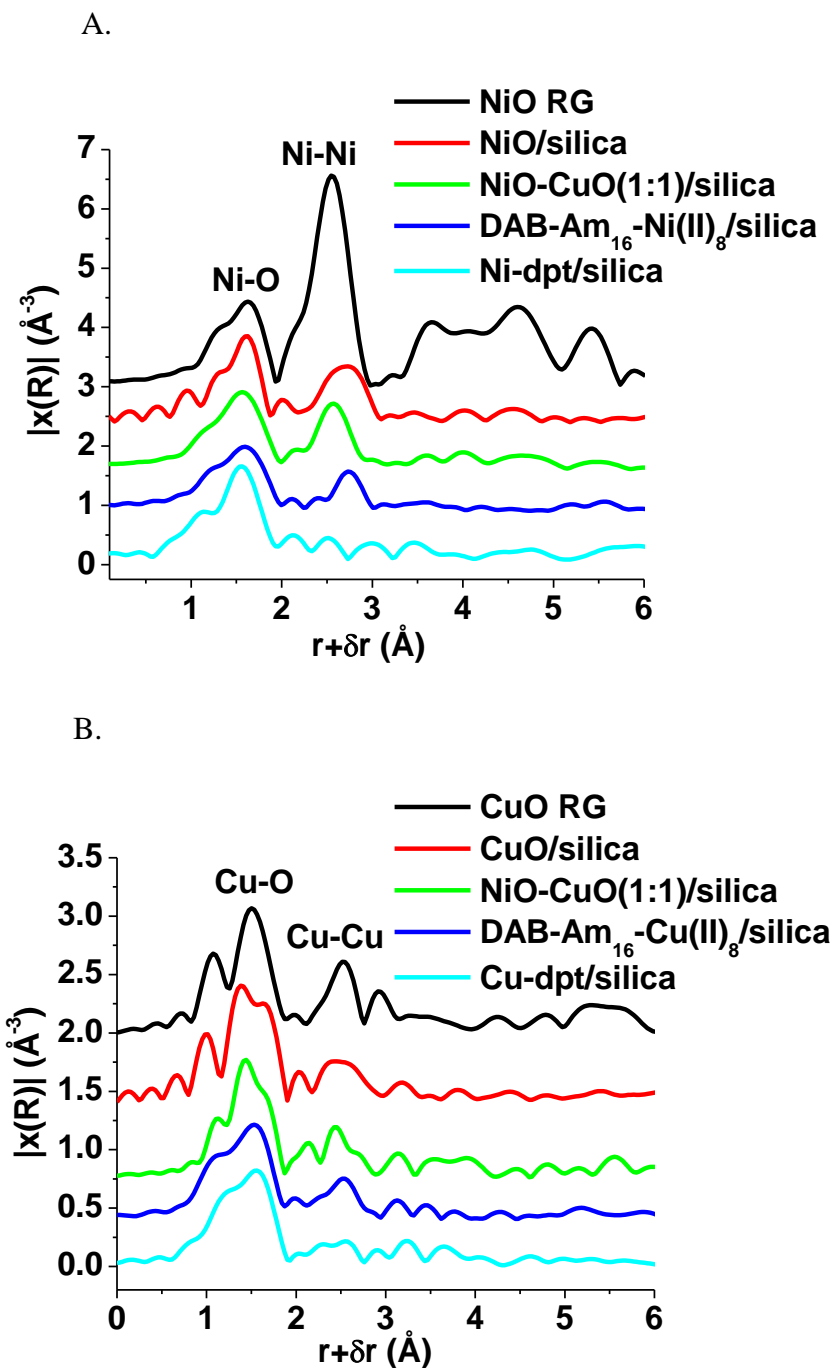
Figure 3.6 Fourier transforms of the EXAFS function for silica-supported metal-dendrimer complexes before and after calcination: A. NiO RG (reagent grade), NiO/silica, NiO-CuO(1:1)/silica, DAB−Am$_{16}$−Ni(II)$_8$/silica, and Ni-dpt/silica; B. CuO RG, CuO/silica, NiO-CuO(1:1)/silica, DAB−Am$_{16}$−Cu(II)$_8$/silica, and Cu-dpt/silica.

Table 3.1 EXAFS function of fitting parameters for Ni(II) compounds

Sample	Atom	N (Coordination)	σ^2 (Debye-Waller Factor)	R (Å) (Bond distance)	S_0^2 (Amplitude reduction factor)	E_0 (edge shift)	χ^2 (Reduced chi squared)
NiO reagent grade	O	6	0.007	2.07 ± 0.01	0.94	-1.91	0.011
	Ni	12	0.007	2.94 ± 0.01			
NiO/silica	O	4.22 ± 0.59	0.005	2.01 ± 0.01	0.94	-2.07	0.020
	Ni	8.06 ± 2.70	0.015	3.05 ± 0.01			
DAB-Am$_{16}$⁻ Ni(II)$_8$/silica	N	2.53 ± 0.52	0.004	2.00 ± 0.01	0.94	-2.03	0.005
	O	2.43 ± 0.48	0.004	2.09 ± 0.01			
	Si	2	0.004	2.91 ± 0.05		14.18	
	Ni	2	0.007	3.19 ± 0.03			
NiO-CuO(1:1) /silica	O	6	0.009	2.05 ± 0.01	0.94	-3.33	0.020
	Ni/Cu	4.48 ± 0.49	0.009	2.98 ± 0.01			
Ni-dpt/silica	O	6.47 ± 0.68	0.006	2.05 ± 0.01	0.94	-5.85	0.011
	Si	2	0.014	2.81 ± 0.01			

47

Table 3.2 EXAFS function of fitting parameters for Cu(II) compounds.

Sample	Atom	N (Coordination)	σ^2 (Debye-Waller Factor)	R (Å) (Bond distance)	S_0^2 (Amplitude reduction factor)	E_0 (edge shift)	$\chi 2$ (Reduced chi squared)
CuO reagent grade	O	2.84 ± 0.42	0.006	1.93 ± 0.02	0.90	4.13	0.012
	O	2	0.038	2.60 ± 0.09			
	Cu	4	0.009	2.89 ± 0.02			
	Cu	4	0.009	3.07 ± 0.02			
	Cu	2	0.009	3.16 ± 0.02			
CuO/silica	O	4.15 ± 0.90	0.005	1.94 ± 0.02	0.90	4.75	0.011
	O	2	0.022	2.35 ± 0.12		3.46	
	Cu	6	0.020	2.90 ± 0.09			
DAB-Am$_{16}$-Cu(II)$_8$/silica	O	2.97 ± 0.48	0.007	1.95 ± 0.01	0.90	-4.74	0.007
	O	2	0.038	2.77 ± 0.05		-5.33	
	Cu	1.39 ± 1.24	0.011	2.91 ± 0.05			
NiO-CuO(1:1) /silica	O	3.54 ± 0.01	0.003	1.96 ± 0.01	0.90	0.29	0.010
	O	2	0.004	2.86 ± 0.01		6.05	
	Cu	4	0.010	3.03 ± 0.04			
	Cu	4	0.010	3.21 ± 0.04			
	Cu	2	0.010	3.29 ± 0.04			
Cu-dpt/silica	O	2.68 ± 0.30	0.005	1.96 ± 0.01	0.90	-3.63	0.010
	O	2	0.011	2.94 ± 0.04			
	Si	0.73 ± 0.81	0.005	3.06 ± 0.09			

The total number of O and N in the first shell was fixed to five for DAB–Am$_{16}$–Ni(II)$_8$/silica, and the resulting data indicated 2.53 ± 0.52 atoms of N and 2.43 ± 0.48 atoms of O, with a Ni-N bond distance of 2.00 ± 0.01 Å and a Ni-O bond distance of 2.09 ± 0.01 Å. However, O and N are also indistinguishable in EXAFS due to their proximity in the periodic table;[12] thus, differentiation between amines groups of the dendrimer and –OH groups on the silica surface is difficult for DAB–Am$_{16}$–Ni(II)$_8$ impregnated on silica (Scheme 3.2A).

To gain further insight into the structure of the metal ion–dendrimer complexes on silica, the EXAFS spectra of Ni-dpt on silica were studied. The "dpt" ligand possesses two primary amine groups, one secondary amine group (Scheme 3.3A), and is a good model of the terminal amino groups of DAB-Am$_{16}$. Upon examination of the EXAFS of Ni-dpt/silica complex, 6.47 ± 0.68 atoms of O in the first coordination shell were observed with the Ni-O bond distance being 2.05 ± 0.01 Å, which is similar to Ni-O bond distance recorded for DAB–Am$_{16}$–Ni(II)$_8$ (2.09 ± 0.01 Å). This value is also in agreement with previously recorded Ni-O bonds.[27] Thus, Ni-dpt complex is presumed to attach to silica surface via –OH groups (Scheme 3.3B). Based on all of these outcomes, we conclude the Ni(II) binds to DAB-Am$_{16}$ via two terminal amino groups and one tertiary amino group, and Ni(II) binds to the silica through two silanol sites.[13] Unlike DAB–Am$_{16}$–Ni(II)$_8$, there was no apparent second coordination shell for the Ni-dpt/silica complex, indicating the absence of a long-range ordered structure in Ni-dpt/silica samples.

Fourier transforms of the EXAFS spectra for CuO/silica and its precursor compounds are displayed in Figure 3.6B; the fitting parameters are listed in Table 3.2. Analysis of EXAFS for CuO/silica yielded two different Cu-O bond distances, 1.94 ± 0.02 Å (4.15 ± 0.90 O atoms) and 2.35 ± 0.12 Å (fitting for two O atoms). The second shell consists of six Cu atoms with a Cu-Cu bond distance of 2.90 ± 0.09 Å (fitting for 6 Cu atoms). The Cu-Cu bond distance indicates that

49

these particles have a long range order similar to NiO/silica particles. The RG CuO also displayed similar bond distances (Cu-O = 1.93 ± 0.02 Å (2.84 ± 0.42 O atoms) and 2.60 ± 0.09 Å (fitting for two O atoms), Cu-Cu = 2.89 ± 0.02 Å (fitting for 4 Cu atoms)).[28-30] In addition, RG CuO possessed two other Cu-Cu bond distances (3.07 ± 0.02 Å and 3.16 ± 0.02 Å). Despite two additional Cu-Cu bond distances, most of the CuO/silica bond distances are in agreement with the RG CuO, confirming the presence of CuO on the silica support after calcination.
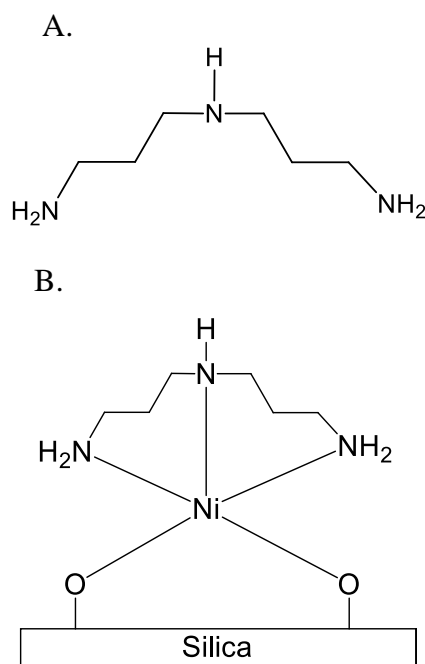
Scheme 3.3 A. Structure of dpt and B. Ni-dpt chemisorbed on silica.

The first shell of the DAB$-$Am$_{16}$$-$Cu(II)$_8$ complex contained Cu-O bonds with 1.95 ± 0.01 Å (2.97 ± 0.48 O atoms) and two Cu-O bonds with 2.77 ± 0.05 Å (fitting for two O atoms). The Cu-O bond distance of 1.95 ± 0.01 Å for the DAB$-$Am$_{16}$$-$Cu(II)$_8$ is in good agreement with the previously reported Cu-O bond distances for oxygen coordinated Cu(II) compounds,[12, 31] thus confirming the presence of Cu-O bonds. It is difficult to distinguish Cu-N from Cu-O due to the proximity of N and O in the periodic table. However, successful fitting of Cu-O bond distances supports the hypothesis that the DAB$-$Am$_{16}$$-$Cu(II)$_8$ complex binds to the silica surface via

surface –OH groups. The presence of Cu-Cu bond distance of 2.91 ± 0.05 Å (1.39 ± 1.24) indicates a long range ordered structure on silica. Evaluation of the EXAFS data for the Cu-dpt/silica model compound indicated two different Cu-O bond distances of 1.96 ± 0.01 Å (2.68 ± 0.30 O atoms) and 2.94 ± 0.04 Å (fitting for two O atoms), similar to those in DAB–Am$_{16}$–Cu(II)$_8$, but the lack of second coordination shell Cu-Cu distance indicates the absence of a long range ordered structure.

3.2.6 Transmission electron microscopy (TEM) studies of nanoparticles by the WI-D method

Based on the proposed interaction of the DAB–Am$_{16}$–M(II)$_8$ complex on silica and the resulting anchored metal-oxide nanoparticles, the MO/silica species were examined by TEM. A representative bright-field TEM image of NiO/silica nanoparticles after calcination at 500 °C for 5 h, and the corresponding size distribution histogram, are shown in Figure 3.7A and 3.7B, respectively. NiO/silica nanoparticles with low size dispersity (14%) and an average diameter 3.6 ± 0.5 nm (223 nanoparticles) were observed on the silica support. Similar results were obtained for CuO/silica nanoparticles with low size dispersity (11%) and an average diameter of 3.6 ± 0.4 nm (Figure 3.8). These sizes and dispersities for amorphous silica-supported NiO and CuO nanoparticles are unprecedented. We attribute the low size dispersity to the anchoring of the metal-oxide precursor and the metal-oxide species to the silica surface. Such anchoring would be expected to reduce mobility of the metal species, thereby leading to small nanoparticles with low size dispersity. Extended calcination time (24 h vs 5 h at 500 °C) leads to a slightly larger nanoparticle size (at 95% confidence interval), Figure 3.7C and 3.7D, indicative of a thermally activated process.[32] However, this small increase in NiO nanoparticle size points to a strong interaction of the nanoparticles with the silica surface, as noted by the outcomes for the EXAFS studies.

51

A.

B.

5 h, 500 °C calcination
d = 3.6 ± 0.5 nm
Population = 223

C.

D.

24 h, 500 °C calcination
d = 4.3 ± 0.4 nm
Population = 114

Figure 3.7 Representative bright-field TEM images and corresponding nanoparticle size distributions for silica-supported NiO nanoparticles prepared using the WI-D method with calcination at 500 °C for 5 h (A and B) and 24 h (C and D).

5 h, 500 °C calcination
d = 3.6 ± 0.4 nm
Population = 233

Figure 3.8 Representative bright-field TEM image and corresponding nanoparticle size distribution of silica-supported CuO nanoparticles prepared using the WI-D method with calcination at 500 °C for 5 h.

52

NiO-CuO/silica nanoparticles with different Ni:Cu molar ratios (1:1, 1:3, 1:10, 10:1, and 3:1) were prepared using the WI-D method. NiO-CuO(1:1)/silica nanoparticles with a low size dispersity (11%) and an average diameter of 3.6 ± 0.4 nm were observed by TEM, as displayed in Figure 3.9. High-angle annular dark-field (HAADF) images of NiO-CuO/silica nanoparticles with different Ni:Cu ratio are displayed in Figure 3.10. The average diameter of the NiO-CuO/silica nanoparticles were not affected by their Ni:Cu composition as observed by HAADF images. Synthesis of mixed metal-oxide nanoparticles on silica with similar size and size dispersity to their monometallic counterparts was a great success in the preparation of surrogates to combustion-generated nanoparticles.

Figure 3.9 Representative bright-field TEM image and corresponding nanoparticle size distribution of silica-supported NiO-CuO (1:1) nanoparticles prepared using the WI-D method with calcination at 500 °C for 5 h.

Figure 3.10 High-angle annular dark-field (HAADF) image of silica-supported NiO-CuO (A. 1:1, B. 1:3, C. 1:1 D. 3:1) nanoparticles prepared using the WI-D method with calcination at 500 °C for 5 h.

3.2.7 Single-particle energy-dispersive X-ray spectroscopy (EDS) studies

Mixed NiO-CuO nanoparticles of various composition were analyzed using single-particle EDS to obtain the Ni:Cu composition in individual nanoparticles.[33-35] The representative single-particle energy-dispersive X-ray spectra obtained for NiO-CuO/silica nanoparticles with different Ni:Cu solution phase molar ratios (1:1, 1:3, 1:10, 10:1, and 3:1) are displayed in Figure 3.11. Both the Ni Kα line (7.5 KeV) and Cu Kα line (8.0 KeV) were routinely observed in spectra when the electron beam was focused on individual nanoparticles. No detectable Ni or Cu signal was found in bare silica regions or on the TEM grid, supporting the presence of metal species only within the nanoparticles. The integrated intensity of the Kα line for Ni and Cu was used to quantify the atomic % of Ni and Cu in individual mixed metal-oxide nanoparticles using

the Cliff-Lorimer method.[36-39] The average atomic % of Ni and Cu in NiO-CuO nanoparticles prepared with various Ni:Cu ratios in the starting solutions by the WI-D method is displayed in Table 3.3. The metal composition of the mixed metal-oxide nanoparticles follows roughly that of the solutions. These outcomes point to a fairly uniform binding of the DAB–Am$_{16}$–M(II)$_8$ species on the silica surface and the lack of any preferential accumulation of a given metal ion in the metal-oxide nanoparticles during the calcination process. In addition, based on the similar crystallographic habits of NiO and CuO,[40-43] it is expected that there would be a distribution of Ni(II) and Cu(II) in the nanoparticles that reflects the Ni(II):Cu(II) ratio on starting solutions.

Figure 3.11 Representative single-particle EDS for NiO-CuO nanoparticles supported on silica, prepared by the WI-D method; Ni:Cu molar ratio A. 1:1, B. 1:3, C. 1:10, and D. 10:1 (Si from silica support and Au from TEM grid).

55

Table 3.3 Average atomic % of Ni and Cu in mixed NiO-CuO nanoparticles obtained using various Ni:Cu molar ratios in solutions (WI-D method).

Solution Phase Ratio	Average Atomic % in Nanoparticles	
Ni:Cu	Ni	Cu
1:1	54.3 ± 4.8	45.7 ± 4.7
1:3	28.5 ± 3.4	71.5 ± 7.9
1:10	11.1 ± 2.1	88.9 ± 4.9
10:1	88.3 ± 8.6	11.7 ± 3.8
3:1	80.5 ± 4.5	19.5 ± 3.2

3.3 Wetness impregnation of metal ion solutions (WI-M)

3.3.1 Preparation of solutions

The standard Ni(II) and Cu(II) solutions prepared in section 3.2.1 were also used in this section for the WI-M method. The stoichiometric amount of metal species was added to silica each time to achieve 5% weight coverage of metal oxide on the silica surfaces after calcination.

3.3.2 Preparation method

An aliquot of the aforementioned standard solutions of $Ni(NO_3)_2$ was mixed with a similar volume of methanol, and was transferred to a round-bottom flask containing silica. The mixture was stirred every 10 min for 1 h, and the solvent was removed by rotary evaporation to impregnate $Ni(NO_3)_2$ on silica. Subsequent calcination at 500 °C for 5 h in breathing air (20% O_2 + 80% N_2) converted $Ni(NO_3)_2$ to NiO nanoparticles. CuO nanoparticles were prepared from the standard $Cu(NO_3)_2$ solutions using a similar procedure. The amounts of $Ni(NO_3)_2$ and $Cu(NO_3)_2$ were varied to obtain different Ni:Cu ratios in the mixed NiO-CuO nanoparticles prepared by the WI-M method.

56

3.3.3 Transmission electron microscopy (TEM) studies of nanoparticles by the WI-M method

NiO nanoparticles prepared by wetness impregnation of $Ni(NO_3)_2$ in methanol (WI-M) led to similar nanoparticle sizes to the ones prepared by WI-D. NiO/silica nanoparticles with low size dispersity (14%) and average diameter of 2.9 ± 0.4 nm (172 nanoparticles) were observed after calcination at 500 °C for 5 h (Figure 3.12); this value is statistically smaller (at 95% confidence interval) than the nanoparticles made using the WI-D method.
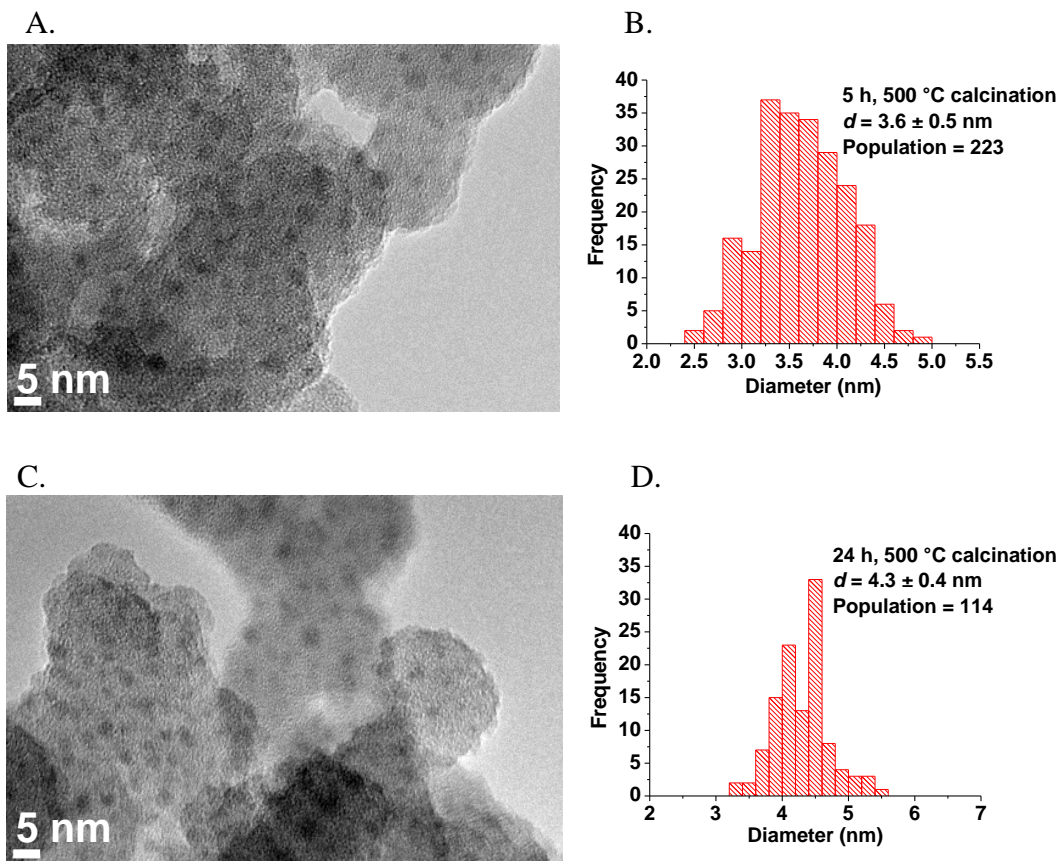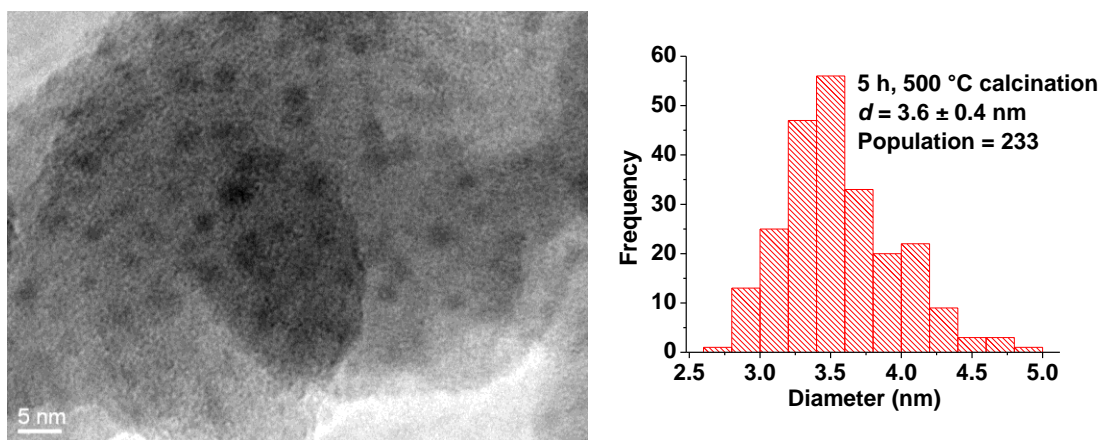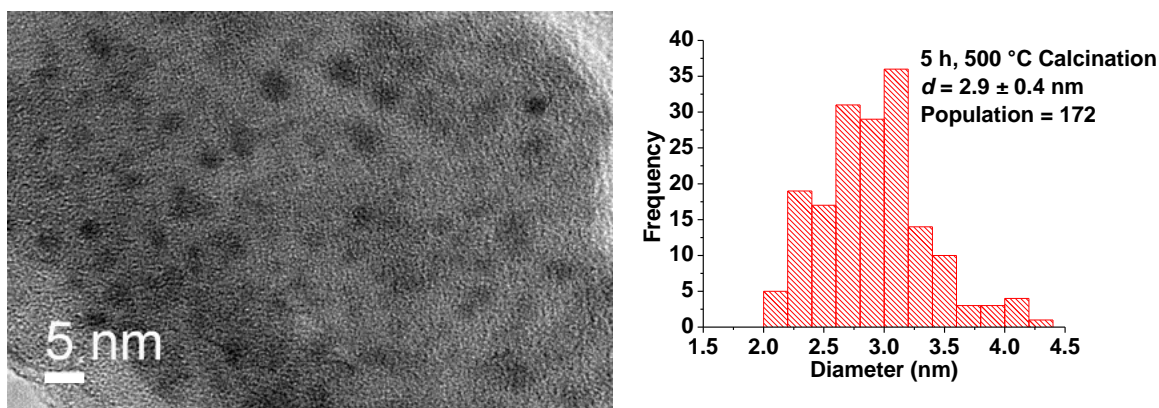

Figure 3.12 Representative bright-field TEM image and corresponding nanoparticle size distribution of silica-supported NiO nanoparticles prepared by the WI-M method with calcination at 500 °C for 5 h.

NiO-CuO/silica nanoparticles with different Ni:Cu molar ratios (1:1, 1:3, 1:10, 10:1, and 3:1) were also prepared using the WI-M method. NiO-CuO(1:1)/silica nanoparticles with low size dispersity (13%) and average diameter of 3.1 ± 0.4 nm were observed by TEM as displayed in Figure 3.13. TEM images of other mixed metal-oxide nanoparticles are displayed in Figure 3.14, and upon their examination, it is found that nanoparticles are produced with similar size and size dispersity regardless of the Ni:Cu ratio. The ability to prepare metal-oxide nanoparticles < 5 nm in diameter even without the dendrimer template is further support for my hypothesis that the metal ions are anchored to the silica surface via silanol groups (Si–OH),[22, 24] as discussed in

section 3.2.6. Binding of metal ions to the silica surface is proposed to limit their mobility on the surface, thus nanoparticles < 5 nm in diameter were resulted.
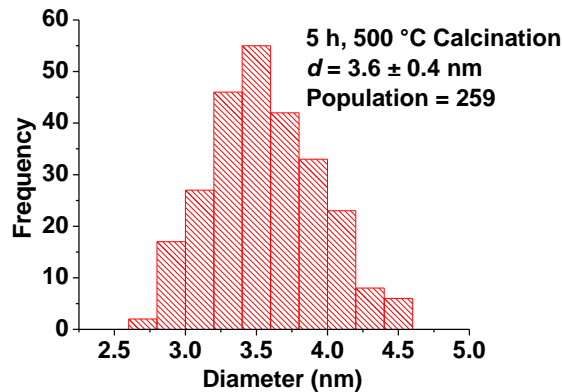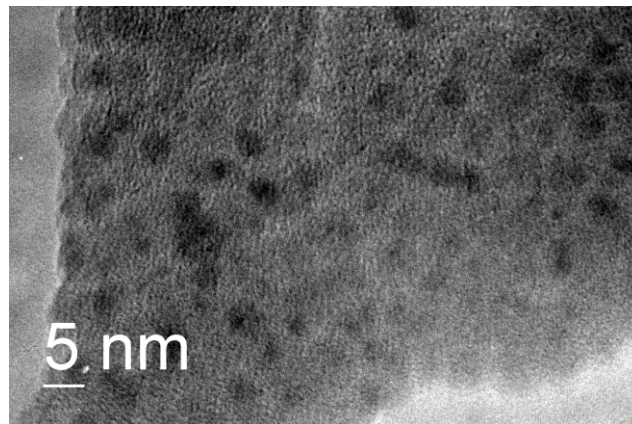

Figure 3.13 Representative bright-field TEM image and corresponding nanoparticle size distribution of silica-supported NiO-CuO (1:1) nanoparticles prepared using the WI-M method with calcination at 500 °C for 5 h.
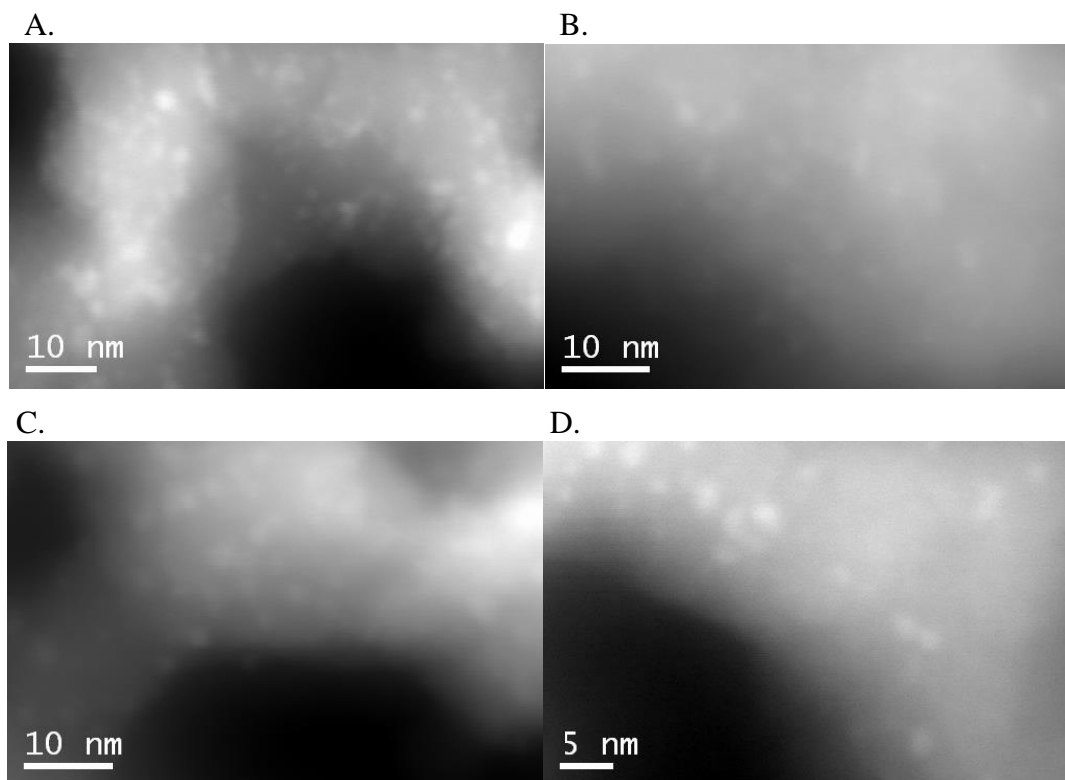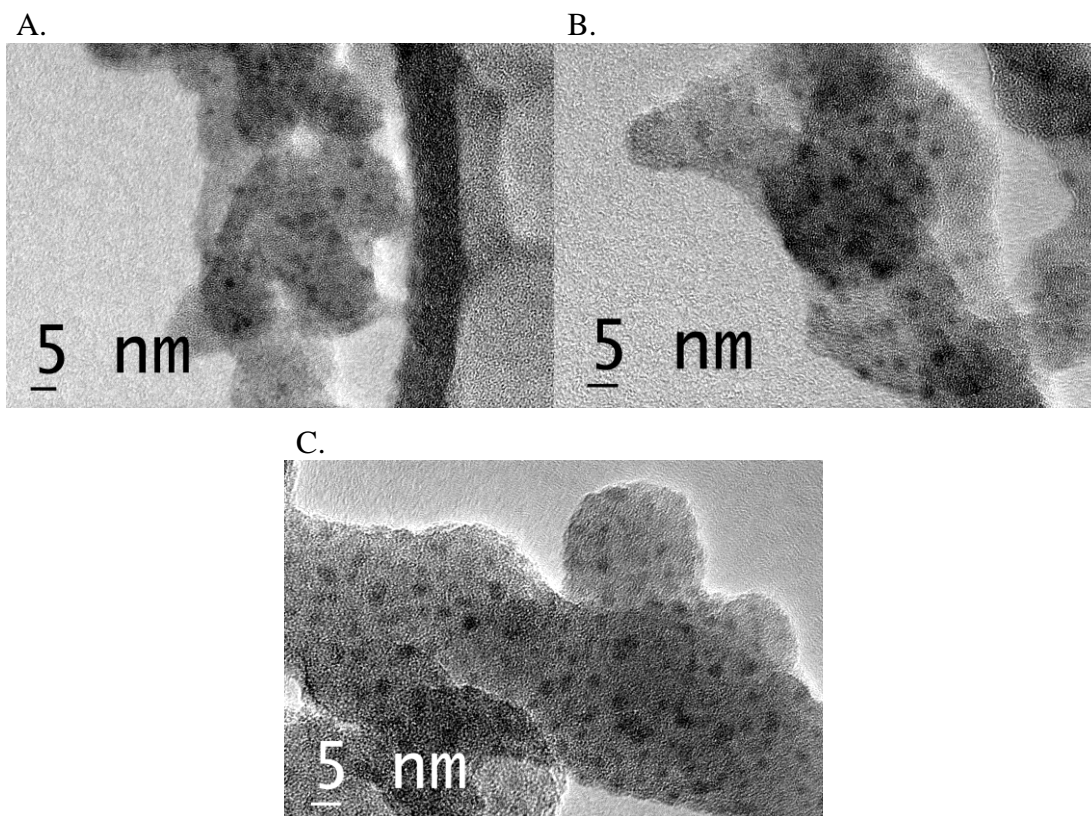

Figure 3.14 Representative TEM images of silica-supported NiO-CuO nanoparticles prepared using the WI-M method with different solution phase Ni:Cu molar ratios with calcination at 500 °C for 5 h. A. 1:3, B. 1:10, and C. 3:1.

3.3.4 Energy-dispersive X-ray spectroscopy (EDS) studies

Representative single-particle energy-dispersive X-ray spectra obtained for NiO-CuO/silica nanoparticles with different solution phase Ni:Cu molar ratios (1:1, 1:3, 1:10, 10:1, and 3:1) are displayed in Figure 3.15. Both the Ni $K\alpha$ line (7.5 KeV) and Cu $K\alpha$ line (8.0 KeV) were routinely observed in spectra when the electron beam was focused on individual nanoparticles. No detectable Ni or Cu signal was found in bare silica regions or on the TEM grid, supporting the presence of metal species only within the nanoparticles. The peak corresponding to the gold TEM grid (Au) was observed in some spectra, but it was, in most cases, overlapped with the large Si peak of the silica support.
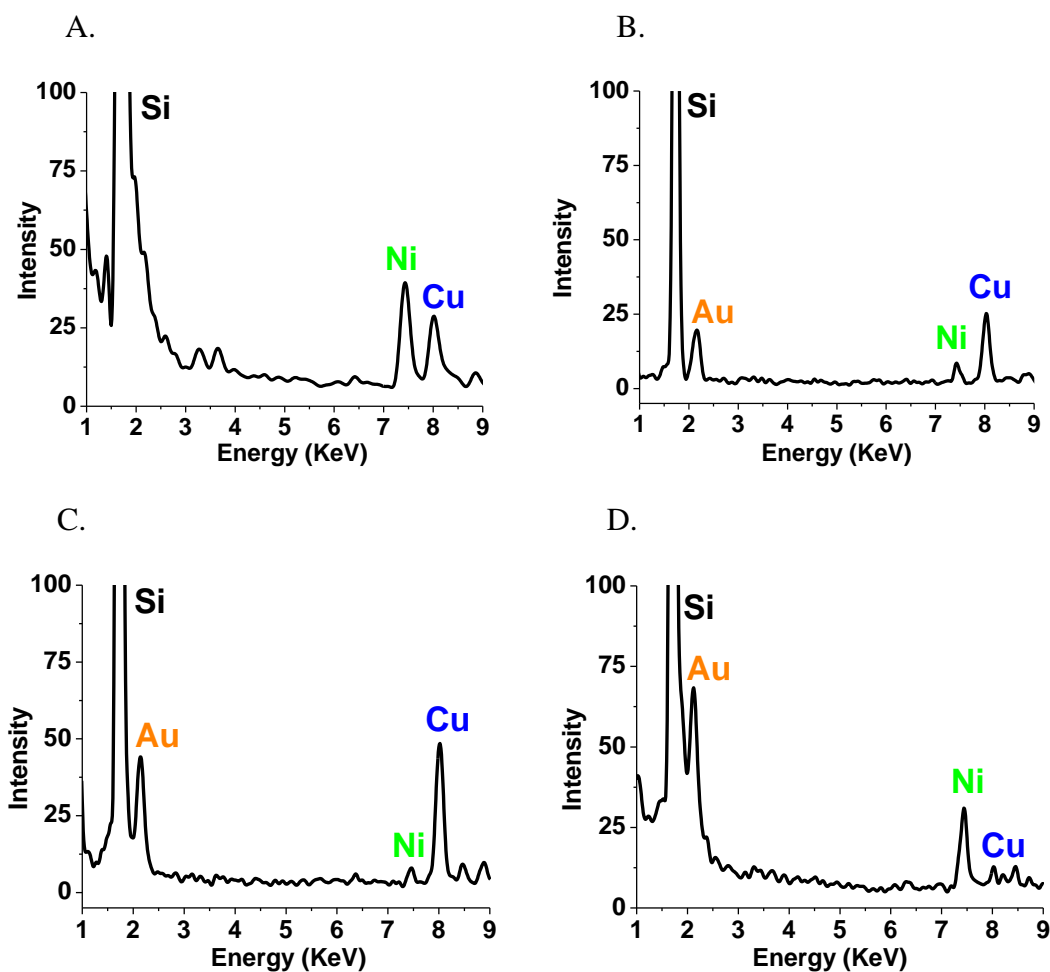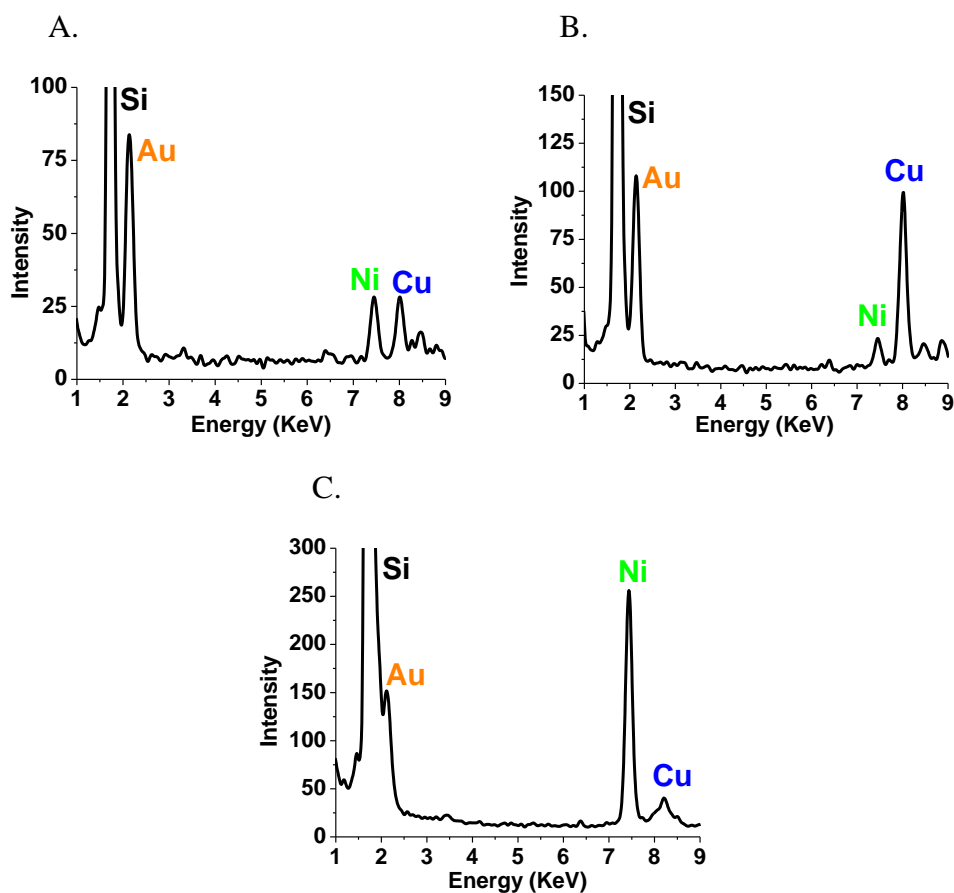
Figure 3.15 Representative single-particle EDS for NiO-CuO nanoparticles supported on silica, prepared by the WI-M method; Ni:Cu molar ratio A. 1:1, B. 1:10, and C. 10:1 (Si from silica support and Au from TEM grid).

59

The average atomic % of Ni and Cu in NiO-CuO nanoparticles prepared with various solution phase Ni:Cu molar ratios by the WI-M method is given in Table 3.4. The composition of the mixed metal-oxide nanoparticles follows roughly that of the solutions. These outcomes point to a fairly uniform binding of the M(II) species on the silica surface and the lack of any preferential accumulation of a given metal ion in the metal-oxide nanoparticles during the calcination process. The ability to manipulate Ni(II):Cu(II) ratio in NiO-CuO nanoparticles by changing the solution phase Ni:Cu molar ratio was a great success achieved in both the WI-D and the WI-M methods.

Table 3.4 Average atomic % of Ni and Cu in mixed NiO-CuO nanoparticles obtained using various Ni:Cu molar ratios in solutions (WI-M method).

Solution Phase Ratio	Average Atomic % in Nanoparticles	
Ni:Cu	Ni	Cu
1:1	53.4 ± 8.5	46.6 ± 5.5
1:3	29.2 ± 5.3	70.8 ± 7.6
1:10	12.2 ± 1.8	87.8 ± 5.4
10:1	90.8 ± 3.8	9.2 ± 1.5
3:1	78.7 ± 4.6	21.3 ± 3.9

3.4   Incipient wetness impregnation (IWI) with methanol and water solutions

3.4.1   Preparation method

Ni(NO$_3$)$_2$·6H$_2$O was dissolved in 3 mL of methanol and mixed thoroughly with 1.0 g of silica (Cab-O-Sil) for 10–15 min. Samples were dried in an oven at 120 °C in an atmospheric pressure for 12 h to remove the solvent, and then they were calcined at 500 °C for 5 h in breathing air (20% O$_2$ + 80% N$_2$). A similar procedure was followed for aqueous

$Ni(NO_3)_2 \cdot 6H_2O$ solutions. In both methods, the amount of Ni(II) in starting solutions was used so that NiO 5% weight coverage was achieved on silica after the calcination.

3.4.2 Effect of solvent and calcination time on the morphology of NiO/silica nanoparticles

NiO/silica nanoparticles prepared by the IWI in methanol possessed low size dispersity (11%) and an average diameter of 3.6 ± 0.4 nm (58 nanoparticles) after calcination at 500 °C for 5 h in breathing air (20% O_2 + 80% N_2). A representative TEM image and the size distribution histogram are displayed in Figures 3.16A and 3.16B. However, increasing the calcination time to 24 h resulted in NiO/silica nanoparticles with an average diameter of 4.6 ± 0.7 nm (111 nanoparticles) as shown in Figure 3.16C. Nanoparticles synthesized after calcination at 24 h were significantly larger (95% confidence interval) than those made after calcination at 5 h (Figure 3.16D). This suggested a thermally activated process where metal-oxide nanoparticles agglomerate to form larger nanoparticles when exposed to higher temperatures for longer periods of time.[32] However, an increment in such a small proportion (1 nm) indicated that the metal ions were bound to the silica via −OH groups on the surface. The strong interaction between Ni(II) and the surface −OH groups restrict the movement of metal ions on the silica surface and led to the formation of nanoparticles < 5nm in diameter.

A significant difference in NiO nanoparticle morphology was observed when water was used as the solvent in the IWI method. Hexagonal-shaped NiO nanoparticles with high size dispersity (29%) were observed by TEM (Figure 3.17A and 3.17B), and the average diameter was much larger compared to the methanol case, with particles having diameter of 49.1 ± 14.4 nm (Figure 3.18A) after calcination at 500 °C for 5 h. This may be due to the hydrolysis of silica surface by water[44] or the formation of $Ni(OH)_2$ in aqueous media.[45] However, nanoparticle size was not significantly affected by the calcination time (Figure 3.18B). Nanoparticles with an average diameter of 52.2 ± 14.0 nm were observed after 24 h calcination, as shown in Figure

61

3.17C and 3.17D. Calcination time was further increased to 48 h, and nanoparticles with an average diameter of 45.6 ± 13.8 nm (Figure 3.18C) were observed (Figure 3.17E and 3.17F). The sizes of these nanoparticles are not significantly different from those of the IWI-water nanoparticles prepared with 5 h and 24 h calcination times (at 95% confidence interval).

A.

B.

C.

D.
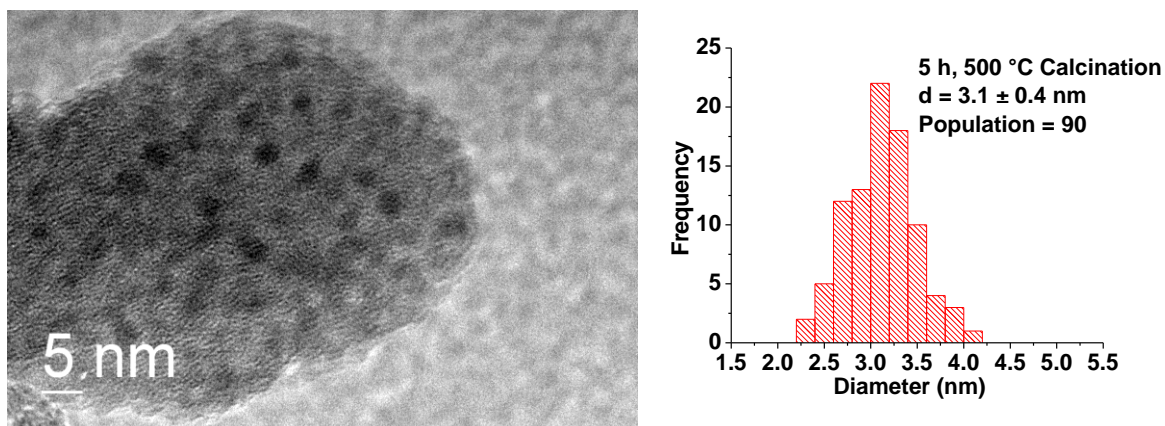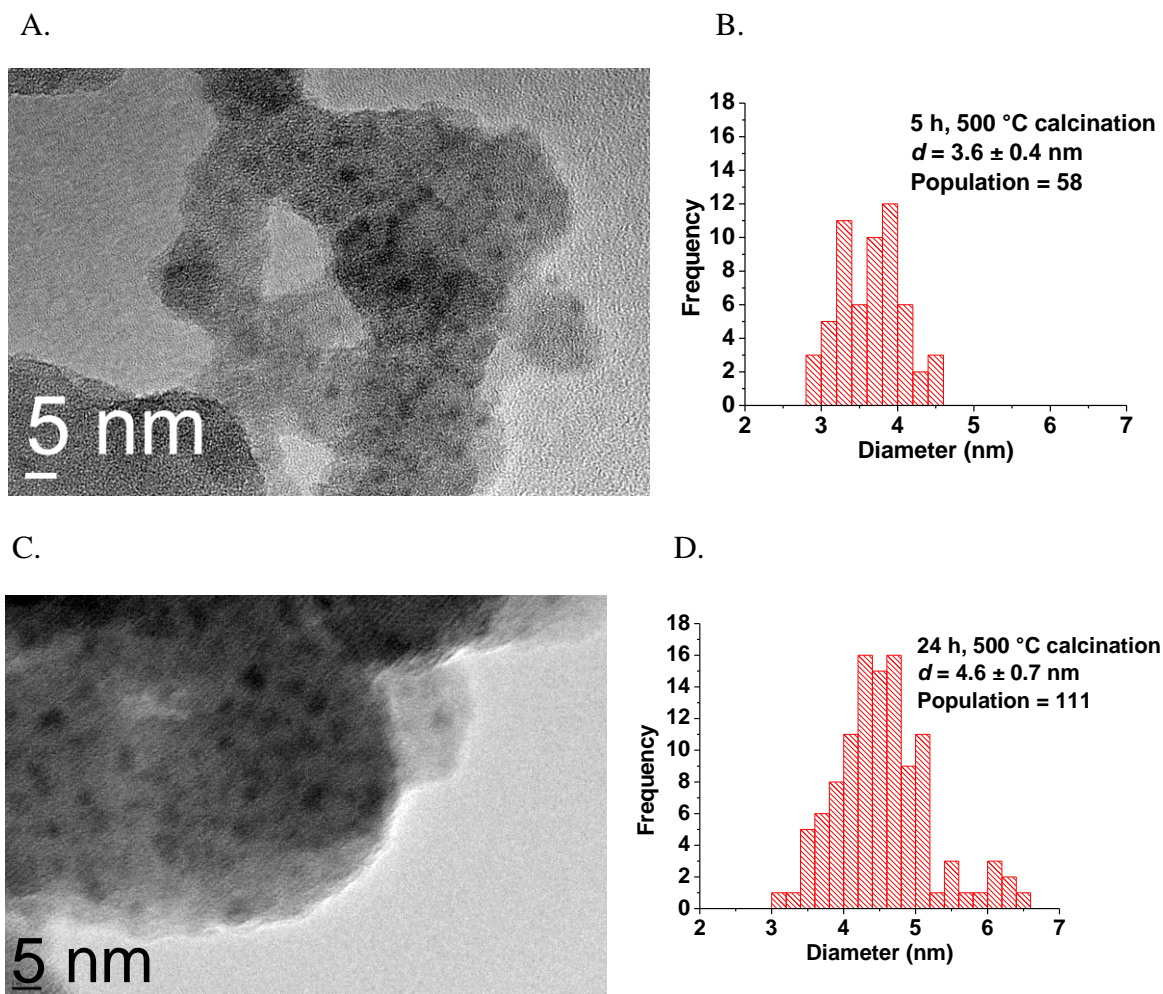

Figure 3.16 Representative bright-field TEM image and corresponding size distribution of silica-supported NiO nanoparticles prepared by the IWI method in methanol (A, B) after 5 h and (C, D) after 24 h calcination at 500 °C.
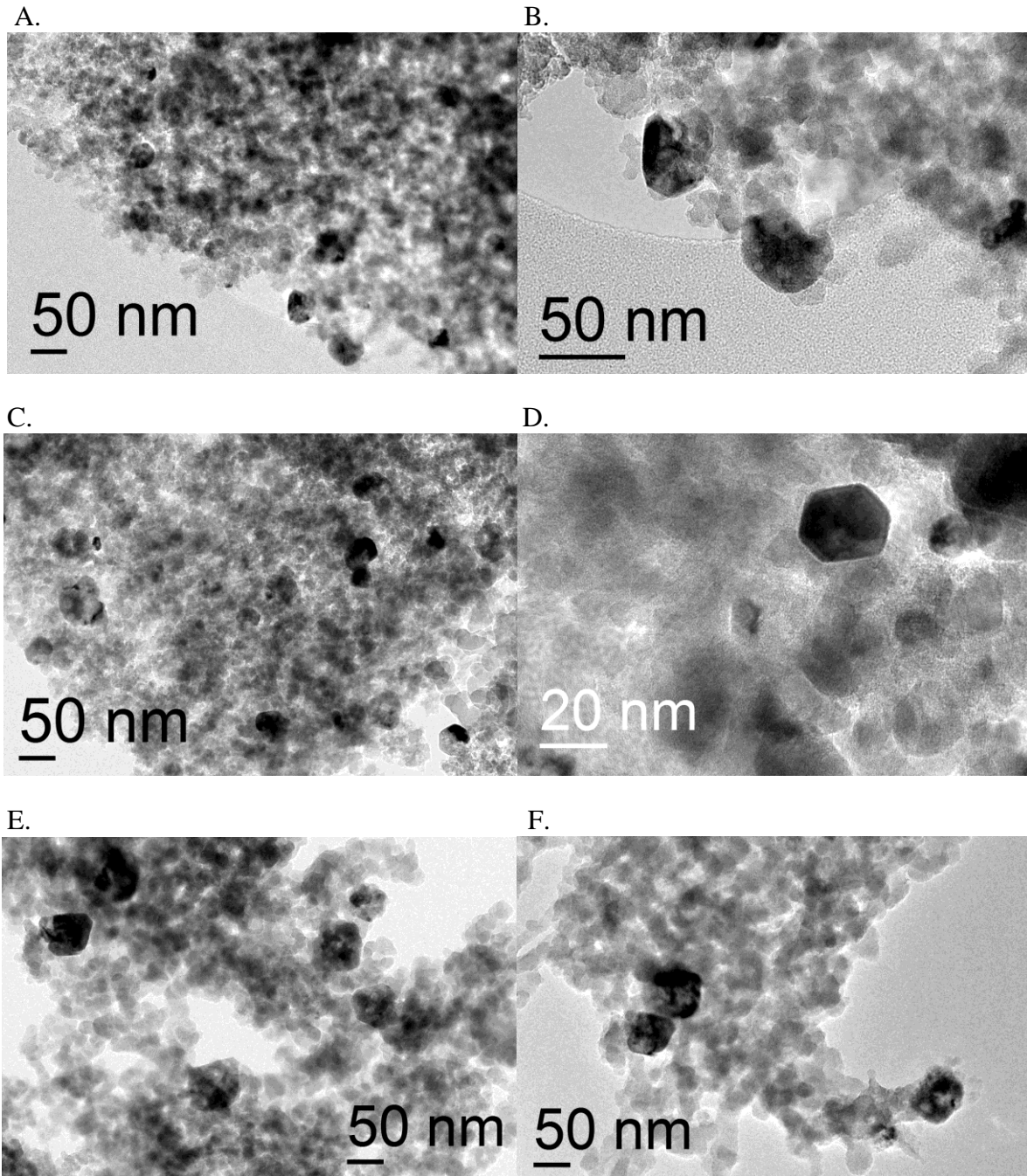
Figure 3.17 Representative bright-field TEM images of silica-supported NiO nanoparticles prepared by the IWI method in water calcination at 500 °C for 5 h (A, B), 24 h (C, D), and 48 h (E, F).

A.

B.

C.
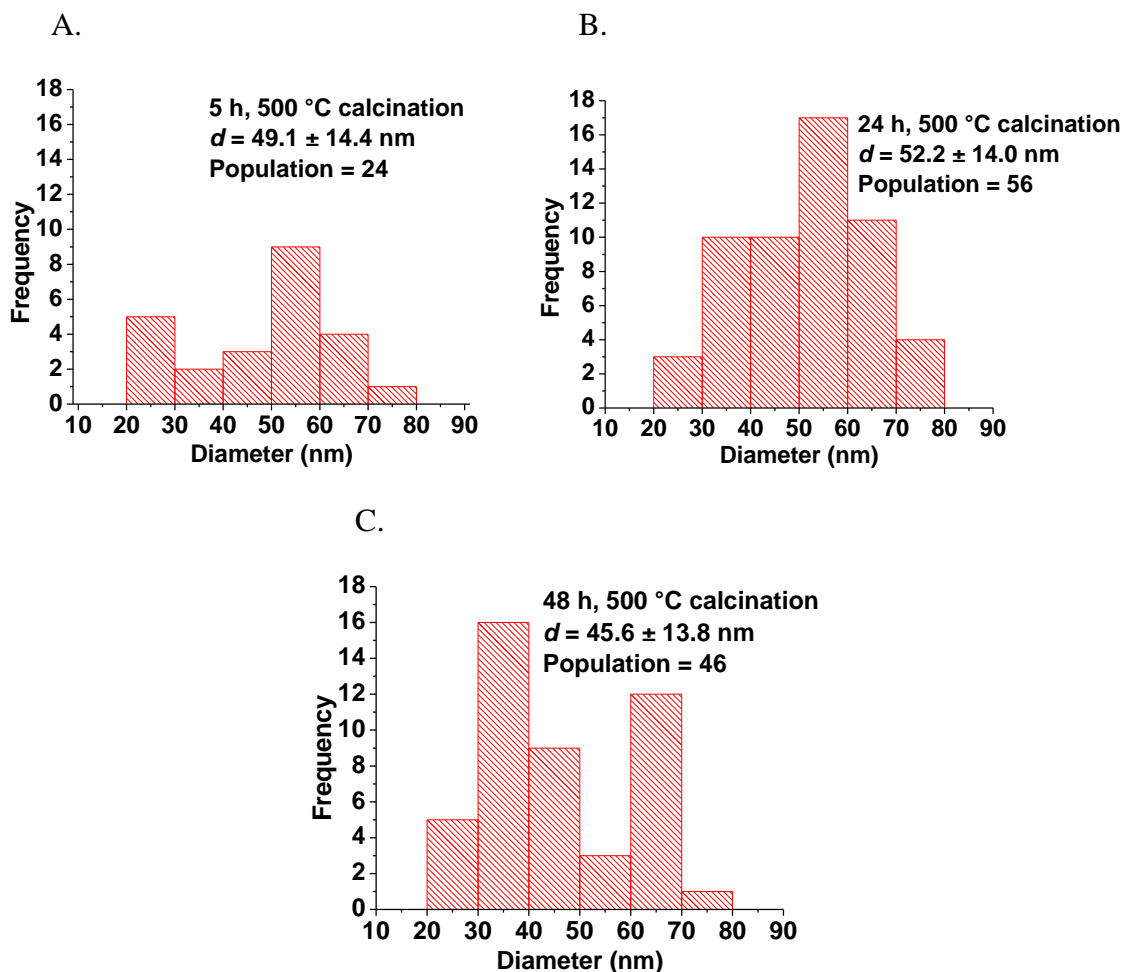
Figure 3.18 Size distribution histograms of silica-supported NiO nanoparticles prepared by the IWI method in water followed by calcination at 500 °C for (A) 5 h, (B) 24 h, and (C) 48 h.

Selected-area electron diffraction (SAED) pattern obtained for NiO nanoparticles prepared by the IWI method in water followed by calcination at 500 °C for 24 h is given in Figure 3.19. The SAED pattern consisted of three crystal planes (111, 200, and 220), which is in agreement with NiO nanoparticles previously reported.[46] This suggests the formation of crystalline NiO nanoparticles by the IWI method in water. However, amorphous silica substrate on each sample scattered the electron beam making it challenging to obtain a SAED pattern.

Also, SAED cannot be performed on regions smaller than 10^{-4} cm diameter because spherical aberration of the objective lens limits it from exploring smaller regions.[47]
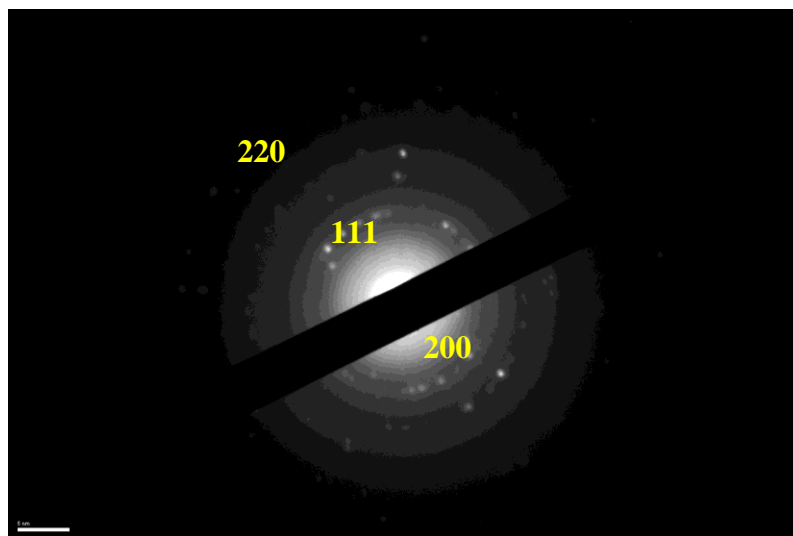
Figure 3.19 Selected-area electron diffraction (SAED) pattern of silica-supported NiO nanoparticles prepared by the IWI method in water (calcination at 500 °C for 24 h).

3.5   References

1.   Lomnicki, S. M.; Wu, H.; Osborne, S. N.; Pruett, J. M.; McCarley, R. L.; Poliakoff, E.; Dellinger, B., Size-selective synthesis of immobilized copper oxide nanoclusters on silica. *Materials Science and Engineering: B* **2010,** *175* (2), 136-142.

2.   Li, W.-C.; Comotti, M.; Schüth, F., Highly reproducible syntheses of active Au/TiO$_2$ catalysts for CO oxidation by deposition–precipitation or impregnation. *Journal of Catalysis* **2006,** *237* (1), 190-196.

3.   Delannoy, L.; El Hassan, N.; Musi, A.; Le To, N. N.; Krafft, J.-M.; Louis, C., Preparation of Supported Gold Nanoparticles by a Modified Incipient Wetness Impregnation Method. *The Journal of Physical Chemistry B* **2006,** *110* (45), 22471-22478.

4.   Lee, D.-S.; Chen, H.-J.; Chen, Y.-W., Photocatalytic reduction of carbon dioxide with water using InNbO$_4$ catalyst with NiO and Co$_3$O$_4$ cocatalysts. *Journal of Physics and Chemistry of Solids* **2012,** *73* (5), 661-669.

5.   Lomnicki, S.; Dellinger, B., Development of Supported Iron Oxide Catalyst for Destruction of PCDD/F. *Environmental Science & Technology* **2003,** *37* (18), 4254-4260.

6.   Nganai, S.; Lomnicki, S.; Dellinger, B., Ferric Oxide Mediated Formation of PCDD/Fs from 2-Monochlorophenol. *Environmental Science & Technology* **2008,** *43* (2), 368-373.

7. Lomnicki, S.; Dellinger, B., A Detailed Mechanism of the Surface-Mediated Formation of PCDD/F from the Oxidation of 2-Chlorophenol on a CuO/Silica Surface. *The Journal of Physical Chemistry A* **2003,** *107* (22), 4387-4395.

8. Lomnicki, S.; Truong, H.; Vejerano, E.; Dellinger, B., Copper Oxide-Based Model of Persistent Free Radical Formation on Combustion-Derived Particulate Matter. *Environmental Science & Technology* **2008,** *42* (13), 4982-4988.

9. Vejerano, E.; Lomnicki, S. M.; Dellinger, B., Formation and Stabilization of Combustion-Generated, Environmentally Persistent Radicals on Ni(II)O Supported on a Silica Surface. *Environmental Science & Technology* **2012,** *46* (17), 9406-9411.

10. Adhiya, A.; Wesdemiotis, C., Poly(propylene imine) dendrimer conformations in the gas phase: a tandem mass spectrometry study. *International Journal of Mass Spectrometry* **2002,** *214* (1), 75-88.

11. Velarde-Ortiz, R.; Larsen, G., A Poly(propylene imine) (DAB-Am$_{64}$) Dendrimer as Cu^{2+} Chelator for the Synthesis of Copper Oxide Clusters Embedded in Sol−Gel Derived Matrixes. *Chemistry of Materials* **2002,** *14* (2), 858-866.

12. Floriano, P. N.; Noble; Schoonmaker, J. M.; Poliakoff, E. D.; McCarley, R. L., Cu(0) Nanoclusters Derived from Poly(propylene imine) Dendrimer Complexes of Cu(II). *Journal of the American Chemical Society* **2001,** *123* (43), 10545-10553.

13. Mitran, E.; Dellinger, B.; McCarley, R. L., Highly Size-Controlled, Low-Size-Dispersity Nickel Nanoparticles from Poly(propylene imine) Dendrimer−Ni(II) Complexes. *Chemistry of Materials* **2010,** *22* (24), 6555-6563.

14. Reijme, M. A.; Maas, A. J. H.; Viitanen, M. M.; Denier van der Gon, A. W.; Brongersma, H. H.; Bosman, A. W.; Meijer, E. W., Intramolecular segregation in polymers and macromolecules studied by low-energy ion scattering. *Surface Science* **2001,** *482–485, Part 2* (0), 1235-1240.

15. Crooks, R. M.; Zhao, M.; Sun, L.; Chechik, V.; Yeung, L. K., Dendrimer-Encapsulated Metal Nanoparticles: Synthesis, Characterization, and Applications to Catalysis. *Accounts of Chemical Research* **2000,** *34* (3), 181-190.

16. Mossanek, R. J. O.; Preda, I.; Abbate, M.; Rubio-Zuazo, J.; Castro, G. R.; Vollmer, A.; Gutiérrez, A.; Soriano, L., Investigation of surface and non-local screening effects in the Ni 2p core level photoemission spectra of NiO. *Chemical Physics Letters* **2011,** *501* (4–6), 437-441.

17. Preda, I.; Mossanek, R. J. O.; Abbate, M.; Alvarez, L.; Méndez, J.; Gutiérrez, A.; Soriano, L., Surface contributions to the XPS spectra of nanostructured NiO deposited on HOPG. *Surface Science* **2012,** *606* (17–18), 1426-1430.

18.   Soriano, L.; Preda, I.; Gutiérrez, A.; Palacín, S.; Abbate, M.; Vollmer, A., Surface effects in the Ni 2p X-ray photoemission spectra of NiO. *Physical Review B* **2007,** *75* (23), 233417.

19.   Peck, M. A.; Langell, M. A., Comparison of Nanoscaled and Bulk NiO Structural and Environmental Characteristics by XRD, XAFS, and XPS. *Chemistry of Materials* **2012,** *24* (23), 4483-4490.

20.   Grosvenor, A. P.; Biesinger, M. C.; Smart, R. S. C.; McIntyre, N. S., New interpretations of XPS spectra of nickel metal and oxides. *Surface Science* **2006,** *600* (9), 1771-1779.

21.   Mu, R.; Fu, Q.; Liu, H.; Tan, D.; Zhai, R.; Bao, X., Reversible surface structural changes in Pt-based bimetallic nanoparticles during oxidation and reduction cycles. *Applied Surface Science* **2009,** *255* (16), 7296-7301.

22.   Hathaway, B. J.; Lewis, C. E., Electronic properties of transition-metal complex ions adsorbed on silica gel. Part I. Nickel(II) complexes. *Journal of the Chemical Society A: Inorganic, Physical, Theoretical* **1969**, 1176-1182.

23.   Yang, J. C.; Shul, Y. G.; Louisb, C.; Che, M., In situ EXAFS study of the nucleation and crystal growth of Ni particles on SiO$_2$ support. *Catalysis Today* **1998,** *44* (1–4), 315-325.

24.   Hathaway, B. J.; Lewis, C. E., The electronic properties of transition-metal complex ions adsorbed on silica gel. Part III. Copper(II). *Journal of the Chemical Society A: Inorganic, Physical, Theoretical* **1969**, 2295-2299.

25.   Hathaway, B. J.; Lewis, C. E., Electronic properties of transition-metal complex ions adsorbed on silica gel. Part II. Cobalt(II) and cobalt(III). *Journal of the Chemical Society A: Inorganic, Physical, Theoretical* **1969**, 1183-1188.

26.   Anspoks, A.; Kalinko, A.; Kalendarev, R.; Kuzmin, A., Probing vacancies in NiO nanoparticles by EXAFS and molecular dynamics simulations. *Journal of Physics: Conference Series* **2013,** *430* (15th International Conference on X-Ray Absorption Fine Structure, 2012), 012027/1-012027/4.

27.   Sandstrom, D. R., Ni^{2+} coordination in aqueous NiCl$_2$ solutions: Study of the extended X-ray absorption fine structure. *The Journal of Chemical Physics* **1979,** *71* (6), 2381-2386.

28.   Chen, C. S.; Lai, Y. T.; Lai, T. W.; Wu, J. H.; Chen, C. H.; Lee, J. F.; Kao, H. M., Formation of Cu Nanoparticles in SBA-15 Functionalized with Carboxylic Acid Groups and Their Application in the Water–Gas Shift Reaction. *ACS Catalysis* **2013,** *3* (4), 667-677.

29.   Chang, F. C.; Liao, P. H.; Tsai, C. K.; Hsiao, M. C.; Paul Wang, H., Chemical-looping combustion of syngas with nano CuO–NiO on chabazite. *Applied Energy* **2014,** *113* (0), 1731-1736.

67

30. Klysubun, W.; Thongkam, Y.; Pongkrapan, S.; Won-in, K.; T-Thienprasert, J.; Dararutana, P., XAS study on copper red in ancient glass beads from Thailand. *Analytical & Bioanalytical Chemistry* **2011,** *399* (9), 3033-3040.

31. Lamberti, C.; Bordiga, S.; Salvalaggio, M.; Spoto, G.; Zecchina, A.; Geobaldo, F.; Vlaic, G.; Bellatreccia, M., XAFS, IR, and UV−Vis Study of the CuI Environment in CuI-ZSM-5. *The Journal of Physical Chemistry B* **1997,** *101* (3), 344-360.

32. Railsback, J. G.; Johnston-Peck, A. C.; Wang, J.; Tracy, J. B., Size-Dependent Nanoscale Kirkendall Effect During the Oxidation of Nickel Nanoparticles. *ACS Nano* **2010,** *4* (4), 1913-1920.

33. Gates, A. T.; Nettleton, E. G.; Myers, V. S.; Crooks, R. M., Synthesis and Characterization of NiSn Dendrimer-Encapsulated Nanoparticles. *Langmuir* **2010,** *26* (15), 12994-12999.

34. Tokonami, S.; Morita, N.; Takasaki, K.; Toshima, N., Novel Synthesis, Structure, and Oxidation Catalysis of Ag/Au Bimetallic Nanoparticles. *The Journal of Physical Chemistry C* **2010,** *114* (23), 10336-10341.

35. Reddy, E. P.; Rojas, T. C.; Fernández, A.; Chowdhury, B.; Reddy, B. M., Transmission Electron Microscopy and Energy-Dispersive X-ray Spectroscopy Study of $V_2O_5/TiO_2−ZrO_2$ Catalyst. *Langmuir* **2000,** *16* (9), 4217-4221.

36. Hashimoto, I.; Wakai, E.; Yamaguchi, H., Dependence of the X-ray detector orientation on Cliff-Lorimer factor for quantitative microanalysis in an electron microscope. *Ultramicroscopy* **1990,** *32* (2), 121-126.

37. Nacucchi, M.; Alvisi, M.; Altamura, D.; Pfister, V.; Re, M.; Signore, M. A.; Antisari, M. V., Quantitative EDS analysis in transmission electron microscopy using unconventional reference materials. *IOP Conference Series: Materials Science and Engineering* **2010,** *7* (1), 012020.

38. Watanabe, M.; Williams, D. B., The quantitative analysis of thin specimens: a review of progress from the Cliff-Lorimer to the new ζ-factor methods. *Journal of Microscopy* **2006,** *221* (2), 89-109.

39. Miguens, F. C.; Oliveira, M. L. d.; Marins, R. V.; Lacerda, L. D. d., A new protocol to detect light elements in estuarine sediments by X-ray microanalysis (SEM/EDS). *Journal of Electron Microscopy* **2010,** *59* (5), 437-446.

40. Mainardi, D. S.; Balbuena, P. B., Monte Carlo Simulation of Cu−Ni Nanoclusters: Surface Segregation Studies. *Langmuir* **2001,** *17* (6), 2047-2050.

41. Bohannan, E. W.; Kothari, H. M.; Nicic, I. M.; Switzer, J. A., Enantiospecific Electrodeposition of Chiral CuO Films on Single-Crystal Cu(111). *Journal of the American Chemical Society* **2003,** *126* (2), 488-489.

42. Pabi, S. K.; Joardar, J.; Manna, I.; Murty, B. S., Nanocrystalline phases in Cu-Ni, Cu-Zn and Ni-Al systems by mechanical alloying. *Nanostructured Materials* **1997,** *9* (1–8), 149-152.

43. Hristova, E.; Dong, Y.; Grigoryan, V. G.; Springborg, M., Structural and Energetic Properties of Ni−Cu Bimetallic Clusters. *The Journal of Physical Chemistry A* **2008,** *112* (34), 7905-7915.

44. Lutz, W.; Toufar, H.; Kurzhals, R.; Suckow, M., Investigation and Modeling of the Hydrothermal Stability of Technically Relevant Zeolites. *Adsorption* **2005,** *11* (3/4), 405-413.

45. Chen, S.; Zhu, J.; Zhou, H.; Wang, X., One-step synthesis of low defect density carbon nanotube-doped $Ni(OH)_2$ nanosheets with improved electrochemical performances. *Royal Society of Chemistry Advances* **2011,** *1* (3), 484-489.

46. Dong, Q.; Yin, S.; Guo, C.; Wu, X.; Kumada, N.; Takei, T.; Miura, A.; Yonesaki, Y.; Sato, T., Single-crystalline porous NiO nanosheets prepared from β-$Ni(OH)_2$ nanosheets: Magnetic property and photocatalytic activity. *Applied Catalysis B: Environmental* **2014,** *147* (0), 741-747.

47. Fultz, B.; Howe, J. M., *Transmission Electron Microscopy and Diffractometry of Materials*. 3rd ed.; Springer Berlin Heidelberg New York: 2008; p 758.

CHAPTER 4: THE CATALYTIC ACTIVITY OF SILICA-SUPPORTED, METAL-OXIDE NANOPARTICLE SURROGATES UNDER PYROLYTIC CONDITIONS

Silica-supported NiO, CuO, and NiO-CuO nanoparticle surrogates of fly ash were successfully synthesized in Chapter 3 using the WI-D and the WI-M methods. The catalytic activity of these surrogate fly ash materials for the formation of PCDD/Fs under pyrolysis is investigated here. Monochlorobenzene (MCBz), dichlorobenzene (DCBz), phenol, and 2-monochlorophenol (2-MCP) are well documented as precursors for the formation of PCDD/Fs during municipal solid waste (MSW) incineration (Figure 4.1).[1-4] The reactions of 1,2-DCBz on CuO[5] were previously studied because 1,2-DCBz is a major chlorobenzene precursor found in the exhaust of waste incinerators.[6] Prior understandings of 2-MCP reactions on CuO[7-8] and Fe_2O_3[9] indicate that 2-MCP is also a precursor for PCDD/Fs formation in the post-combustion zone.
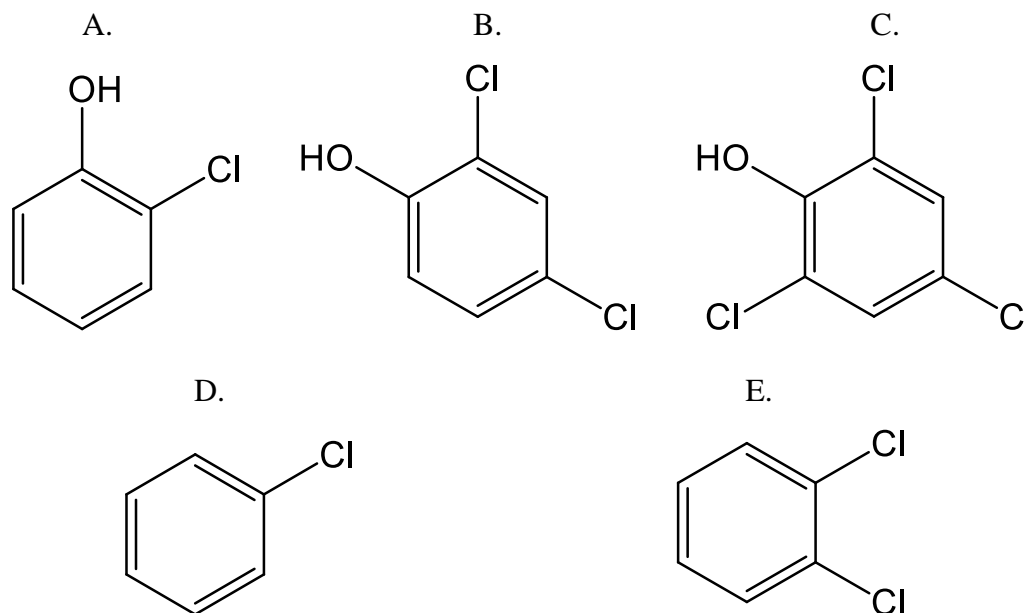
Figure 4.1 Structures of A. 2-monochlorophenol (2-MCP), B. 2,4-dichlorophenol (2,4-DCP), C. 2,4,6-trichlorophenol (2,4,6-TCP), D. monochlorobenzene (MCBz), and E. 1,2-dichlorobenzene (1,2-DCBz).

Ni is a commonly found transition metal in fly ash,[10-12] and the catalytic activity of NiO for the formation of PCDD/Fs has not been investigated to date. The formation of NiO-CuO mixed oxide has also been observed in the presence of oxygen.[13-14] Also, both NiO and CuO have similar crystal structure (face-centered cubic).[15-18] Therefore, it is highly probable that they exist in the form of NiO-CuO mixed particles on fly ash. This chapter is investigated the reactions of 2-MCP on NiO, CuO, and NiO-CuO to determine their catalytic activity for the formation of PCDD/Fs.

4.1   Materials

NiO, CuO, and NiO-CuO (molar ratio 1:1, 1:3, 1:10, 10:1, and 3:1) nanoparticles prepared by the WI-D and the WI-M methods were used as catalysts in this study. Standards of 2-monochlorophenol (2-MCP); 2,4-dichlorophenol (2,4-DCP); 2,4,6-trichlorophenol (2,4,6-TCP); monochlorobenzene (MCBz); and 1,2-dichlorobenzene (1,2-DCBz) were purchased from Sigma-Aldrich Co LLC, St. Louis, MO. Dibenzo-*p*-dioxin (DD), 1-monochlorodibenzo-*p*-dioxin (MCDD), 2,4-dichlorodibenzo-*p*-dioxin (DCDD), and dibenzofuran (DBF) were purchased from Cambridge Isotope Laboratories, Tewksbury, MA. Quartz wool was purchased from Perkin Elmer Inc., Waltham, MA.

4.2   Reaction conditions

Quartz tubes, 18 cm in length and 0.4 cm in diameter, were used as the reactor (Figure 4.2A). A 10mg portion of silica-supported, metal-oxide nanoparticles (catalyst) was placed inside the quartz tube reactor using quartz wool (Figure 4.2B). The length of the catalyst-packed-bed was retained at ~0.4 cm for each experiment. The catalyst was activated at 450 °C for 1 h in breathing air (20% O_2 + 80% N_2) with a flow rate of 5 mL/min before each experiment to remove adsorbed moisture and other contaminants from the surface. All injectors and transfer

71

lines were maintained at 200 °C to avoid condensation of the products. The flow rates of the carrier gas helium (15 mL/min) and the injection rate of 2-MCP (0.21 μL h^{-1}) were maintained to obtain a constant gas phase concentration of 2-MCP (50 ppm) throughout the reaction.[5, 9] The quartz tube with the catalyst was placed inside a thermal reactor (Chapter 2: Figure 2.2B) where the temperature was maintained at 300, 350, 400, 450, 500, or 550 ℃. A fresh quartz tube reactor with catalyst was used for each experiment. The 2-MCP was passed over the catalyst for 1 h, and the products were collected at the front end of the GC column at −60 °C (Cryogenic trap). Subsequently, products were separated and quantified using GC–MS (temperature program: −60 ℃ to 300 ℃ at 10 ℃ min^{-1}). Each catalyst was tested a minimum of three times at each temperature; thus, a data point reflects the average of three experiments with a reported error of ±1 standard deviation.

A.

B.

C.

Figure 4.2 Quartz tube reactors: A. Empty, B. CuO before, and C. CuO after the surface-mediated reaction of 2-MCP (Note: carbonaceous particles). Carrier gas flew from left to right.

The % yields of the products were calculated using Equation 4.1, where [Product] is the amount of the product formed (in moles), and [2-MCP] is the amount of 2-MCP initially injected into the reactor (in moles). *A* is the stoichiometric factor, which is 2 for products with 2 benzene

72

rings (two 2-MCP molecules were utilized to form one MCDD molecule) and 1 for products with 1 benzene ring. All the products were quantified using standard calibration curves.

Equation 4.1 $$\% \, Yield = \left(\frac{A \, [Product]}{[2-MCP]}\right) \times 100$$

4.3 Metal-oxide catalysts prepared by the WI-D method

Silica-supported NiO, CuO, and NiO-CuO (molar ratio 1:1, 1:3, 1:10, 10:1, and 3:1) catalysts were examined in this study under pyrolytic conditions. Each catalyst was tested from 300 °C to 550 °C with 50 °C increments, and the % yields of all the products were recorded as a function of reaction temperature. The amount of unreacted 2-MCP (% recovery) was reported as a function of temperature, as displayed in Figure 4.3. About 86% of 2-MCP were converted to products (~14% recovery), even at the lowest temperature studied (300 °C) for NiO and CuO. However, NiO-CuO mixed catalysts provided lower % recoveries compared to the individual metals, signifying higher rates of 2-MCP conversion on those surfaces (Table 4.1). The nearly-complete conversion of 2-MCP was achieved at temperatures above 450 °C for all the catalysts, as denoted by low % recoveries. However, a fraction of 2-MCP was converted to carbonaceous materials during the reaction,[8, 19] as evidenced by the visible dark gray layer on top of the catalyst after the reaction (Figure 4.2C).

Table 4.1 The % recoveries of 2-MCP over metal-oxide catalysts at 300 °C.

Catalyst	% Recovery
NiO	14.03 ± 0.85%
CuO	12.8 ± 0.43%
NiO-CuO (1:1)	9.53 ± 0.49%
NiO-CuO (1:3)	4.52 ± 0.09%
NiO-CuO (1:10)	1.51 ± 0.12%
NiO-CuO (10:1)	5.95 ± 0.97%
NiO-CuO (3:1)	2.83 ± 0.63%

73
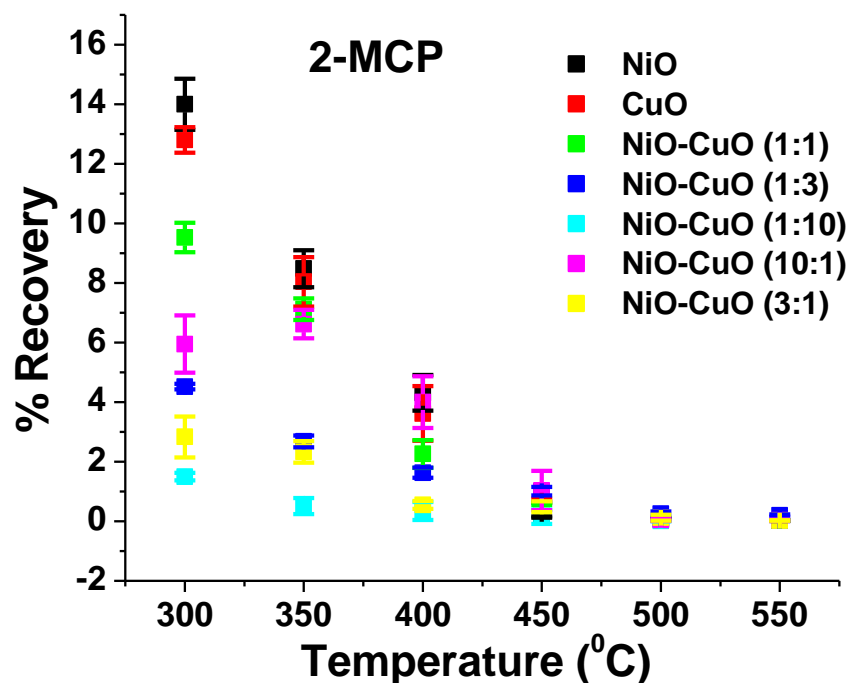
Figure 4.3 % Recoveries of 2-MCP reacted on different silica-supported metal-oxide catalysts (prepared by the WI-D method) from 300 to 550 °C. Experiments were performed in triplicate.

Dichlorophenol (DCP) and trichlorophenol (TCP) were the only chlorophenols formed in this study. DCP was formed with NiO, CuO, and NiO-CuO (1:1, 10:1, and 3:1) catalysts, whereas TCP was formed only with NiO and NiO-CuO (3:1). The highest % yield of DCP was formed on CuO at 300 °C (0.139 ± 0.004%), and comparatively lower % yields were formed on other catalysts at 300 °C, as displayed in Figure 4.4A and Table 4.2. TCP was formed between 300–450 °C only with NiO, whereas it was observed at all temperatures for NiO-CuO (3:1), with the highest % yield recorded at 300 °C (Figure 4.4B and Table 4.2). Both DCP and TCP % yields followed a similar trend to 2-MCP thus, indicating the conversion of these compounds at higher temperatures on metal-oxide catalysts.

74

A.

B.
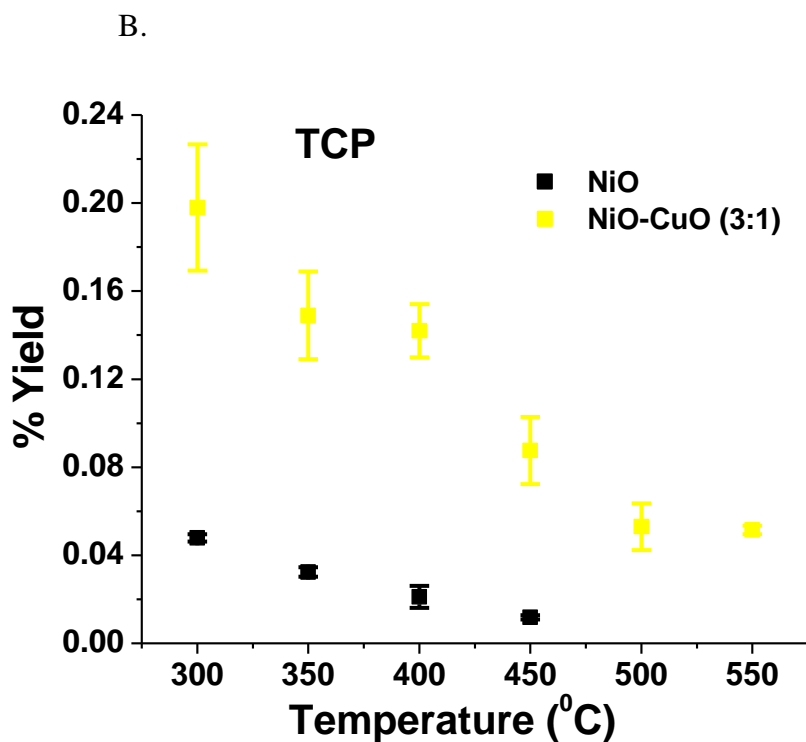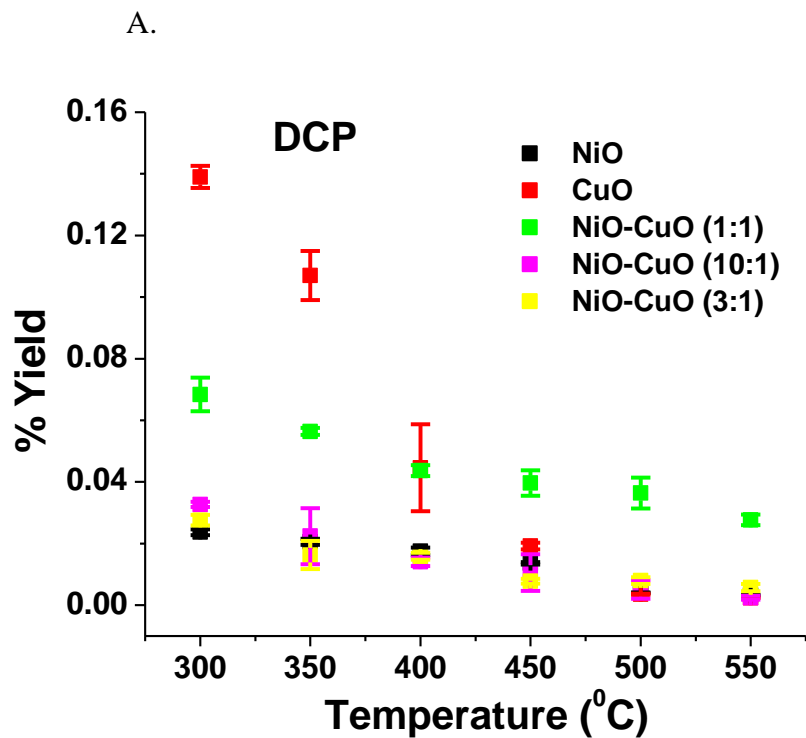
Figure 4.4 % Yields of A. DCP and B. TCP produced on silica-supported, metal-oxide catalysts (prepared by the WI-D method) from 300 to 550 °C. Experiments were performed in triplicate.

75

Table 4.2 The % yields of DCP and TCP on metal-oxide catalysts at 300 °C. Experiments were performed in triplicate.

Catalyst	DCP % yield	TCP % yield
NiO	$0.024 \pm 0.001\%$	$0.048 \pm 0.002\%$
CuO	$0.139 \pm 0.004\%$	Not detected
NiO-CuO (1:1)	$0.068 \pm 0.005\%$	Not detected
NiO-CuO (1:3)	Not detected	Not detected
NiO-CuO (1:10)	Not detected	Not detected
NiO-CuO (10:1)	$0.033 \pm 0.001\%$	Not detected
NiO-CuO (3:1)	$0.028 \pm 0.002\%$	$0.198 \pm 0.003\%$

2,4-DCP and 2,4,6-TCP are typically found in the flue gas of municipal waste incinerators,[2] but it is inconclusive as to which DCP or TCP isomer was formed during the study here. Therefore, three DCP isomers, namely 2,4-DCP, 2,6-DCP, and 3,4-DCP, were studied by GC–MS to determine if differences in the GC retention times and mass spectrometric fragmentation pattern could be observed. Gas chromatograms of the three isomers indicate 2,4-DCP, 2,6-DCP, and 3,4-DCP have retention times of 19.8, 20.3, and 23.2 min, respectively as depicted in Figure 4.5 (GC temperature program: −60 °C to 300 °C at 10 °C min^{-1}). The large difference in retention time of 3,4-DCP in comparison with the other two isomers allows the ability of identifying 3,4-DCP. The 2,4-DCP and 2,6-DCP isomers demonstrated a difference in retention time of 0.5 min, which is enough to distinguish them here. However, when the cryogenically-trapped products of the surface-mediated reaction were analyzed by GC-MS (GC temperature program: −60 °C to 300 °C at 10 °C min^{-1}), the DCP peak shifted between 19.6–20.1 min for each experiment, thus it was difficult to distinguish 2,4-DCP and 2,6-DCP.

Retention times of chlorophenols and chlorobenzenes were compared with that of calibration standards to determine the type of isomer formed during the surface-mediated reaction. The same GC temperature program (−60 ℃ to 300 ℃ at 10 ℃ min^{-1}) used for the

76

product analysis was used for the calibration standard analysis, and the results are displayed in Table 4.3. According to Table 4.3, both the calibration standard of 2,4-DCP has a retention time of 19.5 min, whereas the retention time of the DCP products shift between 19.6–20.1 min, making it impossible to identify comparing with the calibration standards. All three isomers displayed identical mass spectra, thereby making it impossible to distinguish those using MS.
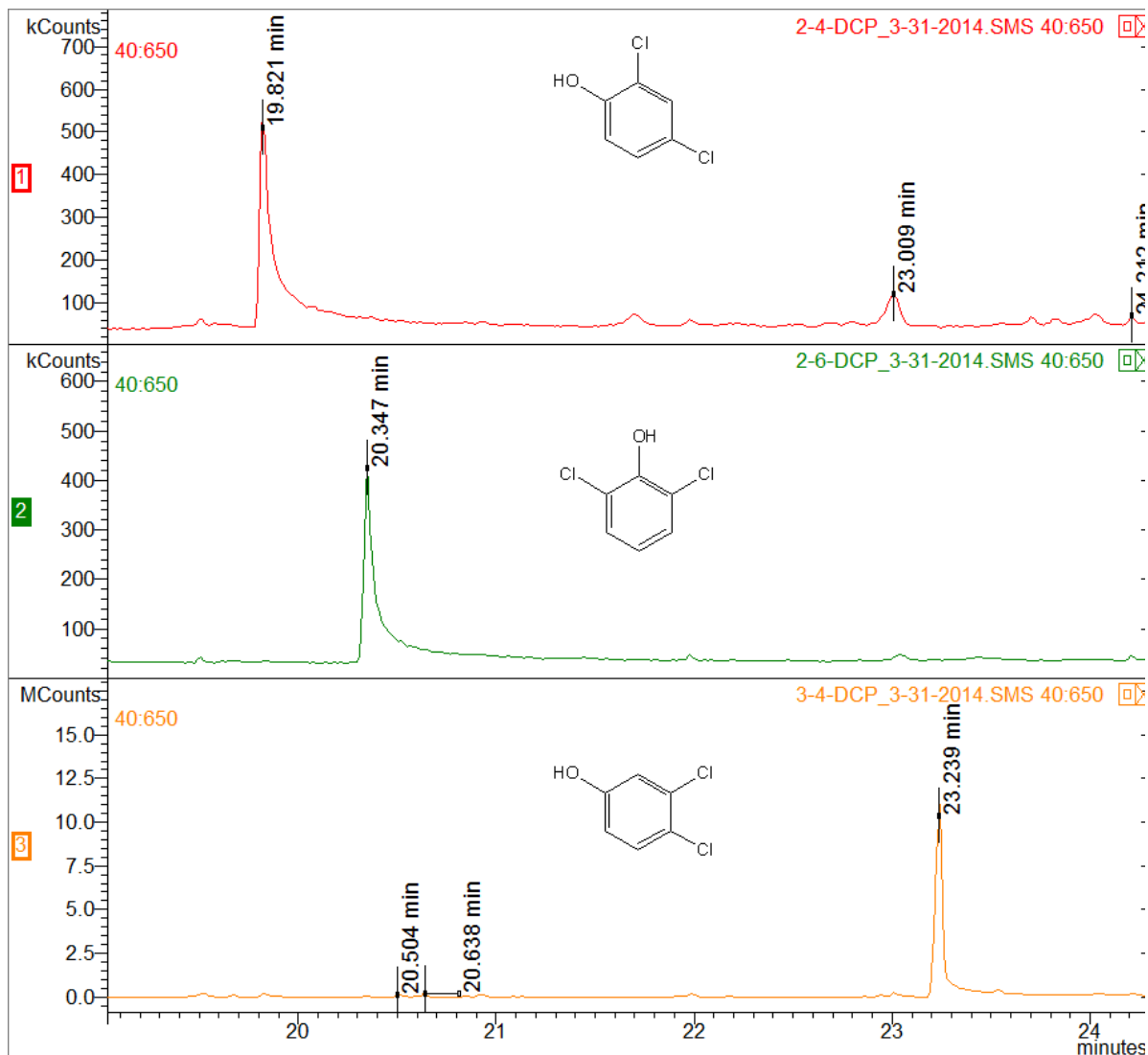
Figure 4.5 GC retention times of different commonly available dichlorophenol (DCP) isomers: 2,4-DCP, 2,6-DCP, and 3,4-DCP.

Table 4.3 Retention time (RT) for products in comparison to the retention times of calibration standards.

Product	*m*/Z	RT (min)	Standard	RT (min)
DCP	162.0	19.6–20.1	2,4-DCP	19.5
TCP	198.0	21.2–21.6	2,4,6-TCP	21.4
DCBz	146.0	16.6–17.0	1,2-DCBz	17.2

DCP = Dichlorophenol, TCP = Trichorophenol, DCBz = Dichlorobenzene

Chlorobenzenes were also generated under pyrolytic conditions. MCBz and DCBz were generated with every catalyst studied, as illustrated in Table 4.4 and Figure 4.6. The % yield of MCBz ($0.126 \pm 0.005\%$) was significantly higher with NiO at 300 °C than all other catalysts at the same temperature (Table 4.4). In the same way, a significantly higher % yield ($0.9 \pm 0.05\%$) of DCBz was observed with NiO-CuO (1:1) at 300 °C while all other catalysts yielded < 0.10% at 300 °C (Table 4.4). Chlorobenzene % yields presented a similar trend to chlorophenols at higher temperatures. The % yields of chlorophenols and chlorobenzenes decreased at temperatures greater than 450 °C, indicating the surface-mediated conversion of them to PCDD/Fs at higher temperatures, which is consistent with the trends of PCDD % yields (discussed later in this Section).

Table 4.4 The % yields of MCBz and DCBz over metal-oxide catalysts at 300 °C from 2-MCP precursor. Experiments were performed in triplicate.

| Catalyst	MCBz % yield	DCBz % yield
NiO	$0.126 \pm 0.005\%$	$0.014 \pm 0.001\%$
CuO	$0.014\% \pm 0.001\%$	$0.063 \pm 0.003\%$
NiO-CuO (1:1)	$0.003\% \pm 0.001\%$	$0.899 \pm 0.005\%$
NiO-CuO (1:3)	$0.003\% \pm 0.001\%$	$0.065 \pm 0.006\%$
NiO-CuO (1:10)	$0.007\% \pm 0.001\%$	$0.013 \pm 0.001\%$
NiO-CuO (10:1)	$0.010\% \pm 0.001\%$	$0.026 \pm 0.005\%$
NiO-CuO (3:1)	$0.009\% \pm 0.001\%$	$0.072 \pm 0.003\%$

78
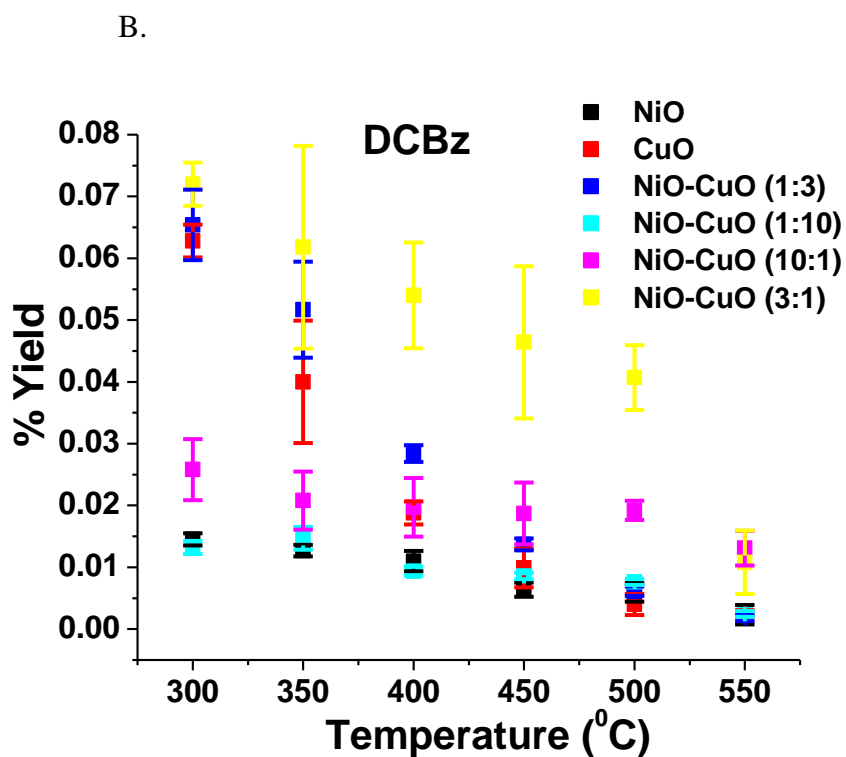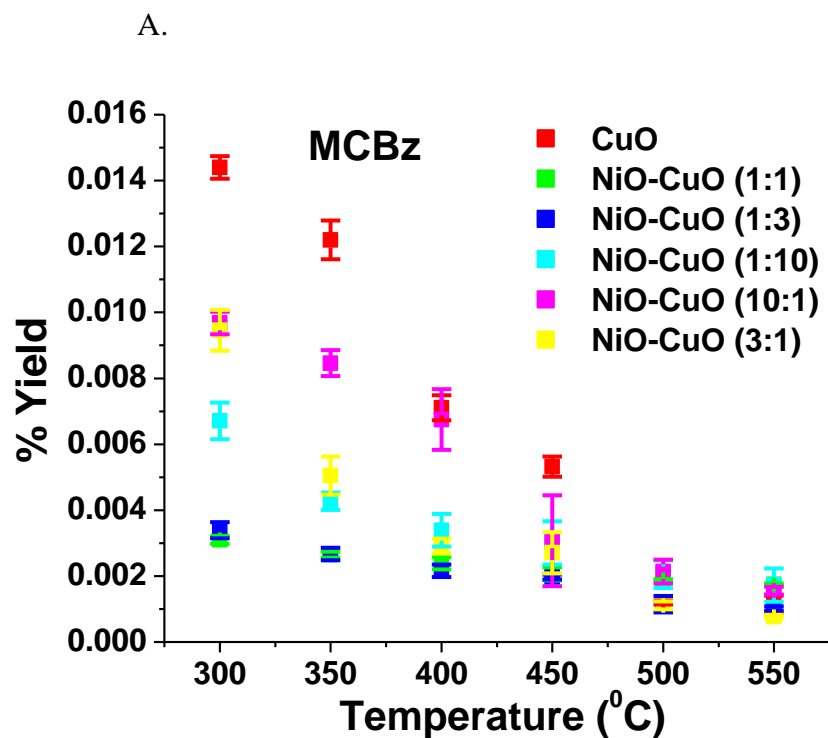
Figure 4.6 % Yields of A. MCBz and B. DCBz produced from 2-MCP on silica-supported, metal-oxide catalysts (prepared by the WI-D) from 300 to 550 °C. Experiments were performed in triplicate.

79

Three dioxin congeners, namely, dibenzo-*p*-dioxin (DD) (Figure 4.7A), monochloro-dibenzo-*p*-dioxin (MCDD) (Figure 4.7B), and dichloro-dibenzo-*p*-dioxin (DCDD) (Figure 4.7C) were identified in the surface-mediated reactions of 2-MCP on metal-oxide catalysts. DD and MCDD was formed with each catalyst tested (Figures 4.8 and 4.9). Moreover, DCDD was also formed with each catalyst except NiO-CuO (1:10) (Figure 4.10). The trends of dioxin % yields over the temperature range were completely different from those of chlorophenols and chlorobenzenes. The % yield decrease of chlorophenols and chlorobenzenes at higher temperatures indicated the conversion of them to dioxins under the conditions studied. For example, low % yields (0.1%–0.2%) of dioxins were observed at 300 °C, but their yields started to increase at above 400 °C, with the highest % yield observed between 400–500 °C for most catalysts; however, the % yields decreased at 550 °C, indicating gas-phase degradation of either dioxins or their precursors.[1, 20]
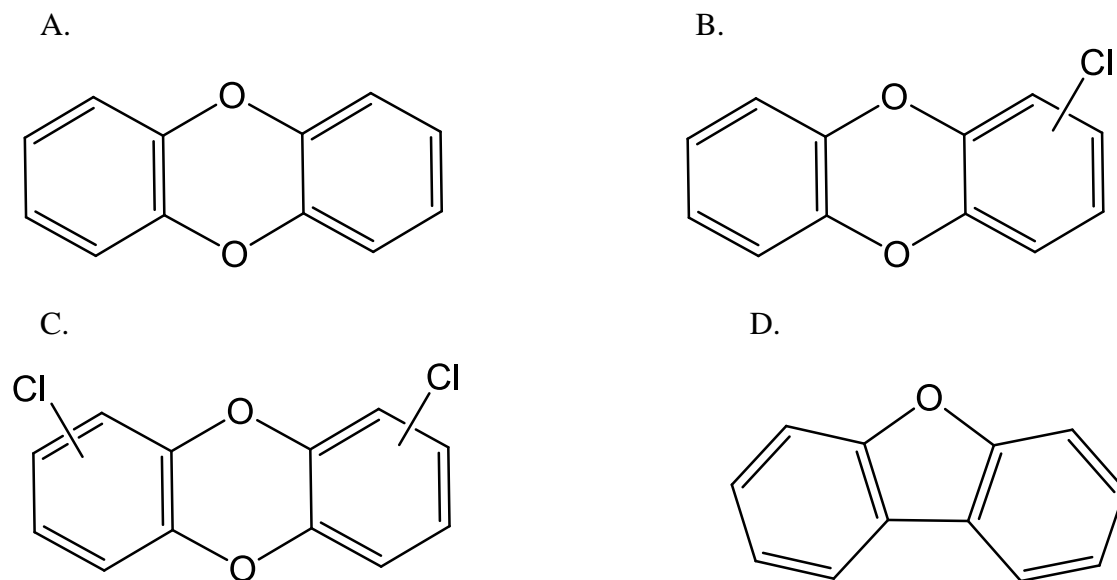
Figure 4.7 Structures of A. dibenzo-*p*-dioxin (DD), B. monochloro-dibenzo-*p*-dioxin (MCDD), C. dichloro-dibenzo-*p*-dioxin (DCDD), and D. dibenzofuran (DBF).

The highest % yields of dioxins were achieved at 350 °C for NiO-CuO (10:1) and NiO-CuO (1:10), but the % yields gradually decreased as the reaction temperature increased (Figure 4.11). The optimum temperature to obtain the highest % yield of dioxins varied from 300 °C to 550 °C, depending on the nature of the catalysts studied.[21-25] The highest % yield of dioxins for each catalyst and its respective temperature are shown in Table 4.5. The highest % yield of DD (2.05 ± 0.04%) and MCDD (1.73 ± 0.19) was recorded for NiO-CuO (1:1) at 450 °C whereas the highest % yield for DCDD (0.98 ± 0.14) was obtained for NiO at the 450 °C.

Figure 4.8 % Yields of dibenzo-*p*-dioxin (DD) produced on silica-supported metal-oxide catalysts (prepared by the WI-D) from 300 to 550 °C. Experiments were performed in triplicate.
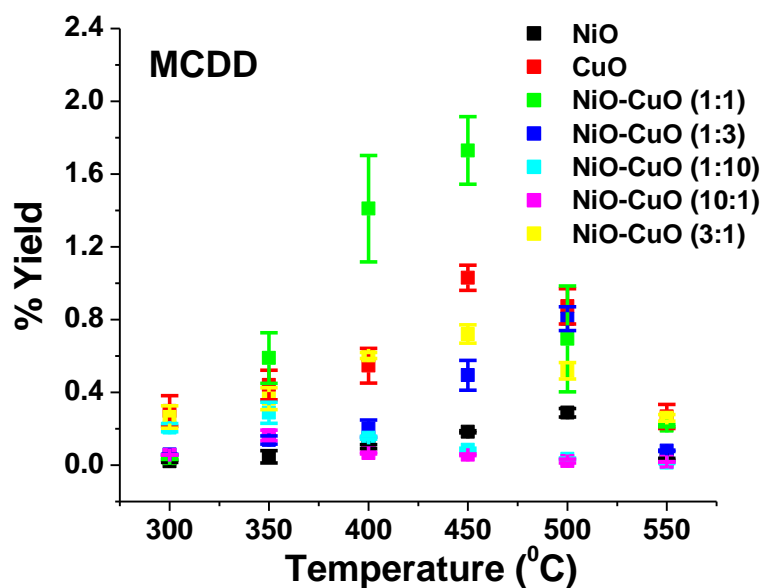
Figure 4.9 % Yields of monochloro-dibenzo-*p*-dioxin (MCDD) produced on silica-supported metal-oxide catalysts (prepared by the WI-D) from 300 to 550 °C. Experiments were performed in triplicate.
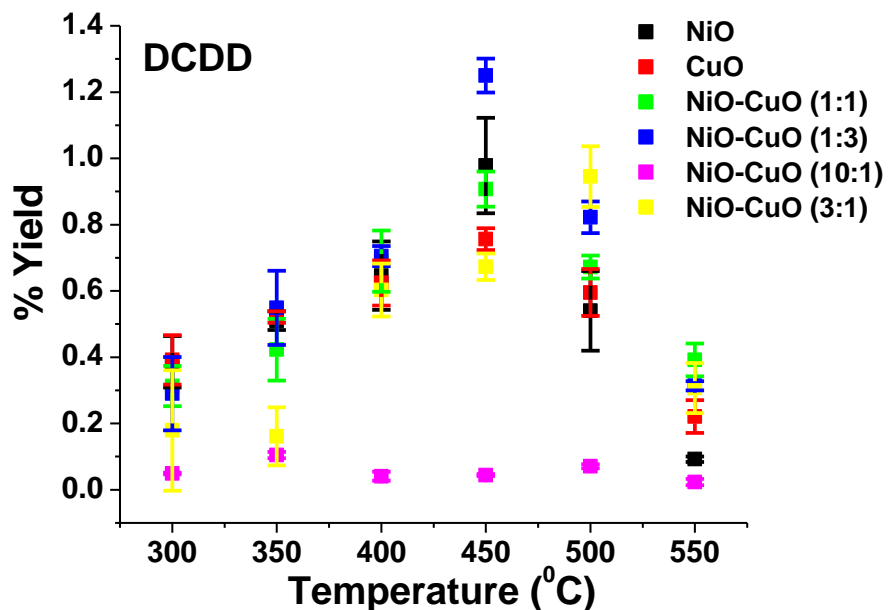
Figure 4.10 % Yields of dichloro-dibenzo-*p*-dioxin (DCDD) produced on silica-supported metal-oxide catalysts (prepared by the WI-D) from 300 to 550 °C. Experiments were performed in triplicate.

82

Table 4.5 The highest % yields of DD, MCDD, and DCDD with respective temperatures. Experiments were performed in triplicate.

Catalyst on Silica	DD		MCDD		DCDD	
	% Yield	Temp (°C)	% Yield	Temp (°C)	% Yield	Temp (°C)
NiO	1.52 ± 0.09	450	0.29 ± 0.02	500	0.98 ± 0.14	450
CuO	1.89 ± 0.17	450	1.03 ± 0.07	450	0.76 ± 0.03	450
NiO-CuO (1:1)	2.05 ± 0.04	500	1.73 ± 0.19	450	0.91 ± 0.05	450
NiO-CuO (3:1)	0.87 ± 0.09	500	0.72 ± 0.05	450	0.94 ± 0.09	500
NiO-CuO (10:1)	0.37 ± 0.04	350	0.16 ± 0.03	350	0.10 ± 0.01	350
NiO-CuO (1:10)	0.60 ± 0.05	350	0.29 ± 0.06	350	–	–
NiO-CuO (1:3)	0.11 ± 0.02	500	0.81 ± 0.07	500	1.25 ± 0.05	450

NiO-CuO mixed catalysts demonstrated strikingly low % yields of DD, MCDD, and DCDD-especially NiO-CuO (1:10) and (10:1)-compared to their individual 100% metal oxides. The exception was NiO-CuO (1:1) producing % yields of DD and MCDD higher than the individual metal oxides at 450 °C. The % recoveries for 2-MCP were lower for mixed metal oxides compared to the individual metal oxides (Figure 4.3 and Table 4.1); thus, a higher conversion rate of precursor (2-MCP) was observed when mixed metal oxides was used. However, the lower dioxin % yields strongly suggest that the majority of the 2-MCP was converted to carbon on the mixed metal-oxide catalysts under these conditions.

Dibenzofuran (DBF) (Figure 4.7D) was produced only with CuO catalysts, and its formation followed a similar trend in % yields to PCDDs under increased reaction temperature (Figure 4.6D). The highest % yield of DBF was 5.74 ± 0.64% at 500 °C (Figure 4.12). DBF % yields followed a similar trend to PCDDs at higher temperature due to their oxidative destruction.[8, 26]
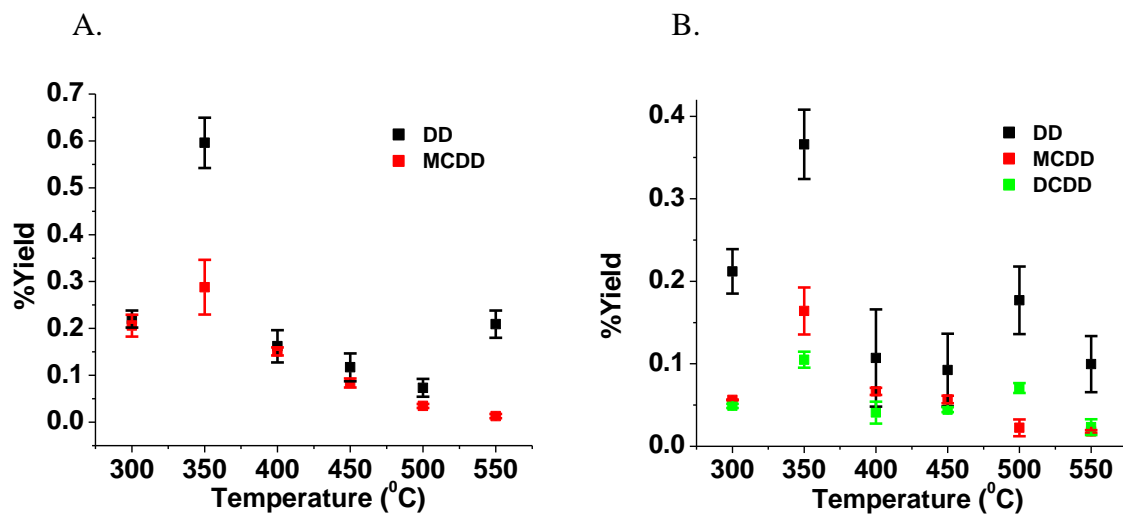
Figure 4.11 % Yields of DD, MCDD, and DCDD on silica-supported NiO-CuO catalysts: A. 1:10 and B. 10:1, (prepared by the WI-D) from 300 to 550 °C. Experiments were performed in triplicate.
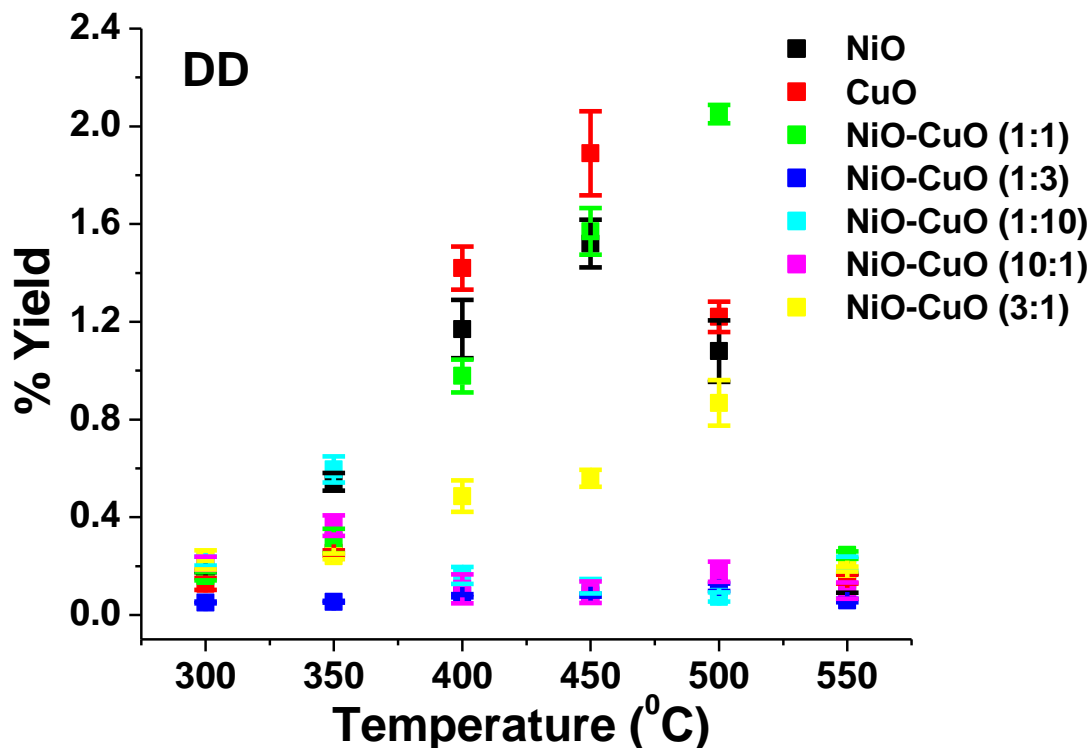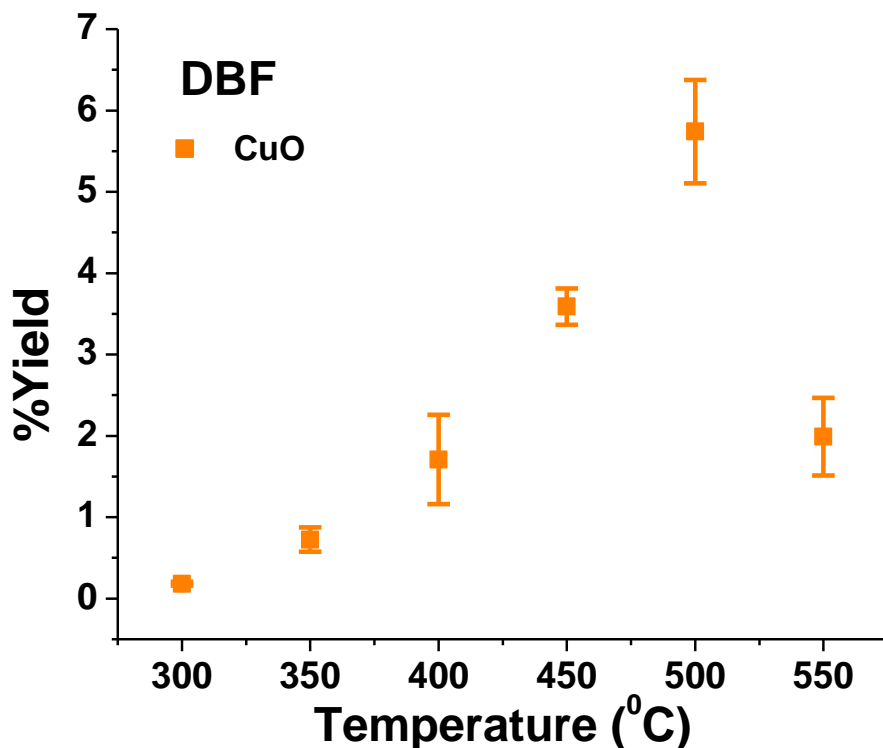

Figure 4.12 % Yields of dibenzofuran (DBF) produced on silica-supported CuO catalyst (prepared by the WI-D) from 300 to 550 °C. Experiments were performed in triplicate.

84

The catalytic activity of silica (not containing metal-oxides) was investigated using the same method. The MS was programmed to start analyzing after the 2-MCP eluted from the GC; hence, large quantities of unreacted 2-MCP would not overwhelm the detector. Significant amounts of MCDD and DCDD were not observed compared to metal-oxide catalysts. However, low % yields DD was observed from 450 to 550 °C due to the reactions of *de novo* synthesis[7, 27-28] and the gas-phase conversion of 2-MCP to DD (Figure 4.13).[1, 8, 23]
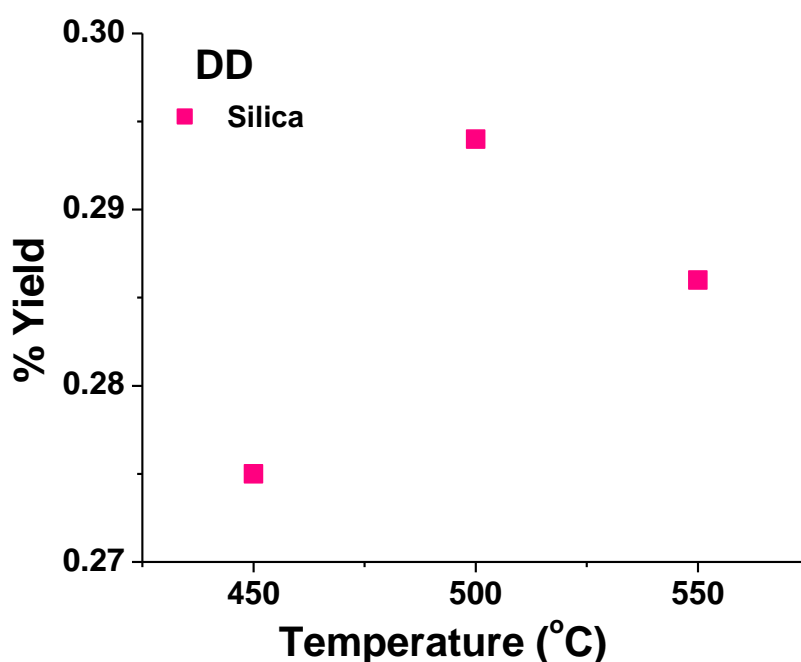
Figure 4.13 % Yields of DD produced on silica from 450 to 550 °C due to *de novo* synthesis and gas-phase conversion of 2-MCP.

4.4   Metal-oxide catalysts prepared by the WI-M method

NiO, CuO, and NiO-CuO (1:1) catalysts were prepared by the WI-M method in order to investigate possible differences in the catalytic activity that may be based on the respective preparation steps in the WI-D and the WI-M methods. A procedure similar to that in Section 4.3 was implemented to test the catalysts prepared by the WI-M method. The precursor 2-MCP %

recoveries are displayed in Figure 4.14 for the three catalysts tested. About 90–95% of 2-MCP was converted to products (5–10% recovery) at 300 °C, and nearly complete 2-MCP conversion was achieved above 450 °C. However, NiO-CuO (1:1) demonstrated lower reactivity in converting 2-MCP compared to NiO and CuO (~86% conversion). There was no significant difference in the 2-MCP % recoveries when catalysts of the WI-D and the WI-M were compared. DCP and TCP were not observed with these catalysts under the reaction conditions, which is strikingly different from WI-D catalysts. Such difference may associate with the difference in the synthetic route of the WI-D catalyst vs the WI-M catalyst.

Figure 4.14 % Recoveries of 2-MCP on silica-supported metal-oxide catalysts (prepared by the WI-M) from 300 to 550 °C. Experiments were performed in triplicate.

MCBz and DCBz were observed by the surface-mediated pyrolysis of 2-MCP on NiO, CuO, and NiO-CuO (1:1) as displayed in Figure 4.15. Significantly higher % yields of MCBz and DCBz were observed with NiO-CuO (1:1) when compared to the other two catalysts. The

86

highest % yields of MCBz (0.045 ± 0.002%) and DCBz (0.207 ± 0.014%) were obtained at 300 °C. The NiO-CuO (1:1) catalyst displayed a higher activity compared to individual metal oxides. Comparison of the results from the WI-D and the WI-M did not display any noticeable difference in the % yields.

All three dioxin congeners previously identified in Section 4.3 were also found when using catalysts prepared by the WI-M method. DD, MCDD, and DCDD were observed with the three catalysts at each temperature studied. DD, MCDD, and DCDD % yields gradually increased with temperature, reaching a maximum around 400–500 °C, followed by a decrease in % yield at 550 °C (Figures 4.16, 4.17, and 4.18), which is in agreement with the % yield trends observed with catalysts prepared by the WI-D method in Section 4.3. NiO-CuO (1:1) generated higher % yields of DD and MCDD compared to individual metal oxides, which is also in agreement with NiO-CuO (1:1) prepared by the WI-D method. However, DBF was not observed with WI-M catalysts at any temperature, indicating the difference in catalytic activity between WI-M and WI-D catalysts. The highest % yields of dioxins and their respective temperatures are depicted in Table 4.6.

Table 4.6 The highest % yields of DD, MCDD, and DCDD with respective temperatures. Experiments were performed in triplicate.

Catalyst on Silica	DD		MCDD		DCDD	
	% Yield	Temp (°C)	% Yield	Temp (°C)	% Yield	Temp (°C)
NiO	1.08 ± 0.08	500	0.40 ± 0.02	450	1.44 ± 0.14	450
CuO	1.83 ± 0.16	450	1.48 ± 0.06	450	0.62 ± 0.03	500
NiO-CuO (1:1)	2.45 ± 0.11	500	1.60 ± 0.05	450	1.15 ± 0.05	450

A.

B.
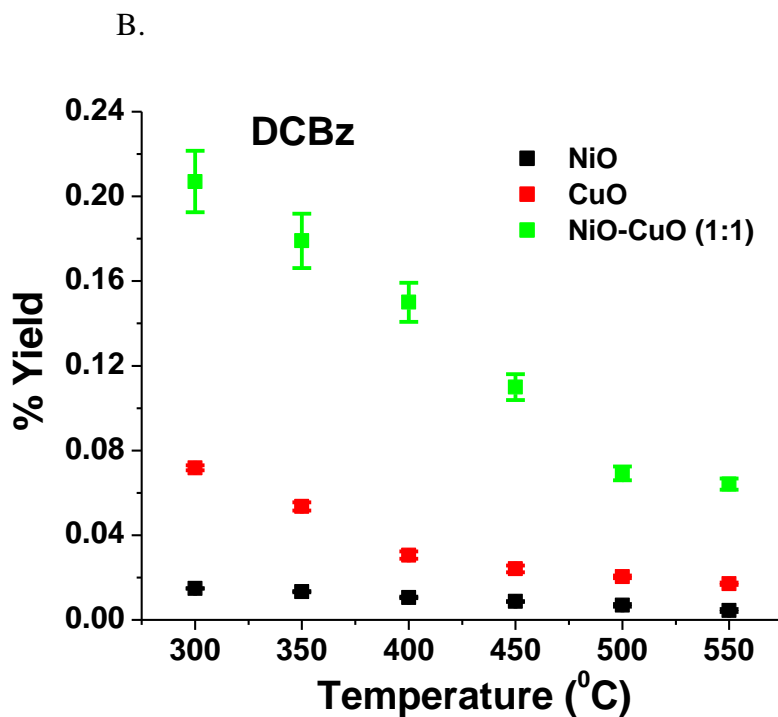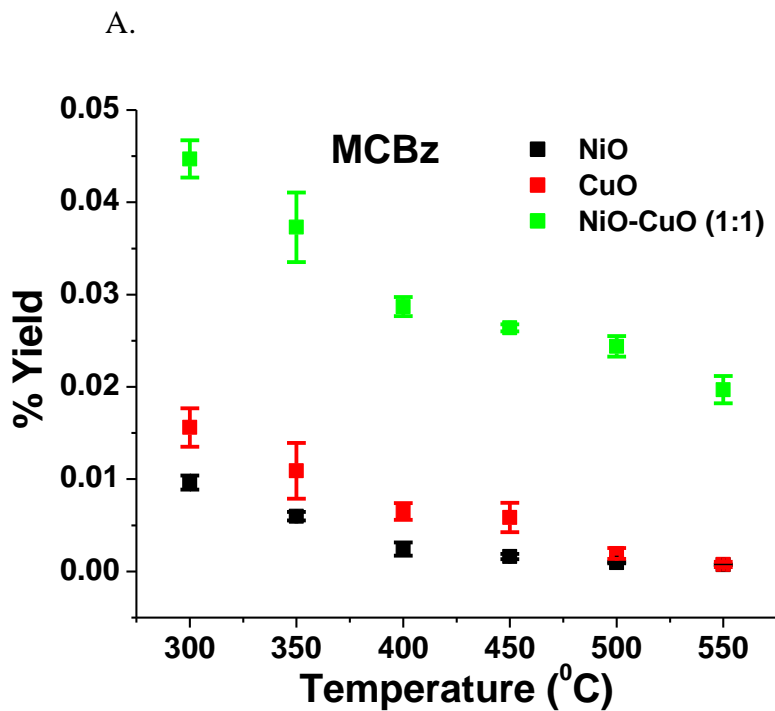
Figure 4.15 % Yields of A. MCBz and B. DCBz produced from 2-MCP on silica-supported, metal-oxide catalysts (prepared by the WI-M) from 300 to 550 °C. Experiments were performed in triplicate.
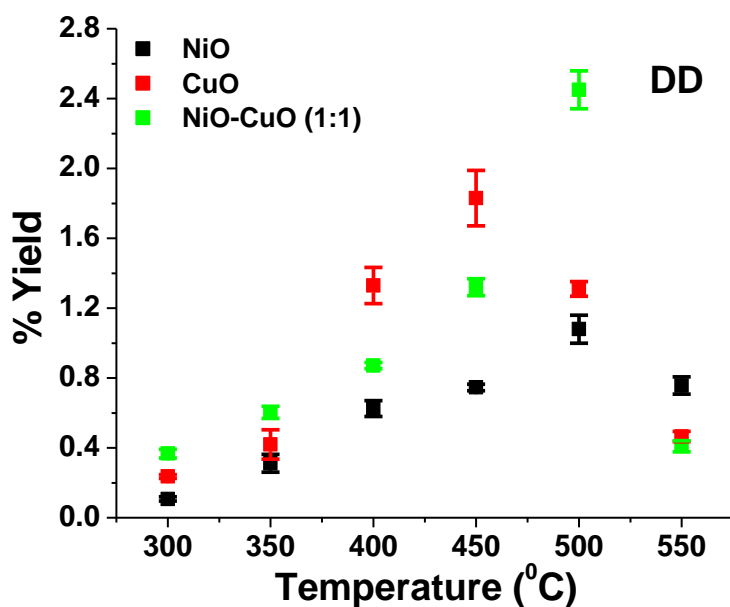
Figure 4.16 % Yields of dibenzo-*p*-dioxin (DD) produced on silica-supported, metal-oxide catalysts (prepared by the WI-M) from 300 to 550 °C. Experiments were performed in triplicate.
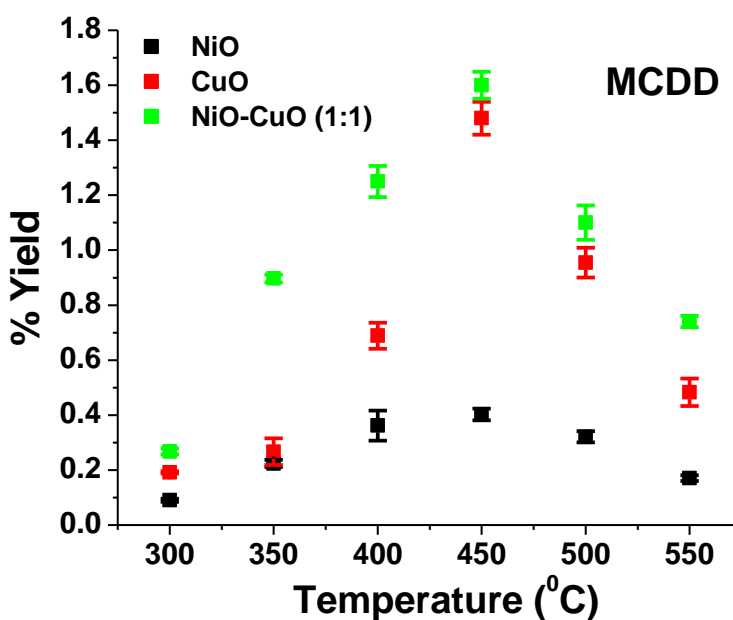
Figure 4.17 % Yields of monochloro-dibenzo-*p*-dioxin (MCDD) produced on silica-supported, metal-oxide catalysts (prepared by the WI-M) from 300 to 550 °C. Experiments were performed in triplicate.

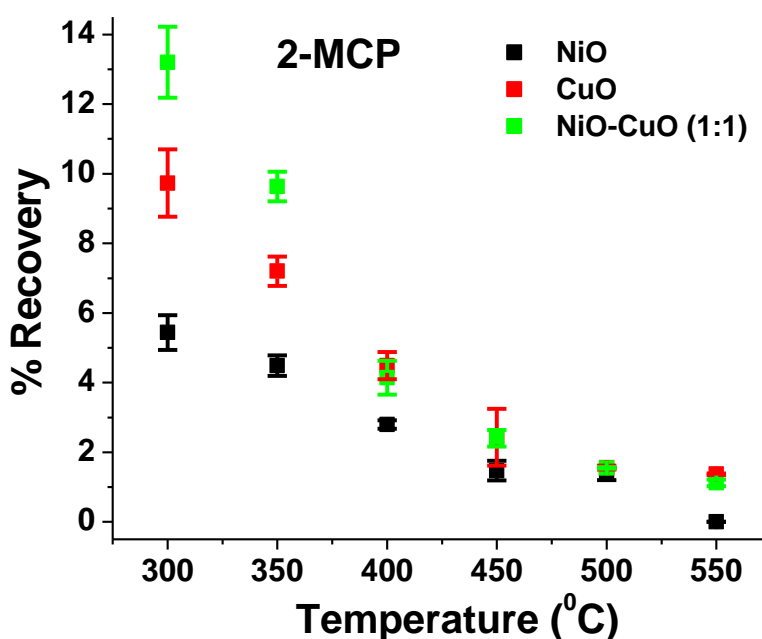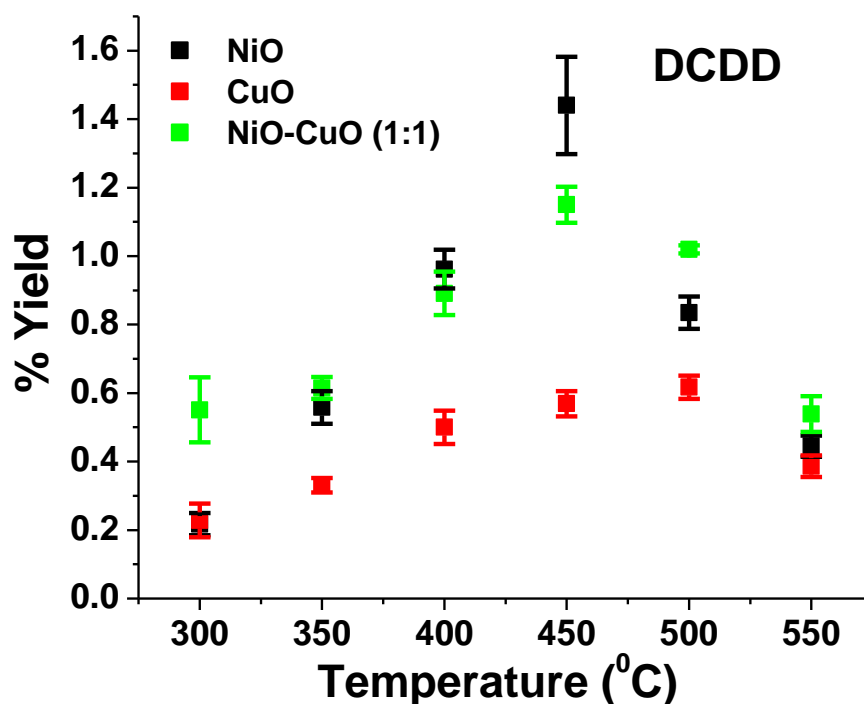Figure 4.18 % Yields of dichloro-dibenzo-*p*-dioxin (DCDD) produced on silica-supported, metal-oxide catalysts (prepared by the WI-M) from 300 to 550 °C. Experiments were performed in triplicate.

4.5   Proposed mechanisms of PCDD/Fs formation

The conversion of precursor molecules (chlorophenols and chlorobenzenes) to PCDD/Fs on transition metal-oxide catalysts has been shown to initiate with the adsorption of 2-MCP to the metal oxides.[3, 28-30] The surface-bound 2-MCP molecule may follow two different pathways on the catalytic surface, namely, the Eley–Rideal pathway or the Langmuir–Hinshelwood pathway.[7-8, 27-28, 31] The Eley–Rideal pathway provides support for the reactions of surface-bound 2-MCP with gas-phase precursor molecules (2-MCP, DCP, TCP, and DCBz); whereas, the Langmuir–Hinshelwood pathway offers a route for the reactions of two surface-bound precursor molecules.

90

The adsorption of 2-MCP onto the catalytic surface occurs at temperatures higher than 150 °C via hydrogen bonding between –OH groups on the metal-oxide sites and the –OH group of 2-MCP, followed by an elimination of a water molecule (Scheme 4.1A–4.1B).[9, 28] Following the proposed mechanism in literature, subsequent reduction of the transition metal center leads to the formation of a stable chlorophenoxyl radical-cation, as depicted in Scheme 4.1C.[5, 9, 28, 32-35] Because the reaction was carried out under pyrolytic conditions (ultra-high pure helium in the gas phase), the metal-oxide sites act as the source of oxygen for oxidation processes.[8] The oxygen exists in different forms (O_2^-, O_2^{2-}, O^-, and O^{2-}) inside the metal-oxide lattice.[36-37] These oxygen species are in dynamic equilibrium with each other and are stabilized by coordination with metal ions. They are indistinguishable at higher temperatures (< 250 °C) due to their rapid interconversion.[36] These oxygen species in the metal-oxide lattice (represented by O_L^- in schemes) react with chlorophenoxyl radical-cations to form a neutral molecule attached to the lattice (Scheme 4.1C – 4.1E).[37] The transfer of electron from the lattice to the benzene ring is compensated by the oxidation of the metal center back to +2 oxidation state. Subsequent hydrolysis of the molecule leads to the formation of surface-bound chlorinated phenol (Scheme 4.1F).

Adsorption of 1,2-DCBz also leads to the formation of chlorophenoxyl radical-cation identical to the one from 2-MCP (Scheme 4.2). Therefore, 1,2-DCBz also converts to surface-bound chlorinated phenol molecules, ultimately forming to PCDD/Fs at higher temperatures as observed by their % yields (Figure 4.5 D and 4.11B). Pyrolytic conditions under helium create an oxygen deficient environment where PCDD/Fs were stable above 325 °C, and 2-MCP was stabilized on the metal-oxide sites rather than becoming oxidized.[7]

91
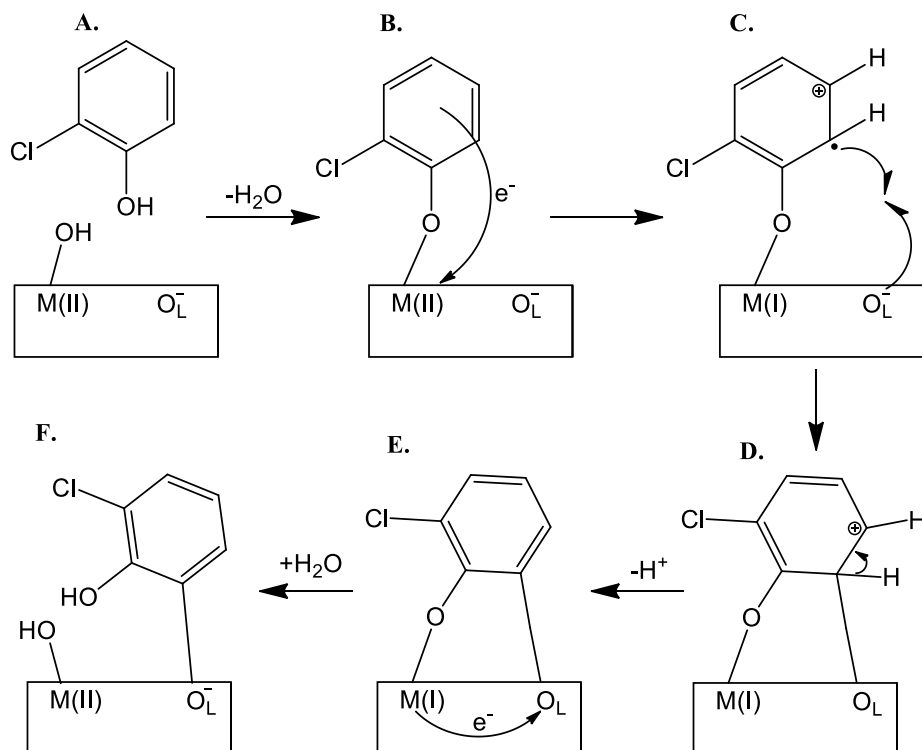
Scheme 4.1 Proposed mechanism for the chemisorption of 2-MCP on metal-oxide sites followed by the formation of surface-bound chlorinated phenol.
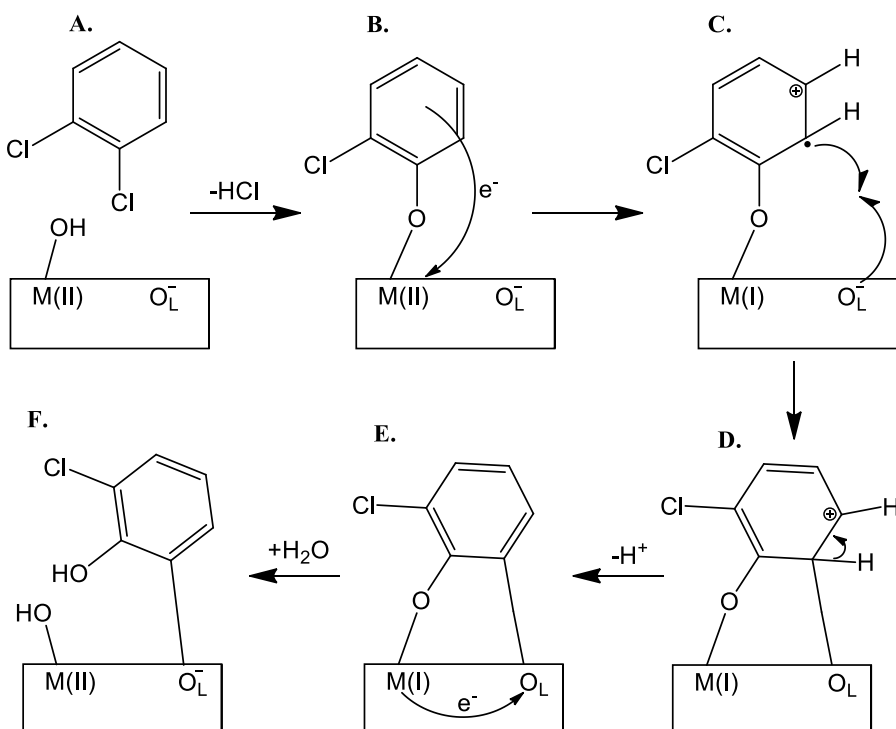
Scheme 4.2 Proposed mechanism for the chemisorption of 1,2-DCBz on metal-oxide sites followed by the formation of surface-bound chlorinated phenol.

The surface-bound chlorinated phenol reacts with gas phase 2-MCP to form DD and MCDD via the Eley–Rideal pathway. A nucleophilic attack of the –OH group in gas-phase 2-MCP on the C–Cl bond of surface-bound chlorinated phenol leads to the formation of DD (Scheme 4.3A); whereas, a nucleophilic attack of the –OH in surface-bound chlorinated phenol on the C–Cl bond of gas-phase 2-MCP leads to MCDD (Scheme 4.3B).[7-8] Due to similarities in the % yields of DD vs MCDD over different catalysts, both pathways are believed to have an equal probability under the reaction conditions studied.

A.

B.
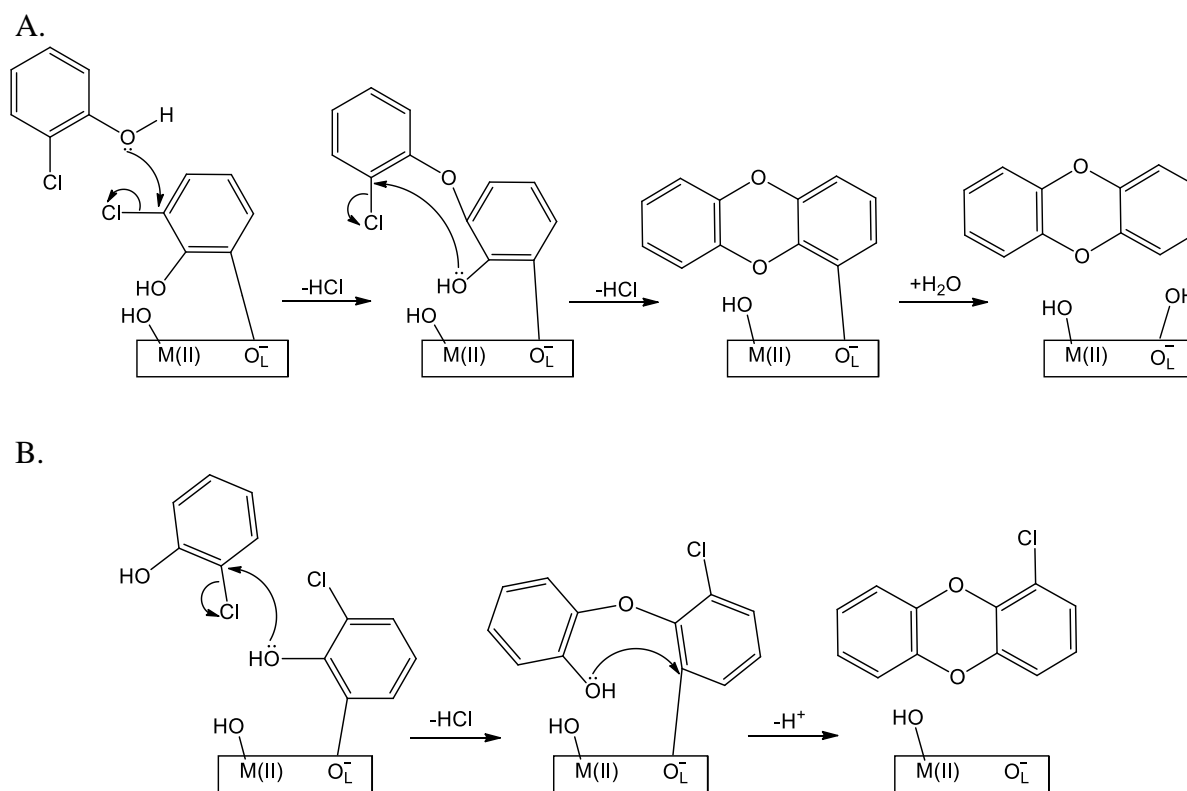
Scheme 4.3 Eley–Rideal reaction pathway of surface-bound chlorinated phenol with gas phase 2-MCP to form; A. DD and B. MCDD.

DCP and TCP, generated during the surface-mediated reactions, are presumed to further react with surface-bound chlorinated phenol to form chlorinated dioxins such as MCDD and DCDD[8] (Scheme 4.4). This is related to the observation of lower % yields of DCP and TCP with increasing reaction temperature for WI-D catalysts. However, DCP or TCP were not observed

with WI-M catalysts, accounting for a difference in catalytic activity of the WI-M catalysts compared to the WI-D catalysts. Such difference in catalytic activity may be due to the difference in synthetic route between the WI-M and the WI-D methods. Previous studies on the reactions of 2-MCP on CuO catalysts suggested that PCDDs are also formed due to the chlorination of DD on the catalytic surface.[7-8] However, there was no such relationship between the % yields of DD and MCDD/DCDD to corroborate surface-assisted chlorination under the conditions studied.
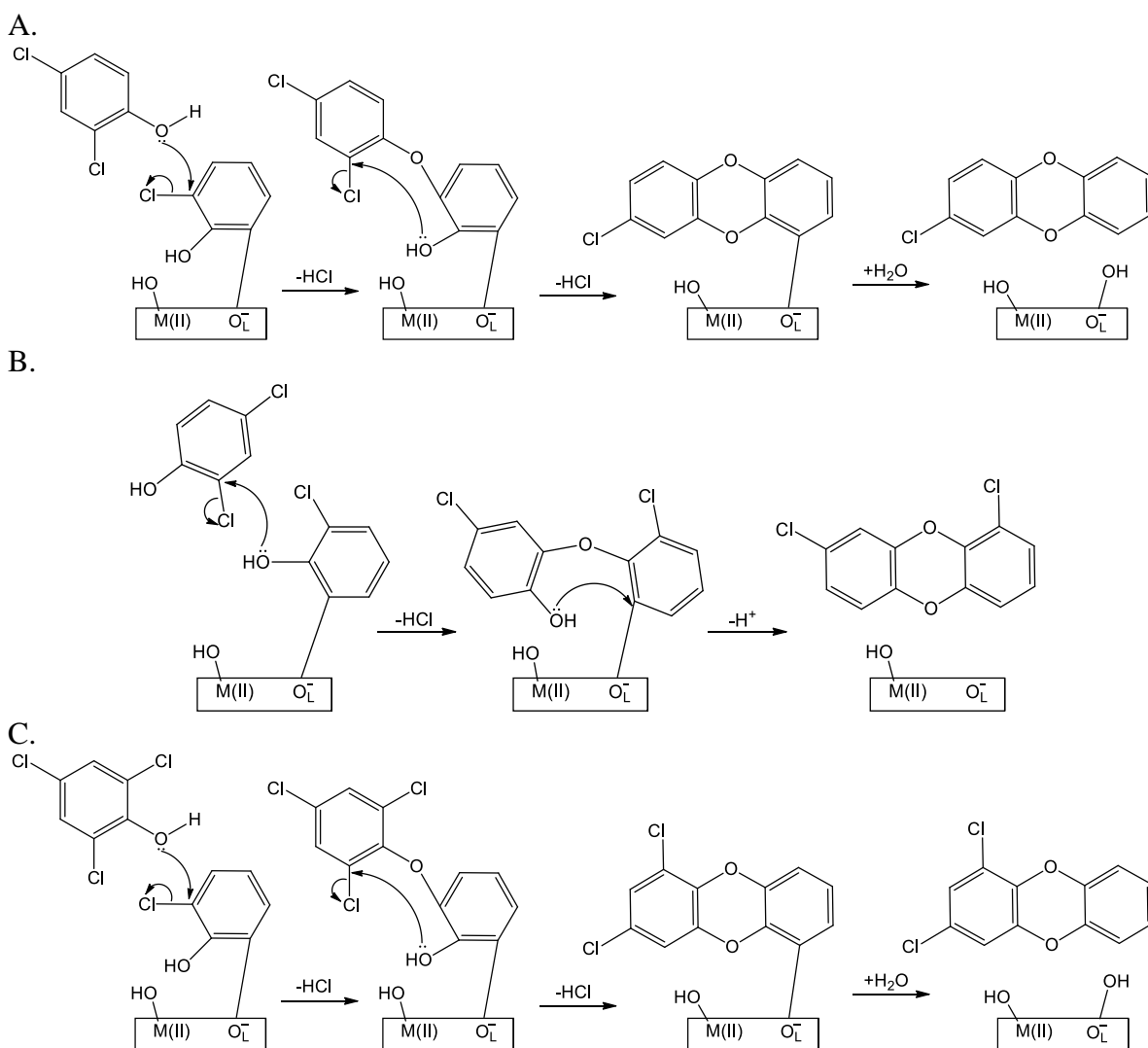
Scheme 4.4 Eley–Rideal reaction pathway of surface-bound chlorinated phenol with gas phase precursor molecules; A. DCP to MCDD, B. DCP to DCDD, and B. TCP to DCDD.

The adsorption of 2-MCP on metal-oxide sites is proposed to occur via elimination of a water molecule, as previously discussed in Scheme 4.1. A nucleophilic attack from a surface – OH group on the C–Cl bond in the aromatic ring leads to the formation of a bidentate intermediate radical-cation, following reduction of the metal center, as illustrated in Scheme 4.5A.[5, 9, 33-34] An electronic rearrangement of the bidentate intermediate radical-cation with the oxidation of metal center leads to the formation of a surface-bound phenoxyl radical (Scheme 4.5B). Formation of DBF occurs via Langmuir–Hinshelwood pathway[38] where two surface-bound phenoxyl radicals react on the catalytic surface, as displayed Scheme 4.6. Each radical then forms a bond between the two aromatic rings, which removes one aromatic ring from the catalytic surface. The –OH group on the free aromatic ring acts as a nucleophile thus, attacking the C–O bond of the surface-bound aromatic ring thereby forming DBF via a transition state (≠).
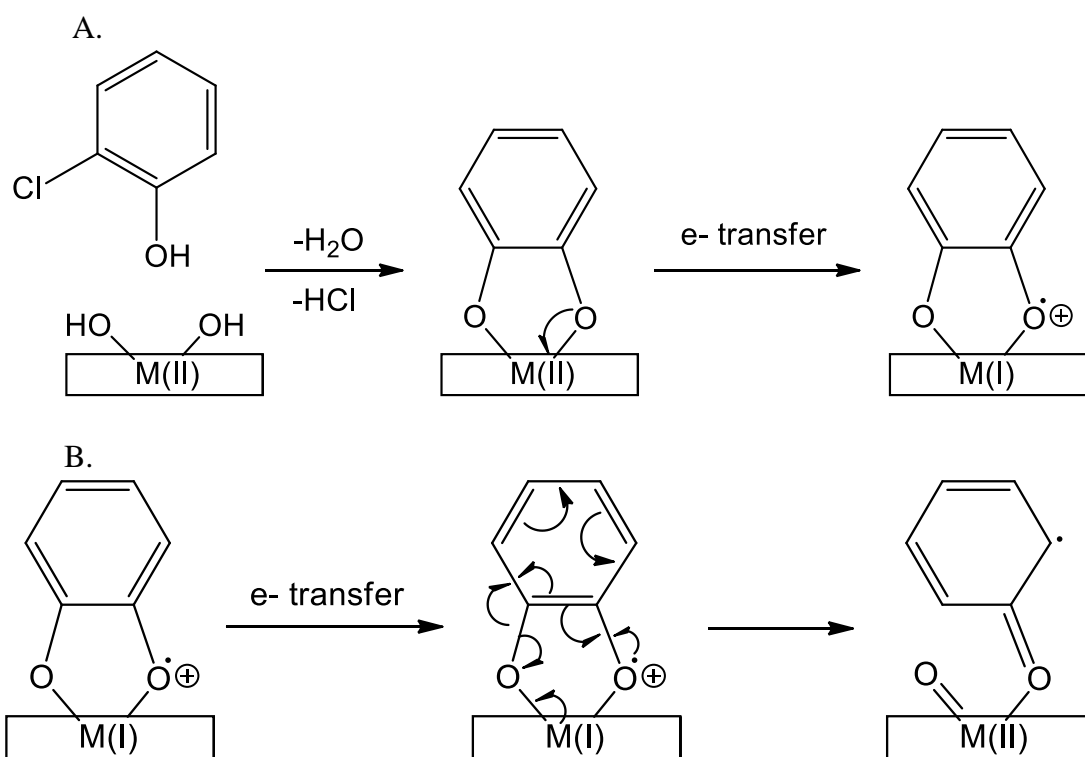
Scheme 4.5 Proposed mechanisms A. Chemisorption of 2-MCP on metal-oxide sites via bidentate intermediate radical-cation and B. Rearrangement of the intermediate to form surface-bound phenoxyl radical.
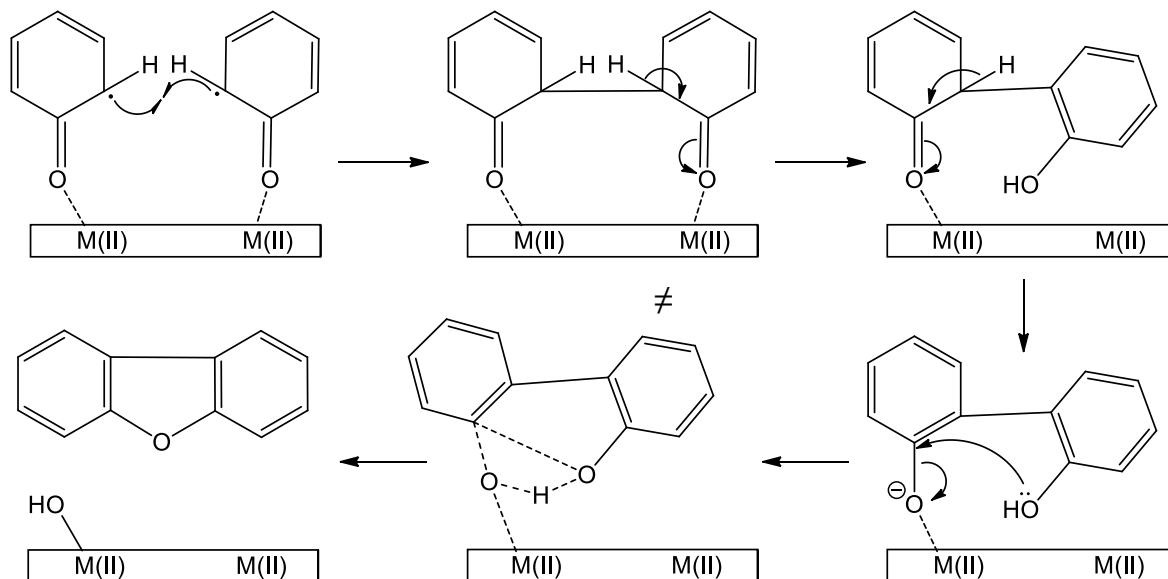
Scheme 4.6 Langmuir–Hinshelwood pathway for the formation of dibenzofuran (DBF) via reaction of two surface-bound phenoxyl radicals.

There are several studies confirming the formation of radicals upon adsorption of precursor molecules (MCBz, DCBz, phenol, and 2-MCP) on silica-supported metal-oxide catalysts of ZnO,[35] CuO,[34] NiO,[33] and Fe_2O_3.[32] The formation of PCDD over DBF depends on whether the formation of chlorophenoxyl radical-cation (Scheme 4.1C) or bidentate intermediate radical-cation (Scheme 4.5A) is favored upon the adsorption of 2-MCP. Reaction of the oxygen species (O_L^-) in the metal-oxide lattice with the chlorophenoxyl radical-cation is driven by the positive charge on the aromatic ring (Scheme 4.1C). However, the rearrangement product of the bidentate intermediate radical-cation (phenoxyl radical) does not have a positive charge as a driving force to react with the oxygen species (O_L^-) (Scheme 4.5B). Hence, a chlorophenoxyl radical-cation converts to surface-bound chlorinated phenol, and further reacts with the gas-phase precursor molecules via the Eley–Rideal pathway to yield DD, MCDD, and DCDD. The phenoxyl radical only reacts with identical species in the proximity to undergo the Langmuir–Hinshelwood pathway to yield DBF. According to this study, DBF was only observed with CuO

catalysts prepared by the WI-D method, and none of the other catalysts produced any DBF or PCDF at any temperature. This is a good indication for the formation of the chlorophenoxyl radical-cation, followed by its conversion to surface-bound chlorinated phenol is favored over the formation of the bidentate intermediate radical-cation, followed by the phenoxyl radical. The Eley–Rideal pathway dominates over the Langmuir–Hinshelwood pathway during these studies to form more dioxins than furans over silica-supported NiO, CuO, and NiO-CuO catalysts.

4.6   Thermogravimetric analysis (TGA) of silica-supported metal oxides

Silica surfaces absorb a great deal of water when exposed to air. The removal of surface bound water (dehydration) was important before the surface-mediated reaction even though the effect of water on the formation of PCDD/Fs has not been clearly interpreted.[39-42] Previous studies illustrated that the surface-bound water molecules are removed at 150 °C while keeping the surface –OH groups intact, which are not removed until 1200 °C.[43] The activation of the catalyst (450 °C in 20% O_2 + 80% N_2) before every reaction removed the surface-bound water and prepared the catalytic surface for the reaction.

Thermogravimetric analysis on metal-oxide catalysts was performed to determine the changes in weight during the surface-mediated reaction. Temperatures and other conditions were maintained similar to the Section 4.2 to mimic the conditions inside the quartz reactor during the surface-mediated reaction. The initial weight of the catalyst (~3 mg) was recorded and the temperature was increased to 450 °C and maintained for 1 h (activation) in breathing air (20% O_2 + 80% N_2). Then helium gas was introduced into the system and held for another 1 h at 450 °C. This procedure was repeated by starting at 450 °C in breathing air and changing the temperature to 350 °C and 550 °C simultaneously with helium. TGA curves of the NiO/silica catalyst for all three temperatures are displayed in Figure 4.19A. A drastic %weight loss (~4%) was observed

97

within the first 10 min indicating the removal of surface-bound water. Another 2% of the weight was lost within the next 30 min indicating the removal of chemically bound water. When the system approached 450 °C, the weight was stabilized, and there was no significant weight loss during the next 60 min. A ~1% weight gain around 100 min was observed when helium was introduced, indicating the adsorption of helium into the pores of the silica. A similar pattern was observed when silica was used in the same process, as displayed in Figure 4.19B. The helium atom is smaller than the O_2 molecule, allowing it to fill up all the silica pores inaccessible to O_2 molecules. Nitrogen is a diatomic molecule (N_2) similar in size to O_2 and as inert as helium, so the experiment was repeated with nitrogen as a substitute for helium. There was no increase in weight% for NiO/silica (Figure 4.20A) and silica (Figure 4.20B) at 100 min when nitrogen was introduced into the system, confirming the previous hypothesis. A substitute for helium presents a better understanding of whether the weight gain is due to filling the pores or a helium-silica specific interaction. Hydrogen (H_2) is a good substitute due to the similar molecular size to helium. However, H_2 is more reactive than helium and is reported to reduce metal-oxides (NiO) on silica surfaces under the temperatures studied.[44] Helium is an inert gas and adsorption on to silica surfaces was presumed not to interfere with the surface-mediated reactions of 2-MCP because 2-MCP binds to the metal-oxide sites via hydrogen bonds followed by resonance stabilization. This drives the binding of 2-MCP to the metal-oxide sites over binding of helium via non-polar interactions.
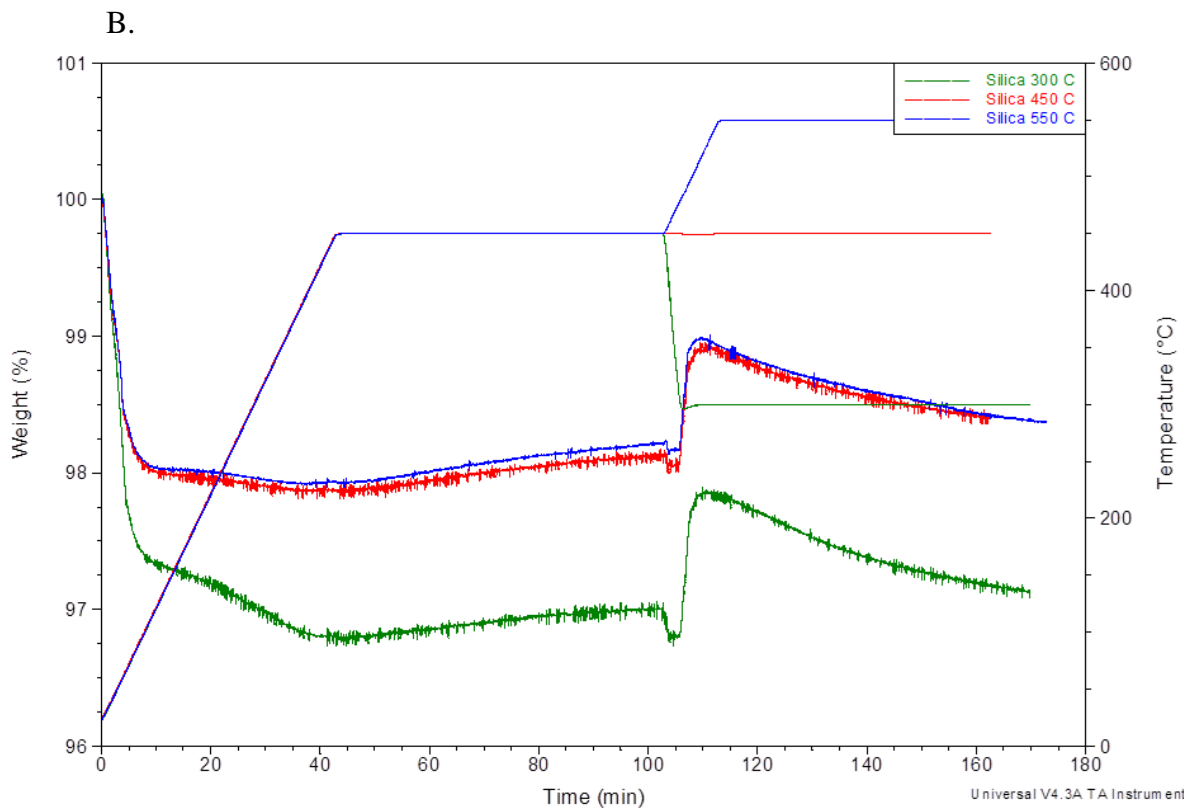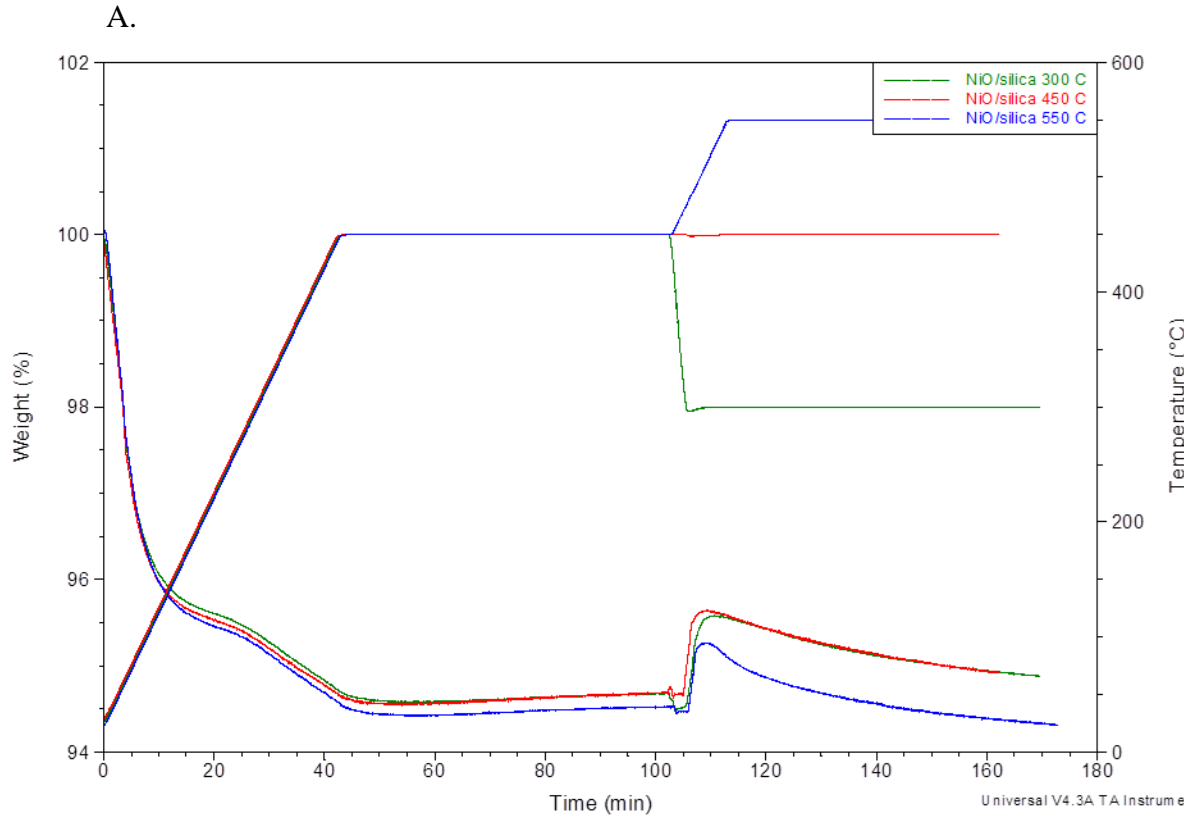
98

Figure 4.19 TGA curve for A. NiO/silica and B. silica, under 20% O_2 + 80% N_2 at 450 °C, followed by 300 °C, 450 °C, and 550 °C under helium atmosphere.
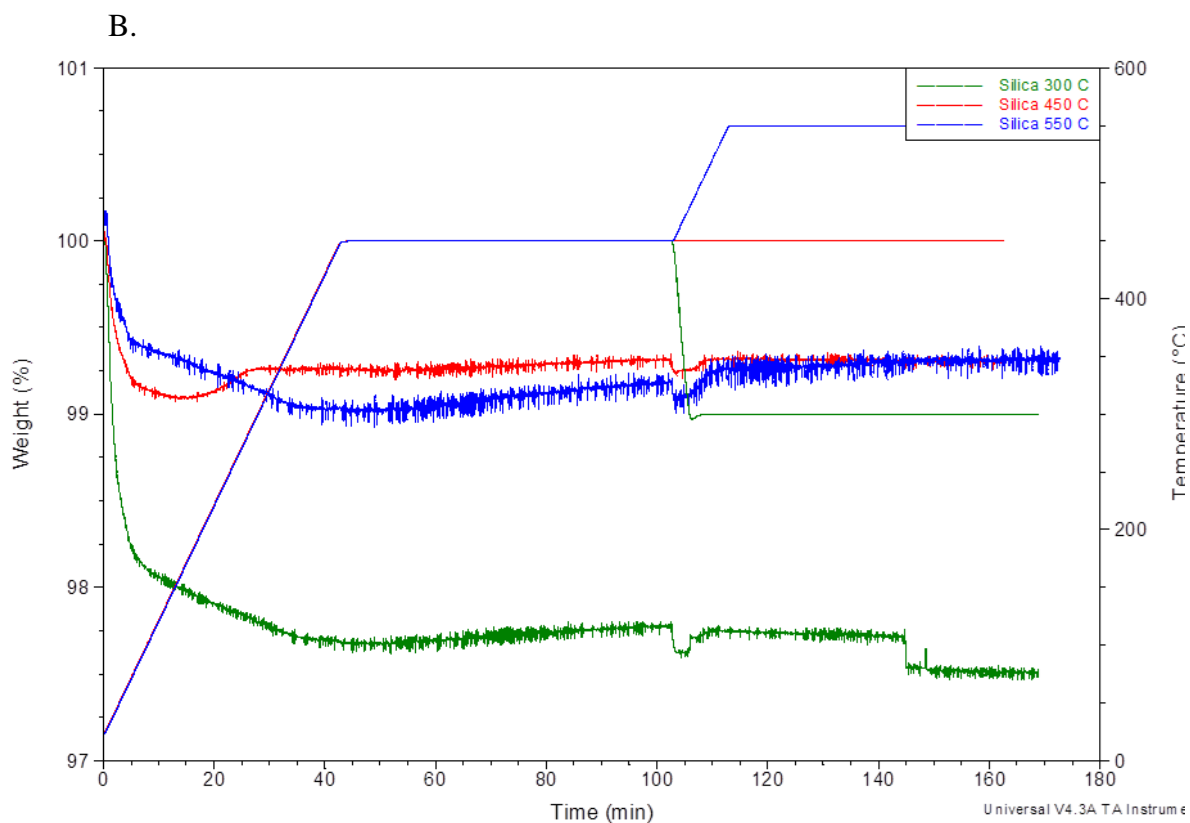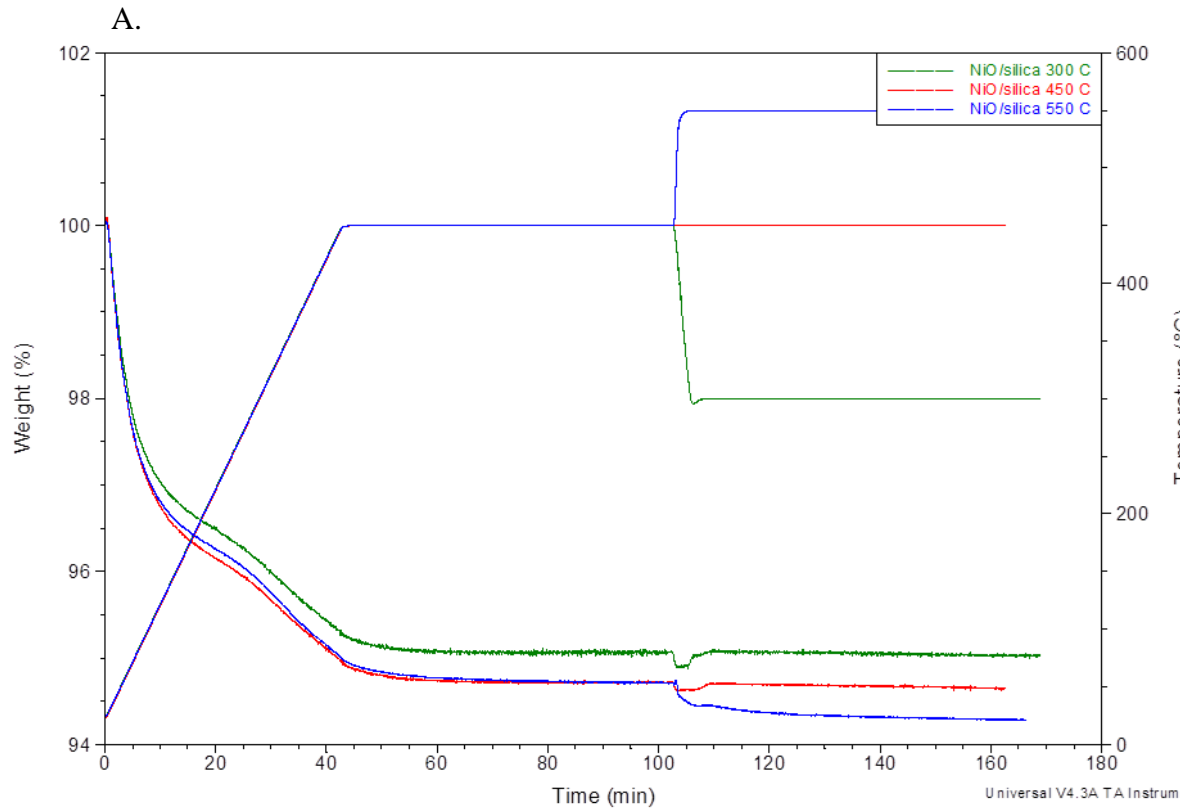
Figure 4.20 TGA curve for A. NiO/silica and B. silica, under 20% O_2 + 80% N_2 at 450 °C, followed by 300 °C, 450 °C, and 550 °C under nitrogen atmosphere.

100

4.7   References

1.   Addink, R.; Olie, K., Mechanisms of Formation and Destruction of Polychlorinated Dibenzo-*p*-dioxins and Dibenzofurans in Heterogeneous Systems. *Environmental Science & Technology* **1995,** *29* (6), 1425-1435.

2.   Briois, C., Temperature and concentration effects on the dioxin and furan formation from a mixture of chlorophenols over fly ash. *Organohalogen Compounds* **2006,** *68*, 1209.

3.   Altarawneh, M.; Dlugogorski, B. Z.; Kennedy, E. M.; Mackie, J. C., Mechanisms for formation, chlorination, dechlorination and destruction of polychlorinated dibenzo-p-dioxins and dibenzofurans (PCDD/Fs). *Progress in Energy and Combustion Science* **2009,** *35* (3), 245-274.

4.   Ryu, J.-Y.; Mulholland, J. A.; Kim, D. H.; Takeuchi, M., Homologue and Isomer Patterns of Polychlorinated Dibenzo-*p*-dioxins and Dibenzofurans from Phenol Precursors: Comparison with Municipal Waste Incinerator Data. *Environmental Science & Technology* **2005,** *39* (12), 4398-4406.

5.   Nganai, S.; Lomnicki, S. M.; Dellinger, B., Formation of PCDD/Fs from the Copper Oxide-Mediated Pyrolysis and Oxidation of 1,2-Dichlorobenzene. *Environmental Science & Technology* **2010,** *45* (3), 1034-1040.

6.   Wienecke, J.; Kruse, H.; Wassermann, O., Organic compounds in the waste gasification and combustion process. *Chemosphere* **1992,** *25* (4), 437-447.

7.   Lomnicki, S.; Dellinger, B., A Detailed Mechanism of the Surface-Mediated Formation of PCDD/F from the Oxidation of 2-Chlorophenol on a CuO/Silica Surface. *The Journal of Physical Chemistry A* **2003,** *107* (22), 4387-4395.

8.   Lomnicki, S.; Dellinger, B., Formation of PCDD/F from the pyrolysis of 2-chlorophenol on the surface of dispersed copper oxide particles. *Proceedings of the Combustion Institute* **2002,** *29* (2), 2463-2468.

9.   Nganai, S.; Lomnicki, S.; Dellinger, B., Ferric Oxide Mediated Formation of PCDD/Fs from 2-Monochlorophenol. *Environmental Science & Technology* **2008,** *43* (2), 368-373.

10.   Chen, Y.; Shah, N.; Huggins, F. E.; Huffman, G. P., Investigation of the Microcharacteristics of $PM_{2.5}$ in Residual Oil Fly Ash by Analytical Transmission Electron Microscopy. *Environmental Science & Technology* **2004,** *38* (24), 6553-6560.

11.   Öberg, T.; Öhrström, T.; Bergström, J., Metal catalyzed formation of chlorinated aromatic compounds: A study of the correlation pattern in incinerator fly ash. *Chemosphere* **2007,** *67* (9), S185-S190.

12.   Allouis, C.; Beretta, F.; D'Alessio, A., Structure of inorganic and carbonaceous particles emitted from heavy oil combustion. *Chemosphere* **2003,** *51* (10), 1091-1096.

13. Eric, H.; Timuçin, M., Equilibrium relations in the system nickel oxide-copper oxide. *MTB* **1979,** *10* (4), 561-563.

14. Kellogg, H. H., Thermodynamic properties of the oxide of copper and nickel. *Journal of chemical and Engineering Data* **1969,** *14* (1), 41-4.

15. Mainardi, D. S.; Balbuena, P. B., Monte Carlo Simulation of Cu−Ni Nanoclusters: Surface Segregation Studies. *Langmuir* **2001,** *17* (6), 2047-2050.

16. Bohannan, E. W.; Kothari, H. M.; Nicic, I. M.; Switzer, J. A., Enantiospecific Electrodeposition of Chiral CuO Films on Single-Crystal Cu(111). *Journal of the American Chemical Society* **2003,** *126* (2), 488-489.

17. Pabi, S. K.; Joardar, J.; Manna, I.; Murty, B. S., Nanocrystalline phases in Cu-Ni, Cu-Zn and Ni-Al systems by mechanical alloying. *Nanostructured Materials* **1997,** *9* (1–8), 149-152.

18. Hristova, E.; Dong, Y.; Grigoryan, V. G.; Springborg, M., Structural and Energetic Properties of Ni−Cu Bimetallic Clusters. *The Journal of Physical Chemistry A* **2008,** *112* (34), 7905-7915.

19. Born, J. G. P.; Mulder, P.; Louw, R., Fly ash mediated reactions of phenol and monochlorophenols: oxychlorination, deep oxidation, and condensation. *Environmental Science & Technology* **1993,** *27* (9), 1849-1863.

20. Marinkovic, N.; Pasalic, D.; Ferencak, G.; Grskovic, B.; Stavljenic Rukavina, A., Dioxins and human toxicity. *Archives of Industrial Hygiene and Toxicology* **2010,** *61* (4), 445-453.

21. Addink, R.; Drijver, D. J.; Olie, K., Formation of polychlorinated dibenzo-*p*-dioxins/dibenzofurans in the carbon/fly ash system. *Chemosphere* **1991,** *23* (8–10), 1205-1211.

22. Stieglitz, L.; Zwick, G.; Beck, J.; Roth, W.; Vogg, H., On the *de novo* synthesis of PCDD/PCDF on fly ash of municipal waste incinerators. *Chemosphere* **1989,** *18* (1–6), 1219-1226.

23. Milligan, M. S.; Altwicker, E., The relationship between *de novo* synthesis of polychlorinated dibenzo-*p*-dioxins and dibenzofurans and low-temperature carbon gasification in fly ash. *Environmental Science & Technology* **1993,** *27* (8), 1595-1601.

24. Addink, R., Bakker, WCM, Olie, K, Influence of H_2O and HCl on the formation of polychlorinated dibenzo-*p*-dioxins/dibenzofurans in a carbon/fly ash mixture. *Organohalogen Compounds* **1992,** *8*, 205 - 208.

25. Schwarz, G., Stieglitz, L, Roth, W Formation Conditions of Several Polychlorinated Compound Classes on Fly Ash of a Municipal Waste Incinerator. *Organohalogen Compounds* **1990,** *3*, 169 - 172.

26. Gullett, B. K.; Bruce, K. R.; Beach, L. O.; Drago, A. M., Mechanistic steps in the production of PCDD and PCDF during waste combustion. *Chemosphere* **1992,** *25* (7–10), 1387-1392.

27. Alderman, S. L.; Dellinger, B., FTIR Investigation of 2-Chlorophenol Chemisorption on a Silica Surface from 200 to 500 °C. *The Journal of Physical Chemistry A* **2005,** *109* (34), 7725-7731.

28. Alderman, S. L.; Farquar, G. R.; Poliakoff, E. D.; Dellinger, B., An Infrared and X-ray Spectroscopic Study of the Reactions of 2-Chlorophenol, 1,2-Dichlorobenzene, and Chlorobenzene with Model CuO/Silica Fly Ash Surfaces. *Environmental Science & Technology* **2005,** *39* (19), 7396-7401.

29. Milligan, M. S.; Altwicker, E. R., Chlorophenol Reactions on Fly Ash. 1. Adsorption/Desorption Equilibria and Conversion to Polychlorinated Dibenzo-*p*-dioxins. *Environmental Science & Technology* **1995,** *30* (1), 225-229.

30. Milligan, M. S.; Altwicker, E. R., Chlorophenol Reactions on Fly Ash. 2. Equilibrium Surface Coverage and Global Kinetics. *Environmental Science & Technology* **1995,** *30* (1), 230-236.

31. Farquar, G. R.; Alderman, S. L.; Poliakoff, E. D.; Dellinger, B., X-ray Spectroscopic Studies of the High Temperature Reduction of Cu(II)O by 2-Chlorophenol on a Simulated Fly Ash Surface. *Environmental Science & Technology* **2003,** *37* (5), 931-935.

32. Vejerano, E.; Lomnicki, S.; Dellinger, B., Formation and Stabilization of Combustion-Generated Environmentally Persistent Free Radicals on an $Fe(III)_2O_3$/Silica Surface. *Environmental Science & Technology* **2010,** *45* (2), 589-594.

33. Vejerano, E.; Lomnicki, S. M.; Dellinger, B., Formation and Stabilization of Combustion-Generated, Environmentally Persistent Radicals on Ni(II)O Supported on a Silica Surface. *Environmental Science & Technology* **2012,** *46* (17), 9406-9411.

34. Lomnicki, S.; Truong, H.; Vejerano, E.; Dellinger, B., Copper Oxide-Based Model of Persistent Free Radical Formation on Combustion-Derived Particulate Matter. *Environmental Science & Technology* **2008,** *42* (13), 4982-4988.

35. Vejerano, E.; Lomnicki, S.; Dellinger, B., Lifetime of combustion-generated environmentally persistent free radicals on Zn(ii)O and other transition metal oxides. *Journal of Environmental Monitoring* **2012,** *14* (10), 2803-2806.

36. Khachatryan, L.; Lomnicki, S.; Dellinger, B., An expanded reaction kinetic model of the CuO surface-mediated formation of PCDD/F from pyrolysis of 2-chlorophenol. *Chemosphere* **2007,** *68* (9), 1741-1750.

37. Gabriele Centi, F. C., Ferruccio Trifiro, *Selective oxidation by heterogeneous catalysis*. Kluwer Academic/Plenum Publishers, 233 Spring Street, New York, NY 10013: 2001.

103

38. Vejerano, E. P.; Holder, A. L.; Marr, L. C., Emissions of Polycyclic Aromatic Hydrocarbons, Polychlorinated Dibenzo-*p*-Dioxins, and Dibenzofurans from Incineration of Nanomaterials. *Environmental Science & Technology* **2013,** *47* (9), 4866-4874.

39. Jay, K.; Stieglitz, L., On the mechanism of formation of polychlorinated aromatic compounds with copper(II) chloride. *Chemosphere* **1991,** *22* (11), 987-996.

40. Wania, F.; Lenoir, D., Copper-pronoted reactions of polybroninated dibenzo-*p*-dioxins (PBrDD). *Chemosphere* **1990,** *21* (3), 417-432.

41. Stieglitz, L.; Zwick, G.; Beck, J.; Bautz, H.; Roth, W., The role of particulate carbon in the *de novo* synthesis of polychlorinated dibenzodioxins and-furans in fly-ash. *Chemosphere* **1990,** *20* (10–12), 1953-1958.

42. Ross, B. J.; Lacombe, D.; Naikwadi, K. P.; Karasek, F. W., Investigation of the effect of water, acids, and bases in the gas stream in the catalytic formation of PCDD and PCDF over MSW fly ash. *Chemosphere* **1990,** *20* (10–12), 1967-1972.

43. Zhuravlev, L. T., The surface chemistry of amorphous silica. Zhuravlev model. *Colloids and Surfaces A: Physicochemical and Engineering Aspects* **2000,** *173* (1–3), 1-38.

44. Syed-Hassan, S. S. A.; Li, C.-Z., NiO reduction with hydrogen and light hydrocarbons: Contrast between SiO_2-supported and unsupported NiO nanoparticles. *Applied Catalysis A: General* **2011,** *398* (1–2), 187-194.

CHAPTER 5: SUMMARY, CONCLUSIONS, AND FUTURE DIRECTION

5.1   Summary and conclusions

The overall goal of the research presented herein was to determine the catalytic characteristics of silica-supported surrogate fly ash composed of NiO, CuO, and NiO-CuO for the formation of PCDD/Fs under simulated cool-zone conditions (< 600 °C and oxygen-depleted) of a municipal solid waste (MSW) incinerator. Transition metal oxides are present in the form of nanometer-sized particles on "real" fly ash formed by MSW incineration, as confirmed by previous TEM studies.[1-2] The challenge of this study was to prepare surrogate fly ash with nanometer-sized, metal-oxide particles similar to those found in real fly ash. Three different methods were employed to synthesize NiO, CuO, and NiO-CuO surrogate fly ash: wetness impregnation of metal ion−dendrimer complexes (WI-D), wetness impregnation of metal ion solutions (WI-M), and incipient wetness impregnation (IWI), all followed by calcination at 500 °C for 5 h.

For the first time NiO, CuO, and NiO-CuO nanoparticles with low size dispersity and < 5 nm in average diameter were synthesized using the WI-D method in methanol. Dendrimers were used as chelating agents to avoid nanoparticle agglomeration. Metal ion solutions were mixed with dendrimer solutions and impregnated into silica; followed by calcination at 500 °C for 5 h. Metal−dendrimer complexes on the silica surface before and after calcination were studied for the first time using XPS, XANES, and EXAFS. The absence of the peak for the N 1s region in high-resolution XPS indicated the dendrimer was removed upon calcination, leaving only metal-oxide nanoparticles on the silica surface. EXAFS fitting parameters provided information of the metal−dendrimer complexes binding to the silica surface via −OH groups. EXAFS also depicted the presence of metal-oxides on the silica surface after calcination, supporting the results of XPS.

105

NiO nanoparticles with an average diameter 3.6 ± 0.5 nm was observed by TEM. The silica support acted as an immobilizing surface, so the metal ions were attached uniformly on the silica surface via surface Si–OH groups.[3-5] Therefore, nanoparticles with low size dispersity and < 5 nm in diameter were formed by the WI-D method. However, the nanoparticle average diameter was increased significantly (at 95% confidence interval) with increasing calcination time to 24 h. The prolonged exposure to higher temperatures lead to agglomeration of the nanoparticles, but the size difference of NiO/silica nanoparticles before and after the calcination (3.6 ± 0.5 nm vs 4.3 ± 0.4 nm) was less than 1 nm and is a good indication that they were anchored on the silica surface so that their mobility is restricted even at 500 °C for 24 h.

The ability of the silica support to immobilize metal ions on the surface was further examined by preparing NiO, CuO, and NiO-CuO surrogate fly ash without the dendrimer via the WI-M method with methanol solvent. NiO nanoparticles with an average diameter of 2.9 ± 0.4 nm, and CuO nanoparticles with an average diameter of 3.1 ± 0.4 nm were observed by TEM after calcination at 500 °C for 5 h. In the same way, NiO nanoparticles prepared by the IWI method in methanol possessed an average diameter of 3.6 ± 0.5 nm after calcination at 500 °C for 5h. This observation is in agreement with the immobilization of metal ions on the silica surface via binding to surface Si–OH groups.[3-5] However, NiO nanoparticles with an average diameter of 49.1 ± 14.4 nm were observed when they were prepared by the IWI method in water. Water hydrolyzes the silica surface by dissociating the silanol groups,[6] thus preventing metal ions from anchoring on the silica surface. Also, hydrolysis of Ni(II) ions in aqueous media leads to the formation of a $Ni(OH)_2$ precipitate,[7] which leads to the agglomeration of NiO nanoparticles. Therefore, it is important to use methanol as the solvent in order to obtain nanoparticles < 5 nm in diameter during surrogate fly ash synthesis.

106

Mixed NiO-CuO surrogate fly ash on silica was synthesized by the WI-D and the WI-M methods and average diameters of 3.6 ± 0.4 nm and 3.1 ± 0.4 nm were obtained respectively for NiO-CuO (1:1) samples after calcination at 500 °C for 5 h. The metal composition (Ni:Cu) of individual nanoparticles was able to be controlled by altering the amounts of metal ions in the starting solutions. Single-particle EDS indicated that all the metal species are confined inside nanoparticles without any metals being present on the silica surface.

Above-mentioned silica-supported NiO, CuO, and NiO-CuO nanoparticles (surrogate fly ash) were used in this study to determine their ability to catalyze the formation of PCDD/Fs. The reactions were carried out under conditions similar to the cool-zone (< 600 °C) of MSW incinerators. The system for thermal diagnostic studies (STDS)[8-9] was utilized to simulate the conditions of a MSW incinerator. Catalysts prepared by both the WI-D and the WI-M methods were evaluated for their potential to convert 2-monochlorophenol (2-MCP) precursor to PCDD/Fs under pyrolytic conditions.

Catalytic studies indicated that approximately 86% of 2-MCP was converted to products (~14% recovery) even at the lowest temperature studied (300 °C) on NiO and CuO. However, NiO-CuO mixed catalysts demonstrated over 90% conversion (< 10% recovery) of 2-MCP at 300 °C, suggesting a higher catalytic activity compared to the individual metals. The nearly-complete conversion of 2-MCP was achieved at temperatures above 450 °C for all the catalysts. However, a major fraction of 2-MCP was converted to carbon during the reaction under pyrolytic conditions (helium atmosphere). Another fraction of the 2-MCP was converted to precursors, like dichlorophenol (DCP), trichlorophenol (TCP), monochlorobenzene (MCBz), and dichlorobenzene (DCBz). The % yields of DCP, TCP, MCBz, and DCBz decreased as the reaction temperature increased, indicating further conversion of these precursor molecules on the

107

catalytic surface. Dibenzo-*p*-dioxin (DD), monochloro dibenzo-*p*-dioxin (MCDD), and dichloro dibenzo-*p*-dioxin (DCDD) were observed as dioxin products. The only furan observed was dibenzofuran (DBF), which was formed only using CuO catalysts prepared by the WI-D method.

These results indicate the importance of NiO and CuO in fly ash as catalysts for the PCDD/Fs formation. The most striking observation was that the NiO-CuO mixed catalysts produced low % yields of PCDD/Fs compared to individual metal oxides. There were several differences in the catalytic activity between the catalysts prepared by the WI-D vs the WI-M methods. DCP and TCP, which were formed with the WI-D catalyst, did not form with the WI-M catalysts. Also, DBF was formed with CuO prepared by the WI-D method, whereas no furans were observed with CuO prepared by the WI-M method. The difference in the catalytic activity may be due to the difference in the synthetic route of WI-D vs WI-M.

5.2   Future Direction

A previous study has found clusters of several metals/metal-oxides in fly ash,[1] leading me to investigate mixed NiO-CuO surrogate fly ash as a catalyst for PCDD/Fs formation. Because Fe is commonly found in fly ash along with Ni and Cu,[1-2, 10] it is important to synthesize NiO-Fe_2O_3, CuO-Fe_2O_3, and NiO-Fe_2O_3-CuO surrogate fly ash samples, characterize them, and investigate their catalytic activity for the formation of PCDD/Fs. Fly ash from MSW incineration also contains a mixture of silica and alumina;[2] thus it is important to prepare fly ash with alumina, as well as combinations of silica and alumina to investigate the effect of the support on the surface-mediated formation of PCDD/Fs.

5.3   References

1.   Chen, Y.; Shah, N.; Huggins, F. E.; Huffman, G. P., Investigation of the Microcharacteristics of $PM_{2.5}$ in Residual Oil Fly Ash by Analytical Transmission Electron Microscopy. *Environmental Science & Technology* **2004,** *38* (24), 6553-6560.

2. Hower, J. C.; Graham, U. M.; Dozier, A.; Tseng, M. T.; Khatri, R. A., Association of the Sites of Heavy Metals with Nanoscale Carbon in a Kentucky Electrostatic Precipitator Fly Ash. *Environmental Science & Technology* **2008,** *42* (22), 8471-8477.

3. Hathaway, B. J.; Lewis, C. E., Electronic properties of transition-metal complex ions adsorbed on silica gel. Part I. Nickel(II) complexes. *Journal of the Chemical Society A: Inorganic, Physical, Theoretical* **1969**, 1176-1182.

4. Hathaway, B. J.; Lewis, C. E., The electronic properties of transition-metal complex ions adsorbed on silica gel. Part III. Copper(II). *Journal of the Chemical Society A: Inorganic, Physical, Theoretical* **1969**, 2295-2299.

5. Hathaway, B. J.; Lewis, C. E., Electronic properties of transition-metal complex ions adsorbed on silica gel. Part II. Cobalt(II) and cobalt(III). *Journal of the Chemical Society A: Inorganic, Physical, Theoretical* **1969**, 1183-1188.

6. Lutz, W.; Toufar, H.; Kurzhals, R.; Suckow, M., Investigation and Modeling of the Hydrothermal Stability of Technically Relevant Zeolites. *Adsorption* **2005,** *11* (3/4), 405-413.

7. Chen, S.; Zhu, J.; Zhou, H.; Wang, X., One-step synthesis of low defect density carbon nanotube-doped $Ni(OH)_2$ nanosheets with improved electrochemical performances. *Royal Society of Chemistry Advances* **2011,** *1* (3), 484-489.

8. Rubey, W. A.; Grant, R. A., Design aspects of a modular instrumentation system for thermal diagnostic studies. *Review of Scientific Instruments* **1988,** *59* (2), 265-269.

9. Wehrmeier, A.; Lenoir, D.; Sidhu, S. S.; Taylor, P. H.; Rubey, W. A.; Kettrup, A.; Dellinger, B., Role of Copper Species in Chlorination and Condensation Reactions of Acetylene. *Environmental Science & Technology* **1998,** *32* (18), 2741-2748.

10. Öberg, T.; Öhrström, T.; Bergström, J., Metal catalyzed formation of chlorinated aromatic compounds: A study of the correlation pattern in incinerator fly ash. *Chemosphere* **2007,** *67* (9), S185-S190.

APPENDIX: PREPARATION OF STANDARD SOLUTIONS OF Ni(NO₃)₂ AND Cu(NO₃)₂, AND QUANTIFICATION BY ATOMIC ABSORPTION SPECTROSCOPY (AAS)

Preparation of AAS standard series

The Ni(II) stock solution (1000 ppm) was prepared by dissolving 100 mg of Ni metal in 100 mL of aqueous 2% nitric acid. The solution was diluted 10 times with aqueous 2% nitric acid to obtain 100 ppm working solution. Ni(II) standard series (5, 10, 15, 20, 25, 30, 35, and 40 ppm) was prepared by diluting the 100 ppm working solution.

The Cu(II) stock solution (1000 ppm) was prepared by dissolving 100 mg of Cu metal in 100 mL of aqueous 2% nitric acid. The solution was diluted 10 times with aqueous 2% nitric acid to obtain 100 ppm working solution. Cu(II) standard series (4, 6, 8, 10, 12, 14, 16, 18, and 20 ppm) was prepared by diluting the 100 ppm working solution.

Preparation of 1×10^{-2} M solutions of Ni(II) and Cu(II) for quantification

Ni(II) and Cu(II) solutions were prepared in methanol using nickel(II) nitrate hexahydrate and copper(II) nitrate hydrate, respectively. The Ni(II) solution (10 mM = 587 ppm) was prepared by dissolving an appropriate amount of nickel(II) nitrate hexahydrate in methanol (100 mL). The Cu(II) solution (10 mM = 635 ppm) was prepared by dissolving an appropriate amount of nickel(II) nitrate hydrate in methanol (100 mL). An aliquot of 10 mL from each Ni(II) and Cu(II) solution was transferred to two different vials, and methanol was removed by passing nitrogen gas through the solution. The remaining solid residue was suspended in 10 mL of deionized water in each vial before AAS experiment. The concentrations of Ni(II) and Cu(II) solutions were determined to be 1.09×10^{-2} ($\pm 0.01 \times 10^{-2}$) M and 1.02×10^{-2} ($\pm 0.03 \times 10^{-2}$) M, respectively by AAS results.

THE VITA

Nuwan Nilanka Balapitiya Liyanage was born in Colombo, Sri Lanka, to Mr. Balapitiya Liyanage Premarathna and Mrs. Chandra Sellahewa. He had his primary education at the President's College, Maharagama, ordinary level (O/L) education at Dharmapala Vidyalaya, Pannipitiya, and advanced level (A/L) education at Nalanda College, Colombo 10. After successfully finishing school, he attended University of Colombo to pursue a Bachelor's degree in chemistry, graduating in 2007. After working in the Department of Chemistry, University of Colombo for one year as a teaching assistant, he moved to the United States in August 2008 to pursue his Ph.D. at Louisiana State University. In the spring of 2009, he joined the research group of Prof. Robin McCarley where he graduated in analytical chemistry in the fall commencement in December 2014.